

NAVAL POSTGRADUATE SCHOOL

Monterey, California



THESIS

**EFFECTS OF THERMOHALINE GRADIENTS AND THE
COLUMBIA RIVER PLUME ON THE CALIFORNIA
CURRENT SYSTEM**

by

Frank M. Schenk

March 2000

Thesis Advisor:

Mary L. Batteen

Second Reader:

Curtis A. Collins

Approved for public release; distribution is unlimited.

DTIC QUALITY INSPECTED 1

20000525 049

REPORT DOCUMENTATION PAGE			Form Approved OMB No. 0704-0188	
Public reporting burden for this collection of information is estimated to average 1 hour per response, including the time for reviewing instruction, searching existing data sources, gathering and maintaining the data needed, and completing and reviewing the collection of information. Send comments regarding this burden estimate or any other aspect of this collection of information, including suggestions for reducing this burden, to Washington headquarters Services, Directorate for Information Operations and Reports, 1215 Jefferson Davis Highway, Suite 1204, Arlington, VA 22202-4302, and to the Office of Management and Budget, Paperwork Reduction Project (0704-0188) Washington DC 20503.				
1. AGENCY USE ONLY (Leave blank)		2. REPORT DATE March 2000		3. REPORT TYPE AND DATES COVERED Master's Thesis
4. TITLE AND SUBTITLE Effects of Thermohaline Gradients and the Columbia River Plume on the California Current System				5. FUNDING NUMBERS
6. AUTHOR(S) Schenk, Frank M.				
7. PERFORMING ORGANIZATION NAME(S) AND ADDRESS(ES) Naval Postgraduate School Monterey, CA 93943-5000				8. PERFORMING ORGANIZATION REPORT NUMBER
9. SPONSORING / MONITORING AGENCY NAME(S) AND ADDRESS(ES)				10. SPONSORING / MONITORING AGENCY REPORT NUMBER
11. SUPPLEMENTARY NOTES The views expressed in this thesis are those of the author and do not reflect the official policy or position of the Department of Defense or the U.S. Government.				
12a. DISTRIBUTION / AVAILABILITY STATEMENT Approved for public release; distribution is unlimited.				12b. DISTRIBUTION CODE
13. ABSTRACT (maximum 200 words) To study the combined effects of thermohaline gradients and the Columbia River plume on the ocean circulation of the California Current System (CCS), results from three numerical experiments of increasing complexity are examined. In all three experiments, seasonal climatological winds are used to force the model. In the first experiment, the effects of seasonal thermohaline gradients along the western boundary are evaluated. In the second experiment, the additional effects of thermohaline gradients along the northern and southern boundaries are investigated, while in the third experiment, the effect of the Columbia River plume on the CCS is explored. The results from the first two experiments show that thermohaline gradients associated with the North Pacific Central, Pacific sub-Arctic, and Southern waters help to maintain more realistic temperatures and salinities in the CCS, particularly in the coastal regions. The third experiment shows that the Columbia River plume exhibits a strong seasonal signal with poleward flow close to the coast in winter and equatorward flow farther offshore in summer. The plume also has a significant impact on the near-surface stratification and baroclinic structure of the velocity field of the CCS from Washington to San Francisco.				
14. SUBJECT TERMS Primitive equation model, California Current System, currents, meanders, eddies, filaments, Columbia River plume				15. NUMBER OF PAGES 109
				16. PRICE CODE
17. SECURITY CLASSIFICATION OF REPORT Unclassified	18. SECURITY CLASSIFICATION OF THIS PAGE Unclassified	19. SECURITY CLASSIFICATION OF ABSTRACT Unclassified		20. LIMITATION OF ABSTRACT UL

Approved for public release; distribution is unlimited

**EFFECTS OF THERMOHALINE GRADIENTS AND THE COLUMBIA RIVER
PLUME ON THE CALIFORNIA CURRENT SYSTEM**

Frank M. Schenk
Lieutenant, United States Navy
B.S., United States Naval Academy, 1991


Submitted in partial fulfillment of the
requirements for the degree of

**MASTER OF SCIENCE IN METEOROLOGY AND PHYSICAL
OCEANOGRAPHY**

from the

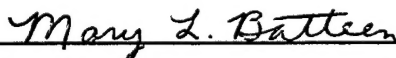
**NAVAL POSTGRADUATE SCHOOL
March 2000**

Author:



Frank M. Schenk

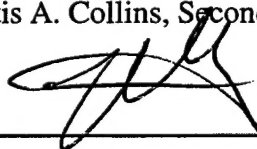
Approved by:



Mary L. Batteen, Thesis Advisor



Curtis A. Collins, Second Reader



Roland W. Garwood, Chairman
Department of Oceanography

ABSTRACT

To study the combined effects of thermohaline gradients and the Columbia River plume on the ocean circulation of the California Current System (CCS), results from three numerical experiments of increasing complexity are examined. In all three experiments, seasonal climatological winds are used to force the model. In the first experiment, the effects of seasonal thermohaline gradients along the western boundary are evaluated. In the second experiment, the additional effects of thermohaline gradients along the northern and southern boundaries are investigated, while in the third experiment, the effect of the Columbia River plume on the CCS is explored. The results from the first two experiments show that thermohaline gradients associated with the North Pacific Central, Pacific sub-Arctic, and Southern waters help to maintain more realistic temperatures and salinities in the CCS, particularly in the coastal regions. The third experiment shows that the Columbia River plume exhibits a strong seasonal signal with poleward flow close to the coast in winter and equatorward flow farther offshore in summer. The plume also has a significant impact on the near-surface stratification and baroclinic structure of the velocity field of the CCS from Washington to San Francisco.

TABLE OF CONTENTS

I. INTRODUCTION.....	1
II. MODEL DECSRIPTION	5
A. MODEL EQUATIONS	5
B. METHOD OF SOLUTION	8
C. FORCING CONDITIONS	11
D. EXPERIMENTAL DESIGN	13
III. RESULTS	15
A. EXPERIMENT 1	15
1. Spin-up Phase	15
2. Quasi-equilibrium Phase	17
B. EXPERIMENT 2	18
1. Spin-up Phase	18
2. Quasi-equilibrium Phase	20
C. EXPERIMENT 3	21
1. Spin-up Phase	22
2. Quasi-equilibrium Phase	23
IV. SUMMARY	25
LIST OF REFERENCES	87
INITIAL DISTRIBUTION LIST	91

LIST OF FIGURES

1. Generalized classical circulation of the California Current System (CCS). The broad, slow surface equatorward California Current (CC) overlies the narrow, poleward California Undercurrent (CUC), along with the Inshore Countercurrent (IC), known as the Davidson Current (DC) north of Point Conception and as the Southern California Eddy (SCE) south of Point Conception 27

2. Domain and climatological winds of the model for the California Current System (CCS) off the Western United States. The domain of the model is bounded by 35.0° N to 47.5° N, 120.0° W to 132.5° W. The climatological (1980-1989) ECMWF winds used in Experiments 1, 2, and 3 in m/s are shown here for (a) January, (b) April, (c) July, and (d) October. Maximum wind vector is 10 m/s 28

3. Plots of Levitus climatological fields used as seasonal forcing along the western boundary (132.5° W) for: (a) temperature and (b) salinity 32

4. Plots of Levitus climatological fields used as seasonal forcing along the northern boundary (47.5° N) for: (a) temperature and (b) salinity 34

5. Plots of Levitus climatological fields used as seasonal forcing along the southern boundary (35.0° N) for: (a) temperature and (b) salinity 36

6. Monthly mean surface salinity conditions recorded at the Columbia River Lightship (46.2° N, 124.2° W), located at the mouth of the Columbia River (Bourke and Glenne, 1971) 38

7. Temperature contours and velocity vectors at 10 m depth for Experiment 1 at days (a) 45, (b) 84, (c) 123, (d) 237, and (e) 270. In all velocity fields presented, to avoid clutter, velocity vectors are plotted every third (fifth) grid point in the cross-shore (alongshore) direction. Contour interval is 1° C; maximum velocity vector is 100 cm/s 39

8. Cross-shore section of meridional velocity (v) at 46° N for Experiment 1 at days (a) 237 and (b) 321. In (a), contour interval is 5 cm/s (10 cm/s) for poleward (equatorward) flow. In (b), contour interval for velocities greater than (less than) 5 cm/s is 10 cm/s (2 cm/s) 44

9. Temperature contours and velocity vectors at 10 m depth for Experiment 1 in the third year of model simulation, time-averaged over the months of (a) May, (b) August, and (c) December. Contour interval is 1° C; maximum velocity vector is 100 cm/s 46

10. Horizontal maps at 10 m depth of (a) mean kinetic energy (MKE), and (b) eddy kinetic energy (EKE) for Experiment 1 in the third year of model simulation, time-averaged for the month of August. Contour interval is 1000 (cm/s)^2 for (a), and 250 (cm/s)^2 for (b) 49
11. Cross-shore section of meridional velocity (v) at 46° N for Experiment 1 in the third year of model simulation time-averaged for the months of (a) October, (b) November, and (c) December. Contour interval is 15 cm/s. The 30 cm/s contour for the coastal, poleward flow shows shoaling of the CUC from October (a) – December (c) 51
12. Salinity contours and velocity vectors at 10 m depth for Experiment 2 on day 126. Contour interval is 0.25 psu; maximum velocity vector is 100 cm/s. The 32.5 and 32.75 isohalines are present off the coast of Washington and Oregon54
13. Temperature contours and velocity vectors at 10 m depth for Experiment 2 on day 237. Contour interval is 1° C ; maximum velocity vector is 100 cm/s 55
14. Cross-shore section of meridional velocity (v) at 47° N on day 183 for (a) Experiment 2 and (b) Experiment 1. Contour interval is 10 cm/s for (a) and (b) 56
15. Cross-shore section of meridional velocity (v) at 37° N on day 141 for (a) Experiment 2 and (b) Experiment 1. Contour interval is 10 cm/s for equatorward flow and 5 cm/s for poleward flow 58
16. Cross-shore section of meridional velocity (v) at 47° N on day 201 for (a) Experiment 2 and (b) Experiment 1. Contour interval is 10 cm/s for equatorward flow in (a) and (b). For poleward flow, the contour interval is 5 cm/s in (a) and 1 cm/s in (b) 60
17. Temperature contours and velocity vectors at 10 m depth for Experiment 2 in the third year of model simulation, time-averaged over the month of August. Contour interval is 1° C ; maximum velocity vector is 100 cm/s 62
18. Cross-shore section of meridional velocity (v) at 42.5° N in the third year of model simulation time-averaged over the month of July for (a) Experiment 2 and (b) Experiment 1. Contour interval is 10 cm/s for equatorward flow and 6 cm/s for poleward flow 63
19. Horizontal maps at 10 m depth of (a) mean kinetic energy (MKE), and (b) eddy kinetic energy (EKE) for Experiment 2 in the third year of model simulation, time-averaged for the month of August. Contour interval is 1000 (cm/s)^2 for (a), and 250 (cm/s)^2 for (b) 65

20. Salinity contours and velocity vectors at 10 m depth for Experiment 3 on day (a) 54, (b) 99, (c) 126, and (d) 201. Contour interval is 0.25 psu; maximum velocity vector is 100 cm/s. Salinity at the mouth of the Columbia River is ~31.72 psu for (a)–(d) 67
21. Cross-shore section for Experiment 3 on day 54 at 47° N for (a) and (c) salinity to 900 m and 150 m depth, respectively; (b) and (d) meridional velocity (v) to 900 m and 150 m depth, respectively. Contour interval for salinity is 0.25 psu for salinity and 5 cm/s for v 71
22. Cross-shore section for Experiment 3 on day 99 at 46.2° N of salinity. Contour interval is 0.25 psu 75
23. Cross-shore section for Experiment 3 on day 126 at 45° N for (a) salinity and (b) meridional velocity (v). Contour interval for salinity is 0.25 psu. Contour interval for v is 5 cm/s 76
24. Cross-shore section of salinity for Experiment 3 on day 201 at (a) 43° N and (b) 42° N. Contour interval for salinity is 0.25 psu 78
25. Cross-shore section for Experiment 3 time-averaged over the month of January at 47° N for (a) salinity and (b) meridional velocity (v). Contour interval for salinity is 0.25 psu. Contour interval for v is 5 cm/s 80
26. Salinity contours and velocity vectors at 10 m depth for Experiment 3 time-averaged for the month of July. Contour interval is 0.2 psu; maximum velocity vector is 100 cm/s. Tongue of Columbia River plume is represented by the 32.0 isohaline 82
27. Cross-shore section of salinity for Experiment 3 time-averaged for the month of July at (a) 45° N and (b) 42° N. Contour interval for salinity is 0.25 psu 83

LIST OF TABLES

1. Values of Constants Used in the Model	85
--	----

ACKNOWLEDGEMENT

I would like to thank my thesis advisor, Dr. Mary Batteen, for her instruction and guidance, which has made this study possible. Her exceptional professional advice, patience, and support were invaluable. Additionally, the constructive advice provided by Dr. Curtis Collins, as second reader, was greatly appreciated as well.

This study would have not been accomplished if it was not for the technical expertise of several individuals: Donna Burych, Arlene Guest, Pete Braccio, Mike Cook, Eldor Magat, and Al Lewis. I am so grateful that these individuals were willing to help assist with the numerous technical computing issues required to accomplish this study.

Above all, I could not have accomplished this study without the love and support of my wife Michele and two children, Frankie and Isabella. I could not have finished this study without their patience, flexibility, and encouragement. Thank you all!

I. INTRODUCTION

The west coast of North America from the Strait of Juan de Fuca to the tip of Baja California is part of an eastern boundary current system known as the California Current System (CCS) (Hickey, 1998). The CCS is comprised of three large-scale currents (see Figure 1): the California Current (CC), the California Undercurrent (CUC), and the Inshore Countercurrent (IC) (Batteen and Vance, 1998).

The CC is a broad (~1000 km), relatively slow (~10-30 cm/s), equatorward year-round surface flow. The current is strongest at the sea surface and generally extends over the upper 500 m of the water column. It has a seasonal maximum in summer to early fall (Hickey, 1998; Batteen and Vance, 1998).

The CUC is a narrow (~10-40 km), relatively weak (~2-10 cm/s), poleward subsurface flow over the continental slope. The current is strongest at depths of ~100-300 m from the surface. It has a seasonal maximum in late spring and summer with peak speeds of ~30-50 cm/s (Hickey, 1998; Batteen and Vance, 1998).

The IC, which is known as the Davidson Current (DC) north of Point Conception, is a broader (~200 km), weak (~5 cm/s), poleward surface flow in fall and winter with a seasonal maximum in winter. There are other ICs known as the Southern California Countercurrent (SCC) to the south, and the Southern California Eddy (SCE) inshore of the Channel Islands within the California Bight (Hickey, 1979, 1998; Batteen and Vance, 1998).

Three types of water masses are found in the CCS: Pacific sub-Arctic, North Pacific Central, and Southern waters. The Pacific sub-Arctic water, characterized by low salinity and temperature and high oxygen and nutrients, is advected equatorward in the CCS by the CC. North Pacific Central water, characterized by high salinity and temperature and low oxygen and nutrients, enters the CCS from the west. Southern water characterized by high salinity, temperature and nutrients, and low oxygen, enters the CCS from the south by the CUC (Lynn and Simpson, 1987).

The only large river plume off the west coast of the U.S. is from the Columbia River (Huyer, 1983; Hickey, 1998). The Columbia River provides over 77% of the drainage between the Strait of Juan de Fuca and San Francisco Bay. On a seasonal basis, the plume flows poleward over the shelf and slope in fall and winter, and equatorward well offshore of the shelf in spring and summer. The Columbia plume is barely visible at a depth of 20 m from the sea surface (Hickey, 1998).

Recent observational studies have shown that the CCS is not the quiescent, stable system of currents with a well-defined, unchanging structure as suggested by Figure 1. Rather, the flow fluctuates greatly in both time and space (Batteen and Vance, 1998). Satellite infrared sea surface temperature (SST) imagery of the CCS has revealed a distinct complex flow structure with seasonal variations. Within the mean, large-scale structure of the CCS there exist perturbations in the form of mesoscale meanders, eddies, filaments, and jets which vary in both space and time (Bernstein *et al.*, 1977; Chelton, 1984; Strub *et al.*, 1991). Dominant mechanisms responsible for the observed large-scale structure within the CCS have been shown to be seasonal variations in alongshore wind

stress (Bakun and Nelson, 1991), coastline irregularities (e.g., Batteen, 1997), bottom topography (e.g., Ikeda *et al.*, 1984), and temperature and salinity variations (Batteen *et al.*, 1995; Batteen and Vance, 1998).

Previous modeling studies (e.g., Batteen *et al.*, 1989; Batteen, 1997) have shown the seasonal variation of the alongshore component of wind stress to be critical in generating realistic horizontal and vertical structures for the CC and CUC. Both baroclinic and barotropic instability mechanisms contributed to the generation of meanders, filaments, and eddies. Additionally, coastline irregularities were shown to help "anchor" upwelling filaments and to enhance growth of meanders and eddies.

In recent observational (Batteen *et al.*, 1995) and numerical modeling studies (Batteen and Vance, 1998) on the combined effect of temperature and salinity on density, it was shown that the distribution of salinity as well as temperature is important in defining the large-scale structure and circulation of the CCS. The modeling study of Batteen and Vance (1998) included wind forcing, coastline irregularities, and seasonal temperature and salinity thermohaline gradients on the western boundary.

In this study, the role of thermohaline gradients on the CCS will be expanded to include seasonal temperature and salinity forcing on the northern and southern boundaries of the model domain. This will allow the influences of the three major water masses (i.e. the Pacific sub-Arctic, North Pacific Central, and Southern waters) on the CCS to be studied. Additionally, the Columbia River plume will be added to the model domain in order to examine its effect on the CCS.

The study is organized as follows: section 2 describes the numerical model, the forcing, and the experimental conditions used in the basic experiment; section 3 includes analysis of the results of the model simulations, and section 4 summarizes the results.

II. MODEL DESCRIPTION

A. MODEL EQUATIONS

The numerical model in this study was originally a coarse resolution model used in closed basin studies by Haney (1974). It has recently been adapted by Batteen (1997) for eddy-resolving, limited EBC regions with open boundaries to the north, south, and west. The model is multi-level, uses non-adiabatic primitive equations, and the beta-plane approximation. It has both baroclinic and barotropic velocity components and uses the hydrostatic and Boussinesq approximations as well as a rigid lid. The governing equations are as follows:

$$\frac{du}{dt} = \frac{-1}{\rho_0} \frac{\partial p}{\partial x} + fv - A_M \nabla^4 u + K_M \frac{\partial^2 u}{\partial z^2} \quad (1)$$

$$\frac{dv}{dt} = \frac{-1}{\rho_0} \frac{\partial p}{\partial y} - fu - A_M \nabla^4 v + K_M \frac{\partial^2 v}{\partial z^2} \quad (2)$$

$$\frac{\partial u}{\partial x} + \frac{\partial v}{\partial y} + \frac{\partial w}{\partial z} = 0 \quad (3)$$

$$\frac{\partial p}{\partial z} = -\rho g \quad (4)$$

$$\rho = \rho_0 [1 - \alpha(T - T_0) + \beta(S - S_0)] \quad (5)$$

$$\frac{dT}{dt} = -A_H \nabla^4 T + K_H \frac{\partial^2 T}{\partial z^2} \quad (6)$$

$$\frac{dS}{dt} = -A_H \nabla^4 S + K_H \frac{\partial^2 S}{\partial z^2} \quad (7)$$

In the above equations, t is time and (x,y,z) is a right-handed Cartesian coordinate system with x pointing toward shore, y alongshore, and z upward. The corresponding velocity components are (u,v,w) . T , S , and p are temperature, salinity and pressure, respectively, and ρ is density. Table 1 provides a list of other symbols found in the model equations, as well as values of constants used throughout the study.

A space-staggered B-scheme (Arakawa and Lamb, 1977) is used for the horizontal finite differencing. This scheme has been shown by Batteen and Han (1981) to be appropriate when grid spacing is approximately the same order as, or less than, the Rossby radius of deformation. The horizontal grid spacing is 8 km in the east-west direction and 11 km in the north-south direction, while the internal Rossby radius of deformation is ~30 km. This horizontal grid resolution should allow realistic spatial resolution of mesoscale features in the CCS, which have typical wavelengths of the order of 100 km (Breaker and Mooers, 1986).

The model uses ten vertical layers, with constant z -levels, at depths of 10, 30, 75, 150, 250, 400, 600, 1226, 2283, and 3656 m. This vertical scheme is designed to concentrate more layers above the thermocline in the dynamically active portion of the ocean, consistent with Haney (1974).

The model domain (Figure 2) is a rectangular region encompassing the west coast of the United States, from 35.0° N to 47.5° N (1408 km alongshore), and from 120.0° W to 132.5° W (1024 km cross-shore). The coastal boundary of the model domain is closed, and has both tangential and normal velocity components set to zero. As in other wind-forced process-oriented studies, bottom topography has been omitted to focus on the roles

played by wind forcing and thermohaline gradients. The constant depth used in the model is 4500 m.

A modified version of the radiation boundary conditions of Camerlengo and O'Brien (1980) is used for the open ocean domain boundaries to the north, south, and west. In particular, whether a boundary grid point is treated as an inflow point or an outflow point for a particular prognostic variable is determined by the sign of a dynamically computed effective group velocity. This group velocity is defined as the ratio of the local time derivative and the local space derivative normal to the boundary. If the boundary grid point is thereby determined to be an inflow point, then the value of the prognostic variable is set to its value at the previous timestep. If the boundary point is determined to be an outflow point, its value is set to that of the nearest interior point. Spatial smoothing is also applied with a 1-2-1 weighting window within five grid points (~50 km) of the open boundaries.

The model uses biharmonic lateral heat and momentum diffusion with the same choice of coefficients (i.e., $2.0 \times 10^{17} \text{ cm}^4/\text{s}$) as in Batteen et al. (1989). Holland (1978) showed that the highly scale-selective biharmonic diffusion acts predominantly on submesoscales, while Holland and Batteen (1986) found that baroclinic mesoscale processes can be damped by Laplacian lateral heat diffusion. As a result, the use of biharmonic lateral diffusion should allow mesoscale eddy generation via barotropic (horizontal shear) and/or baroclinic (vertical shear) instability mechanisms. As in Batteen et al. (1989), weak ($0.5 \text{ cm}^2/\text{s}$) eddy viscosities and conductivity are used. Bottom stress

is parameterized by a simplified quadratic drag law (Weatherly, 1972), as in Batteen et al. (1989).

The method of solution is straightforward with the rigid lid and flat bottom assumptions because the vertically integrated horizontal velocity is subsequently nondivergent. The vertical mean flow can be described by a streamfunction which can be predicted from the vorticity equation, while the vertical shear currents can be predicted after the vertical mean flow is subtracted from the original equations. The other variables, i.e., temperature, salinity, vertical velocity, and pressure, can be explicitly obtained from the thermodynamic energy equation (6), salinity equation (7), continuity equation (3), and hydrostatic equation (4), respectively.

B. METHOD OF SOLUTION

Equations (1) through (7) comprise a closed system of seven scalar equations and seven unknowns, u , v , w , p , ρ , T , and S . The variables, u , v , T , and S are prognostic variables whose time rates of change are predicted from (1), (2), (6) and (7), respectively. Although the diagnostic variables w , p , and ρ can be determined from (3), (4), and (5), respectively, additional constraints are imposed on p and w by the choice of the rigid lid boundary condition. Specifically, the vertically integrated pressure can no longer be obtained by integrating the hydrostatic equation (4) for the free surface, and the vertically-integrated horizontal velocity is subsequently constrained to be non-divergent, i.e.,

$$\int_{-H}^0 \left(\frac{\partial u}{\partial x} + \frac{\partial v}{\partial y} \right) d\varepsilon = 0, \quad (8)$$

which is obtained by integrating (3) and applying the vertical boundary conditions where ε is a dummy variable representing the vertical coordinate.

For any quantity q , let its vertical average be denoted by \bar{q} and its departure (vertical shear) by q' . From (8) the vertical mean flow can then be described by a stream function ψ , such that:

$$\bar{u} = -\frac{1}{H} \frac{\partial \psi}{\partial y}, \quad (9)$$

$$\bar{v} = \frac{1}{H} \frac{\partial \psi}{\partial x}. \quad (10)$$

The stream function ψ is predicted from the vorticity equation, which is derived from the vertical average of (1) and (2). Applying the curl operator and using (9) and (10) the vorticity equation becomes

$$\begin{aligned} \frac{\partial \zeta}{\partial t} &= \frac{\partial}{\partial t} \left[\frac{1}{H} \left(\frac{\partial^2 \psi}{\partial x^2} \right) + \frac{1}{H} \left(\frac{\partial^2 \psi}{\partial y^2} \right) + \frac{\partial \psi}{\partial x} \frac{\partial H^{-1}}{\partial x} + \frac{\partial \psi}{\partial y} \frac{\partial H^{-1}}{\partial y} \right] \\ &= - \left[\frac{\partial}{\partial x} \left(\frac{f}{H} \frac{\partial \psi}{\partial y} \right) - \frac{\partial}{\partial y} \left(\frac{f}{H} \frac{\partial \psi}{\partial x} \right) \right] \\ &\quad - \left[\frac{\partial}{\partial x} \left(\frac{g}{H\rho_0} \int_{-H}^0 \int_z \frac{\partial \rho}{\partial y} d\varepsilon dz \right) - \frac{\partial}{\partial y} \left(\frac{g}{H\rho_0} \int_{-H}^0 \int_z \frac{\partial \rho}{\partial x} d\varepsilon dz \right) \right] \\ &\quad + \frac{\partial}{\partial x} \left(\frac{1}{H} \int_{-H}^0 G dz \right) - \frac{\partial}{\partial y} \left(\frac{1}{H} \int_{-H}^0 F dz \right), \end{aligned} \quad (11)$$

where G and F represent the collective contributions of nonlinear and viscous terms from equations (1) and (2).

The vorticity equation (1) is solved by obtaining an updated value of ζ by applying the leapfrog (or every 11 time steps, the Euler-backward) time-differencing scheme. The associated value of ψ can then be obtained from:

$$\zeta = \frac{1}{H} \left(\frac{\partial^2 \psi}{\partial x^2} \right) + \frac{1}{H} \left(\frac{\partial^2 \psi}{\partial y^2} \right) + \frac{\partial \psi}{\partial x} \frac{\partial H^{-1}}{\partial x} + \frac{\partial \psi}{\partial y} \frac{\partial H^{-1}}{\partial y}, \quad (12)$$

which is an elliptic equation. A solution to (1) is fully prescribed by specifying the values of ψ on the open and closed boundaries of the model domain. Currently, to solve (1), the model uses successive over-relaxation techniques.

The vertical shear current (u' , v') is predicted from (1) and (2) after subtracting the vertical mean flow. The results are:

$$\frac{\partial u'}{\partial t} = \frac{-1}{\rho_0} \frac{\partial p'}{\partial x} + f v' - A_M \nabla^4 u' + K_M \frac{\partial^2 u'}{\partial z^2} + F - \bar{F} - \frac{\tau^y}{\rho_0 H}, \quad (13)$$

$$\frac{\partial v'}{\partial t} = \frac{-1}{\rho_0} \frac{\partial p'}{\partial y} - f u' - A_M \nabla^4 v' + K_M \frac{\partial^2 v'}{\partial z^2} + G - \bar{G} - \frac{\tau^x}{\rho_0 H}. \quad (14)$$

In (13) and (14), p' , which represents the departure of the pressure from the vertical average, is, using (4), expressed in terms of ρ as:

$$p' = \int_z^0 \rho g d\epsilon - \frac{1}{H} \int_{-H}^0 \left(\int_z^0 \rho g d\epsilon \right) dz. \quad (15)$$

The method of solution consists of predicting $\nabla^2 \psi$, ψ , u' , v' , T , and S from (11), (12), (13), (14), (6) and (7), respectively. The total current is then obtained by adding the vertical shear part to the vertical average part, after the latter is obtained from ψ using

(9) and (10). The diagnostics ρ , w , and p' are then obtained explicitly from the equation of state (5), continuity equation (8), and hydrostatic relation (15) respectively.

C. FORCING CONDITIONS

The model is forced from rest with climatological wind fields from a 2.5° by 2.5° grid of European Centre for Medium-Range Weather Forecasts (ECMWF) near-surface wind analyses (Trenberth *et al.*, 1990). The monthly mean stresses based on twice daily wind analyses from 1980-1989 have been interpolated spatially to the 8 by 11 km model resolution and temporally to daily wind values.

Sample wind fields used in the basic study are shown in Figure 2, which depicts the seasonal influence and migration of flow around the North Pacific Subtropical High over the area encompassed by the model domain. The atmospheric pressure pattern for January (Figure 2a) has a low (i.e., the Aleutian Low) to the north and a high (i.e., the North Pacific High) to the south, which results in a wind divergence near 40° N as winds circulate anticyclonically around the Subtropical High and cyclonically around the Aleutian Low. This pattern of poleward winds north of 40° N and equatorward winds to the south continues through February and March. During April (Figure 2b) and May, the Subtropical High has begun its westward and northward expansion, producing increased equatorward winds over most of the model domain and causing the divergence of flow to move north off the Washington coast. In July (Figure 2c), equatorward, upwelling-favorable winds dominate along the entire coastline as the Subtropical High reaches its

maximum extent. By October (Figure 2d), the winds decrease in magnitude throughout the model domain as the Subtropical High once again begins to recede southward. By December, the wind divergence has returned to $\sim 40^\circ$ N.

The effects of thermohaline gradients in the CCS along the western (132.5° W), northern (47.5° N), and southern (35.0° N) boundaries are included using monthly temperature and salinity climatological conditions for the upper seven levels from Levitus *et al.* (1994) and Levitus and Boyer (1994) to initialize the model, and every 10 days to force the model at the boundaries. The seasonal temperature and salinity forcing conditions for the upper seven layers, which are initially assumed to be zonally homogeneous, are shown in Figures 3-5 for the western, northern and southern boundaries, respectively. Since the lower three levels do not exhibit significant horizontal variation in temperature and salinity, constants are assumed for each level. Temperature values used for levels 8, 9, and 10 are 2.56° C, 2.08° C, and 2.00° C, respectively, while the salinity constant used for the lower three levels is 34.7.

Along the boundaries, the temperatures to the south and offshore are generally warmer than those to the north and inshore. Only the upper level temperature conditions (Figures 3a, 4a, and 5a) show significant seasonal variability with a temperature maximum in September and a temperature minimum in February. Below ~ 150 m, both the seasonal temperature fluctuations and temperature gradient weaken. Salinity forcing conditions (Figures 3b, 4b, and 5b), which show less saline water to the north and inshore in the upper 75 m, have no significant seasonal cycle.

The effects of the Columbia River plume on the CCS are included using monthly mean surface salinity conditions. The data used was recorded at the Columbia River Lightship (46.2 N, 124.2 W), located at the mouth of the Columbia River (Bourke and Glenne, 1971). The monthly data (Figure 6) was interpolated to daily values to force the model. The lowest salinities are observed in late spring and early summer due to the annual snow melt (Landry and Hickey, 1989).

D. EXPERIMENTAL DESIGN

Experiment 1 examines the model response to seasonal wind forcing (Figure 2) and thermohaline gradients along the western boundary (Figure 3). Model integrations start from a state of rest and, once a day, the model is updated with ECMWF winds and, every 10 days, the model is updated along the western boundary with temperature and salinity. In Experiment 2, thermohaline gradients along the northern (Figure 4) and southern (Figure 5) boundaries are added to Experiment 1 to investigate the impact of the three major water masses on the CCS. In Experiment 3, the Columbia River plume is added to Experiment 2 to study its effect on the CCS. All three experiments are run for three years to allow the model to reach a state of quasi-equilibrium.

THIS PAGE INTENTIONALLY LEFT BLANK

III. RESULTS

A. EXPERIMENT 1

1. Spin-up Phase

Due to the combination of climatological wind forcing and thermohaline gradients along the western boundary, different oceanic responses are expected depending on the season. During winter, in the poleward end of the model domain, the large high-to-low pressure gradient due to the warm-to-cold temperature gradient establishes an onshore geostrophic flow, while the poleward wind stress results in onshore Ekman flow. On approaching the eastern boundary, the onshore flow turns and forms a poleward boundary current (e.g., Figure 7a). In the equatorward end of the model domain, the smaller pressure gradient and the equatorward wind stress results in weak onshore geostrophic flow, offshore Ekman flow, and a coastal equatorward surface current (e.g., Figure 7b).

As spring approaches and the North Pacific High begins to build, the poleward boundary current along the coast in the northern part of the model domain gradually weakens and turns equatorward (e.g., Figure 7c). Coastal upwelling is first noticeable along the coast south of Cape Mendocino and Point Arena (e.g., Figure 7c).

In summer, the primary upwelling season, the combination of a weakened pressure gradient and increased equatorward winds over the entire model domain lead to a strengthening of equatorward flow all along the coast and a weakening (strengthening) of onshore (offshore) flow. Coastal upwelling becomes more pronounced along the coast,

but has the coldest water found near coastal promontories (e.g., Cape Blanco and Cape Mendocino in Figure 7d). Since promontories are areas of the irregular coastline where the alongshore component of the wind stress is at a local maximum, the CC, upwelling, and growth of filaments should be enhanced in these regions during the upwelling season (Batteen, 1997). The filaments that develop are “anchored” in the vicinity of Cape Blanco and Cape Mendocino (e.g., Figure 7d). The equatorward CC also forms meanders in the vicinity of capes, which intensify and develop into predominantly cyclonic eddies (e.g., Figure 7e).

The subsurface structure of the currents (e.g., Figure 8a) shows that the poleward undercurrent is within ~50 km of the coast and has a core velocity of ~5-10 cm/s centered at ~300 m depth. The core of the surface coastal equatorward current is within ~100 km of the coast and has a typical core velocity of ~50-60 cm/s.

During fall, as expected, the surface poleward flow strengthens in the coastal poleward end of the model domain in response to both the strengthening of the pressure gradient and the return of poleward wind stress in the region. The subsurface structure of the currents (e.g., Figure 8b) shows that in the coastal, poleward end of the model domain, there is an equatorward undercurrent. The undercurrent is within ~30 km of the coast, extends from ~100-500 m depth, and has a core velocity of ~1 cm/s. The core of the surface poleward current is within ~100 km of the coast and has a typical core velocity of ~5 cm/s. The fall model simulation in the poleward end of the model domain is consistent with the observed depths and velocities of both the surface poleward current and the equatorward undercurrent near the coast of Washington (Hickey, 1979, 1998).

2. Quasi-equilibrium Phase

Longer experimental runs show that the system has reached a quasi-steady state and that these features continue to be generated and maintained. Using the results of the longer experimental runs (i.e., year 3 of model simulation time), the model output is time-averaged for the months of May, August, and December to see the seasonal structure of features in the CCS (Figures 9a–9c). The spring results (e.g., Figure 9a) show that equatorward flow along with upwelling is present along the coast, as well as many features such as meanders, eddies, a temperature front, and filaments. By late summer, coastal upwelling is at its maximum with temperatures along the coast as low as 7°C near the coastal promontories (e.g., Figure 9b). During fall (not shown) and winter (e.g., Figure 9c), a coastal, poleward flow is discernible in the northern portion of the model domain. A continuous, meandering, equatorward jet embedded with eddies is also present offshore.

Horizontal maps of the upper layer mean kinetic energy (MKE) and eddy kinetic energy (EKE) are time-averaged for each month during the duration of the upwelling season. Maps of MKE and EKE are suggestive of where the mean and eddy energy sources are to be found (Holland et al., 1983). Typical MKE and EKE results during the upwelling season (e.g., Figures 10a and 10b) show that high values of MKE and EKE are found all along the coastal and offshore axes of the equatorward jet (e.g., compare Figures 10a and 10b with Figure 9b). A comparison of Figures 10a and 10b shows that maximum values of MKE and EKE occur in the same region, i.e., inshore of $\sim 129^{\circ}\text{W}$

and equatorward of $\sim 45^\circ$ N with high values offshore of the coastal promontories of Cape Blanco and Cape Mendocino. Note that the MKE values are larger than the EKE values in the region. This is consistent with the results of Batteen (1997), which showed that the eddies are generated from instabilities of the mean equatorward current and the poleward undercurrent via baroclinic and/or barotropic instability processes.

The combination of wind forcing and thermohaline gradients results in seasonal changes in the currents in the poleward end of the model domain. In particular, in the fall, the reversal of winds from equatorward to poleward combined with the intensification of the alongshore pressure gradient results in a shoaling of the poleward undercurrent off the coast of Oregon and Washington (e.g., Figures 11a-c). These results are consistent with the hypothesis of Hickey (1979, 1998) that a surface poleward current can result from a shoaling of the undercurrent.

B. EXPERIMENT 2

In this experiment, the role of thermohaline gradients on the CCS is expanded to include seasonal temperature and salinity forcing on the northern and southern boundaries of the model domain. This allows the influences of all three water masses (i.e., the North Pacific Central, Pacific sub-Arctic, and Southern waters) on the CCS to be studied.

1. Spin-up Phase

The North Pacific Central water mass continues to input warm water in the upper layers from the west. The signature of the Pacific sub-Arctic water mass is to bring low salinity water in the upper layers from the north. For example, Figure 12 shows a tongue of relatively low salinity water (as a result of the Pacific sub-Arctic water mass along the northern boundary) along the coast in the northern portion of the model domain in the region of coastal, equatorward flow during the spring.

The signature of the Southern water mass is to bring relatively high temperature in the upper layers and higher salinity into the southern portion of the model domain. As a result of the relatively high temperature associated with the Southern waters, the water along the coast is generally warmer in Experiment 2, particularly in regions of upwelling south of Cape Mendocino during the summer (e.g., compare Figure 13 from Experiment 2 with Figure 7d from Experiment 1). As a result, the equatorward flow is slightly weaker in Experiment 2, due to the reduced onshore-offshore temperature gradient. For example, maximum equatorward speeds reach ~55 cm/s in the summer (e.g., Figure 14a) compared to maximum speeds of ~65 cm/s in Experiment 1 (e.g., Figure 14b). Filaments, meanders, and eddies also develop earlier in Experiment 2 (e.g., Figure 13 at day 237 resembles Figure 7e at day 270 for Experiment 1 more than Figure 7d at day 237 for Experiment 1).

In the southern portion of the model domain, the CUC develops earlier and is stronger than the CUC in Experiment 1 (e.g., compare Figure 15a from Experiment 2

with Figure 15b from Experiment 1). The earlier development and stronger velocities of the CUC can be attributed to the influx of the Southern waters. Consistent with the results from the southern portion of the model domain, the CUC develops earlier and is stronger in the northern portion as well (e.g., compare Figure 16a from Experiment 2 with Figure 16b from Experiment 1).

2. Quasi-equilibrium Phase

Longer run times (~ 3 years) of the model simulation show that all of the features simulated in Experiment 1, such as the seasonal cycle of the surface coastal equatorward and poleward currents, upwelling, subsurface poleward and equatorward undercurrents, meanders, eddies, and filaments are also simulated in Experiment 2. As a result of the influence of the Southern waters, the coastal temperatures are considerably warmer (e.g., by 2-3 K in the summer) than Experiment 1 (e.g., compare Figure 17 from Experiment 2 with Figure 9b from Experiment 1). As in Experiment 1, the coldest temperatures are still found offshore of the coastal promontories of Cape Blanco, Cape Mendocino, and Point Arena (e.g., Figure 17).

The mean speeds for the CC are greater in Experiment 2 than in Experiment 1. For example, for the month of July, core velocities are ~20 cm/s for Experiment 2 at 42.5° N (e.g., Figure 18a), while mean speeds are ~50 cm/s for Experiment 1 at the same latitude (e.g., Figure 18b). The mean speeds for the CUC are also greater in Experiment 1 than in Experiment 2. For example, mean speeds of ~12 cm/s are obtained in Experiment

2 (e.g., Figure 18a) compared with mean velocities of ~6 cm/s in Experiment 1 (e.g., Figure 18b).

MKE and EKE values, as expected, are higher for Experiment 1 than Experiment 2 (e.g., compare Figures 19a and 19b from Experiment 2 with Figures 10a and 10b from Experiment 1). Both experiments still exhibit high values of MKE and EKE extending from the coastal promontories.

This experiment illustrates the important role that thermohaline gradients play in the CCS. In particular, the North Pacific Central water mass and the Southern water mass are important sources for input of surface warm waters into the CCS region. The Southern (Pacific sub-Arctic) water mass is an important source of high (low) salinity water in the southern (northern) coastal regions of the model domain. These water masses help to maintain more realistic temperatures and salinities in the CCS, particularly in the coastal regions.

C. EXPERIMENT 3

In this experiment, the effect of the fresh water plume of the Columbia River on the CCS is explored by incorporating monthly mean surface salinity conditions, which have been interpolated to daily values, to force the model at the mouth of the Columbia River. The Columbia River plume, which is ~5-20 m thick, has been observed to extend to ~300 km offshore, as far north as the Strait of Juan de Fuca and as far south as San Francisco (e.g., Hickey, 1998). In general, the Columbia River plume flows northward

close to the coast in the winter and offshore to the southwest in the summer (e.g., Bourke and Glenne, 1971). Fluctuations in the Columbia River plume are thought to be largely wind-driven (e.g., Hickey *et al.*, 1998). It is speculated that the wind-driven frictional currents cause the flow along the plume axis to veer to the right for northward winds or to the left of the plume axis for southward winds. As a result, the plume tends to extend farther offshore during the summer than winter (e.g., Berdeal *et al.*, 2000; Hickey *et al.*, 1998).

1. Spin-up Phase

During winter, the predominantly poleward flow carries the Columbia River plume poleward along the coast (e.g., Figure 20a). During the early part of spring, in response to the spring transition from poleward to equatorward winds, the plume begins to expand offshore (e.g. Figure 20b) as it transitions to the south from a predominantly poleward flow to a predominantly equatorward flow. By late spring, as the equatorward flow intensifies in response to the predominantly equatorward winds, the plume widens and extends farther south to ~ Cape Blanco (e.g. Figure 20c). In summer, the fresh water plume extends offshore from Cape Blanco to the south (e.g., as denoted by the 31.75 isohaline in Figure 20d). Inshore of the fresh water plume, higher salinity water, as a result of upwelling of the Southern water mass below, is present along the coast (e.g., Figure 20d).

Cross-sections of salinity and meridional velocity (e.g., Figures 21-23) are shown north of, in the vicinity of, and south of the mouth of the Columbia River to illustrate the subsurface structure of the Columbia River plume during the different seasons. During winter, when the Columbia River plume is carried poleward along the coast (e.g., Figures 21a-21d), the plume is ~30 km wide and extends to ~45 m depth (Figures 21a and 21c) inshore of the core of the poleward flow (e.g., Figures 21b and 21d). During the early part of spring, the plume widens to ~50 km and extends to ~ 50 m depth (e.g., Figure 22). By late spring, when the Columbia River plume is carried equatorward down the coast (e.g., Figures 23a and 23b), the plume expands to a width of ~75 km and extends to ~55 m depth (e.g., Figure 23a) offshore of the core of the coastal equatorward flow (e.g., Figure 23b). In summer, the plume continues southward with the equatorward flow (e.g., Figure 20d). South of Cape Blanco, the plume is pushed farther offshore by the upwelled Southern water mass (e.g., Figures 24a and 24b).

2. Quasi-equilibrium Phase

Similar to the previous two experiments, the model reaches quasi-equilibrium by year three, and shows that most features continue to be generated and maintained. The Columbia River plume tends to behave in a manner consistent with the spin-up phase results.

In winter, the Columbia River plume travels poleward inshore of the core of the poleward coastal current and extends ~30 km off the coast to ~40 m depth (e.g., Figures

25a and 25b). After the spring transition (not shown), the plume begins to move offshore down the coast with the equatorward CC. During summer, the core of the plume extends south offshore of Cape Blanco (e.g., Figure 26). A cross-section of the plume at 45° N shows the plume extending ~ 50 km from the coast (e.g., Figure 27a), while a cross-section at 42° N show the plume offshore along $\sim 125^{\circ}$ W with a width of ~ 70 km (e.g., Figure 27b).

This experiment shows that the Columbia River plays an important role in the near-surface stratification of the CCS from Washington in winter to as far south as San Francisco in summer. In particular, the Columbia River plume can extend to ~ 50 m depth and is found inshore of the poleward flow in winter and offshore of the core of the CC in summer. The offshore extent of the plume is likely due to the cross-shore Ekman flux, as suggested by Berdeal *et al.* (2000), since the plume occurs farthest offshore in late summer, coinciding with the period of strongest upwelling-favorable winds.

IV. SUMMARY

This study was designed to investigate the role of thermohaline gradients and the Columbia River plume on the CCS. A high-resolution, multi-level, PE model using a realistic coastline, was forced from rest with spatially and temporally varying climatological winds, temperatures and salinities. The Columbia River plume was input into the model by incorporating monthly mean surface salinity conditions, which have been interpolated to daily values, at the mouth of the Columbia River. Towards this end, results from three numerical experiments of increasing complexity were examined.

In Experiment 1, the western boundary of the model domain was forced with seasonal temperature and salinity conditions, which showed that the North Pacific Central water mass was an important source for warm surface waters into the CCS region. The results also showed features found in a classical eastern boundary current system such as an offshore surface equatorward meandering current, a surface equatorward coastal jet, a surface poleward coastal current, a poleward undercurrent, upwelling, a temperature front, meanders, eddies, and filaments.

In Experiment 2, seasonal temperature and salinity forcing were added to the northern and southern boundaries of the model domain. Model results showed that the Southern water mass was also an important source for the input of warm surface waters into the CCS region. The Southern (Pacific sub-Arctic) water mass was an important source of high (low) salinity water into the southern (northern) coastal regions of the model domain.

In Experiment 3, the Columbia River plume, the only large river plume off the west coast of the U.S., was added. Model results showed that the Columbia River plume exhibited a strong seasonal signal. During winter, the plume traveled poleward along the coast. In spring, the plume expanded off the coast as it transitioned from a predominantly poleward flow to a predominantly equatorward flow. By the end of summer, the plume traveled equatorward and offshore with the CC. The plume was found to be mainly a surface feature extending to ~50 m depth during all seasons.

These experiments illustrate the important roles that thermohaline gradients and the Columbia River plume play in the CCS. The thermohaline gradients help to maintain more realistic temperatures and salinities throughout the water column. The Columbia River has a significant impact on both the near-surface stratification and baroclinic structure of the velocity field of the CCS. The influences of the Columbia River plume can extend from the coast of Washington in winter to as far south as San Francisco in summer.

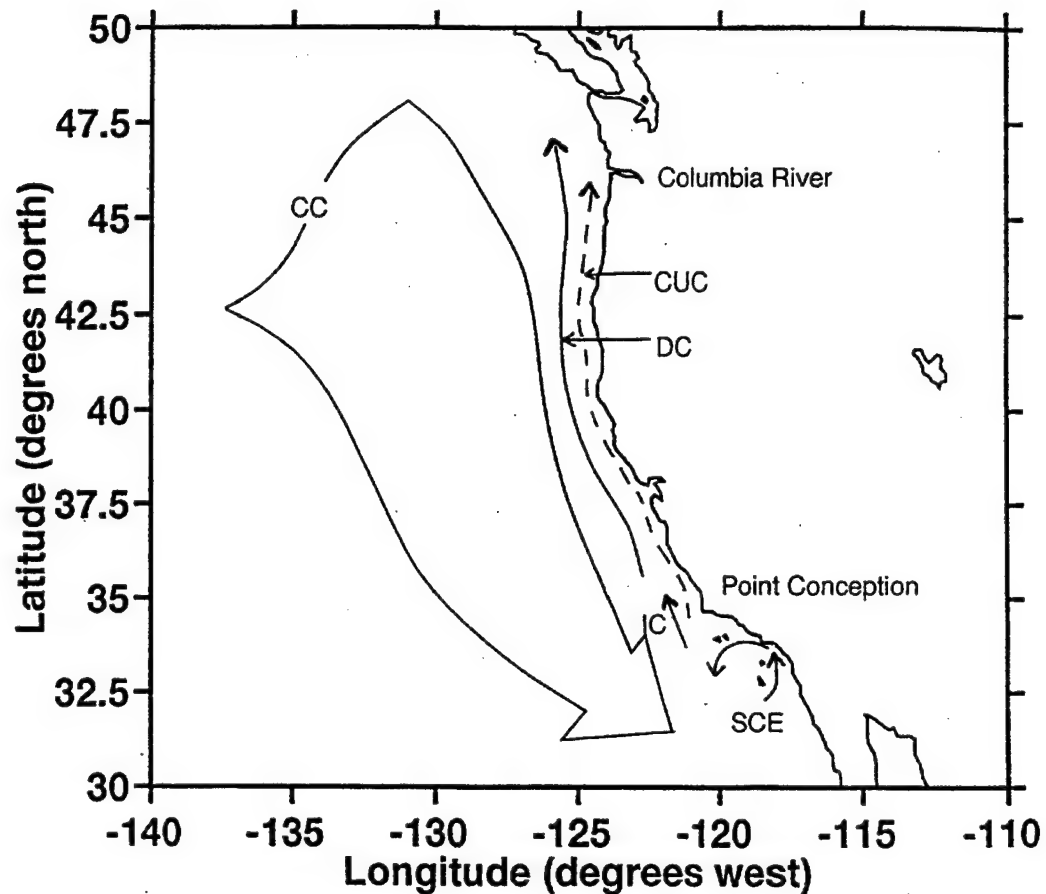
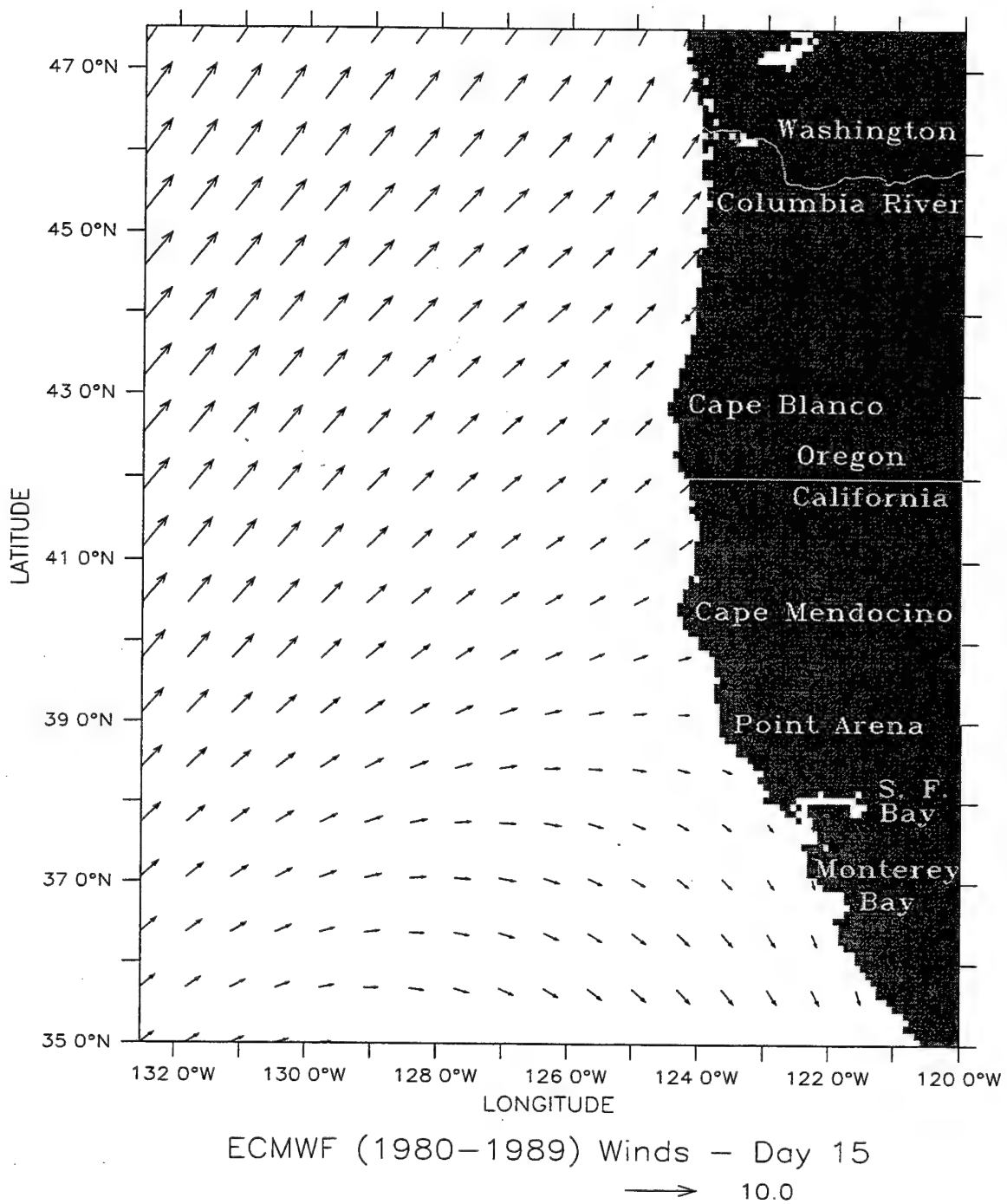
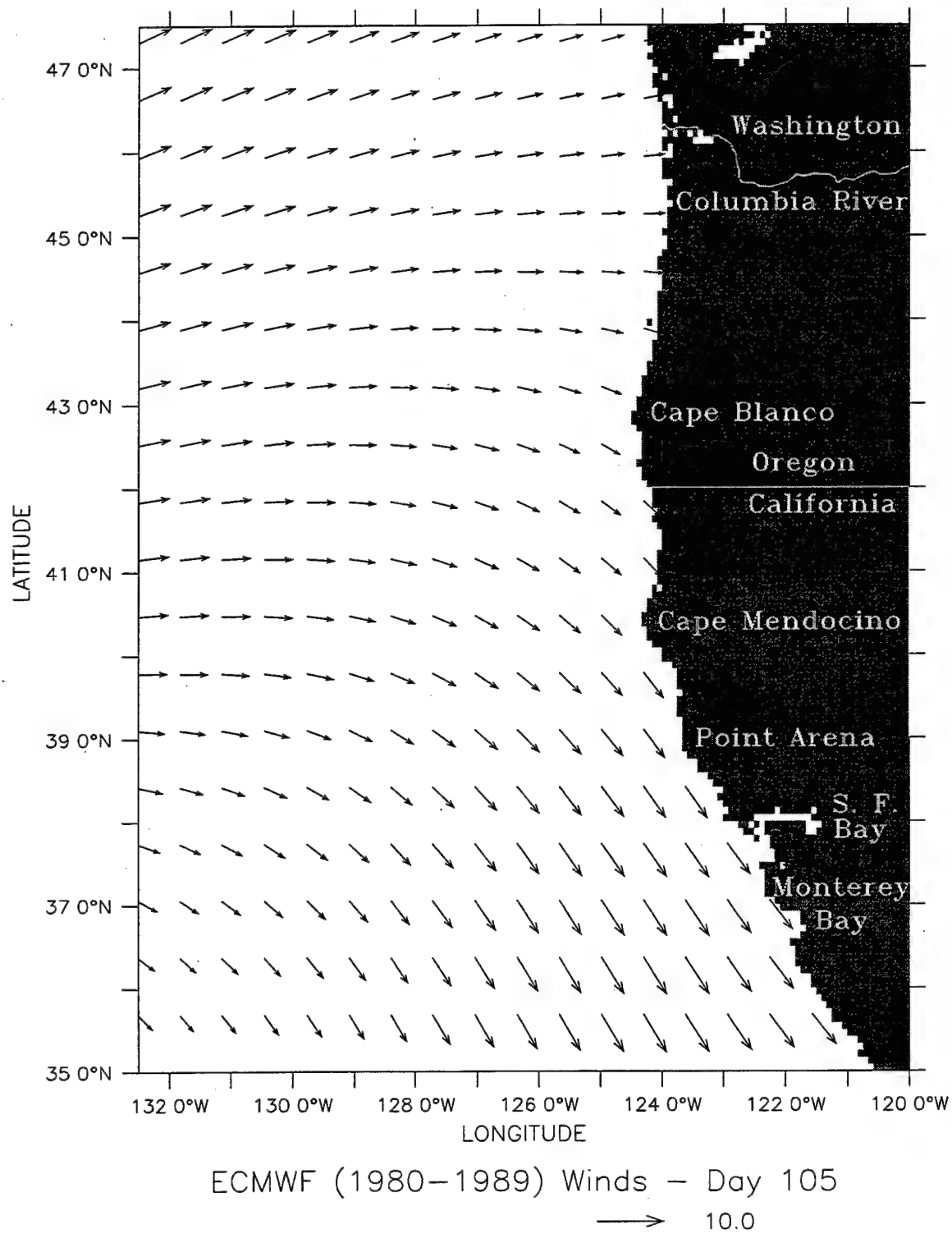


Figure 1. Generalized classical circulation of the California Current System (CCS). The broad, slow surface equatorward California Current (CC) overlies the narrow, poleward California Undercurrent (CUC), along with the Inshore Countercurrent (IC), known as the Davidson Current (DC) north of Point Conception and as the Southern California Eddy (SCE) south of Point Conception.



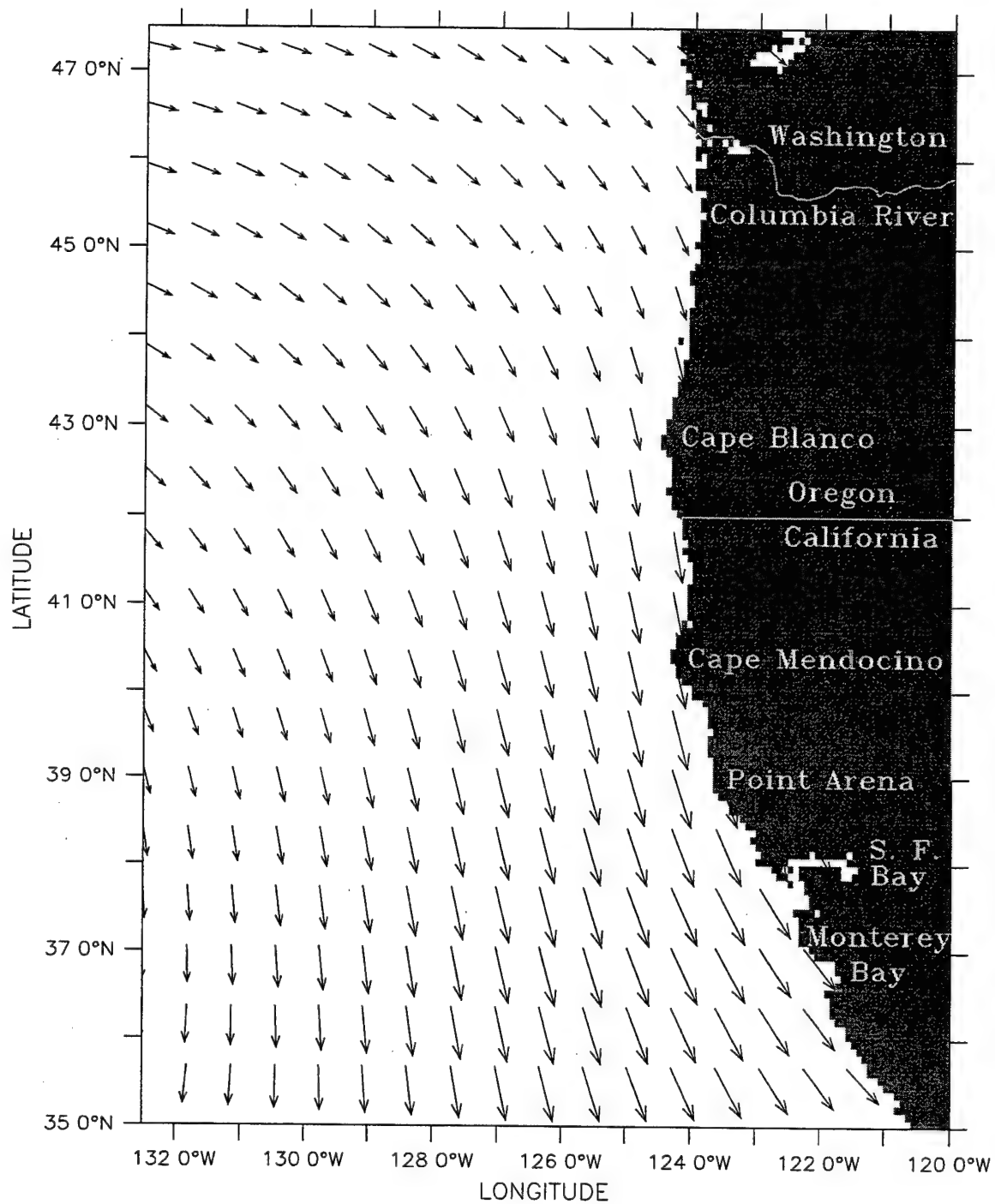
(a)

Figure 2. Domain and climatological winds of the model for the California Current System (CCS) off the Western United States. The domain of the model is bounded by 35.0° N to 47.5° N, 120.0° W to 132.5° W. The climatological (1980-1989) ECMWF winds used in Experiments 1, 2, and 3 in m/s are shown here for (a) January, (b) April, (c) July, and (d) October. Maximum wind vector is 10 m/s.



(b)

Figure 2 continued.

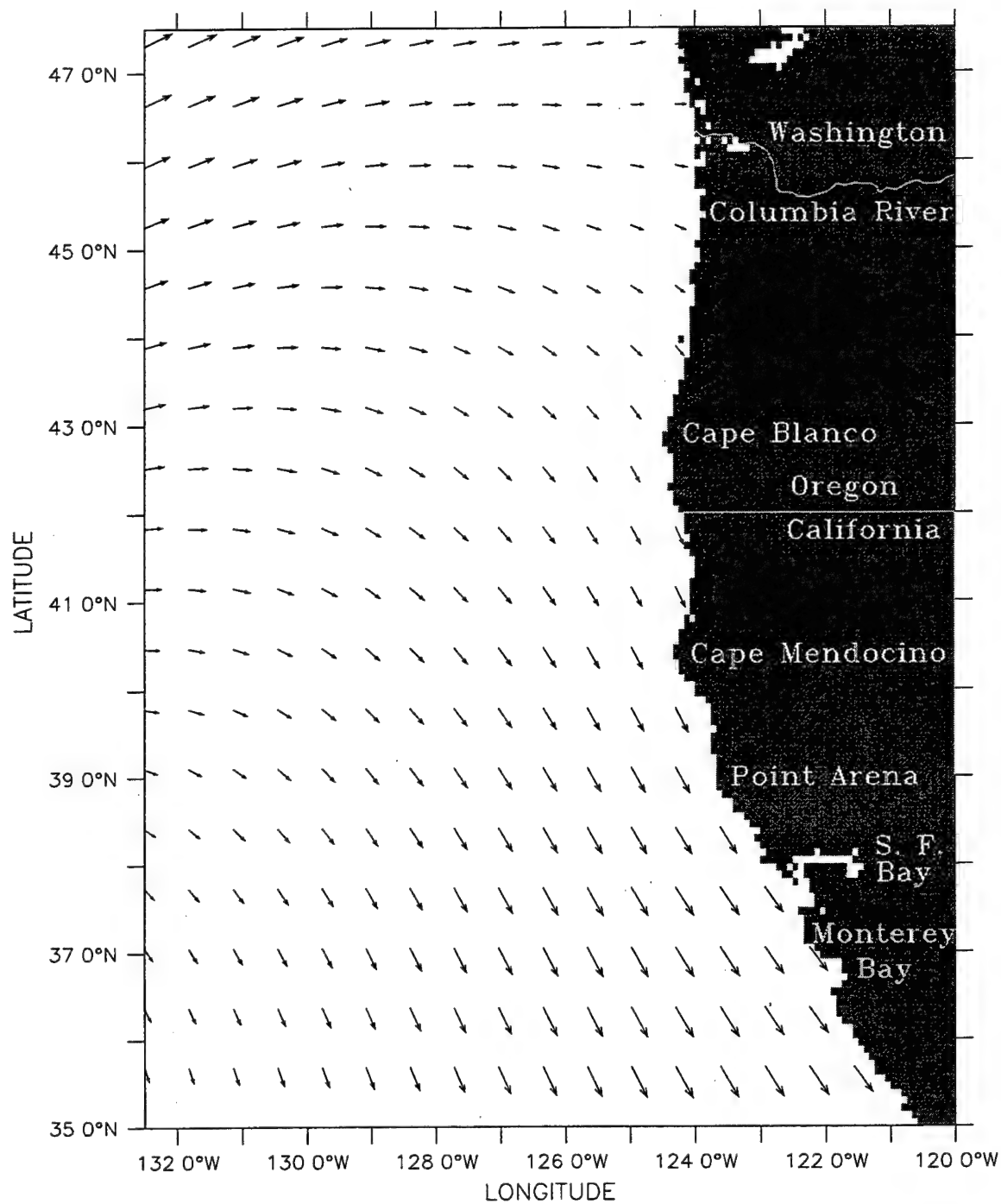


ECMWF (1980-1989) Winds — Day 195

→ 10.0

(c)

Figure 2 continued.

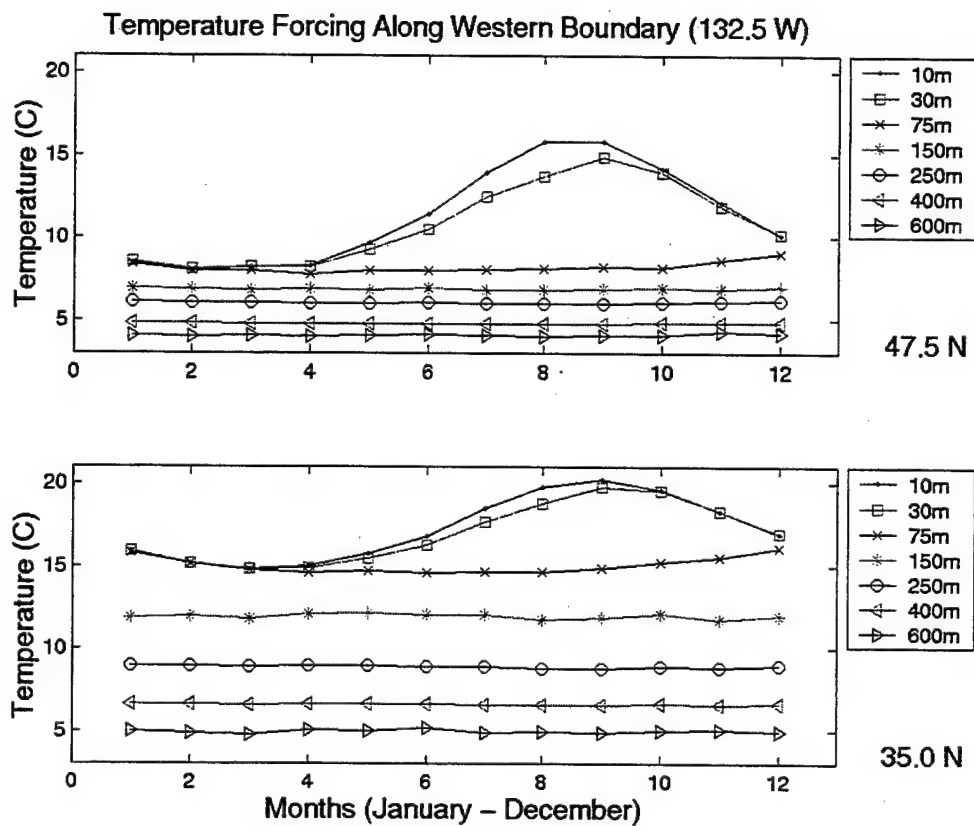


ECMWF (1980-1989) Winds - Day 285

→ 10.0

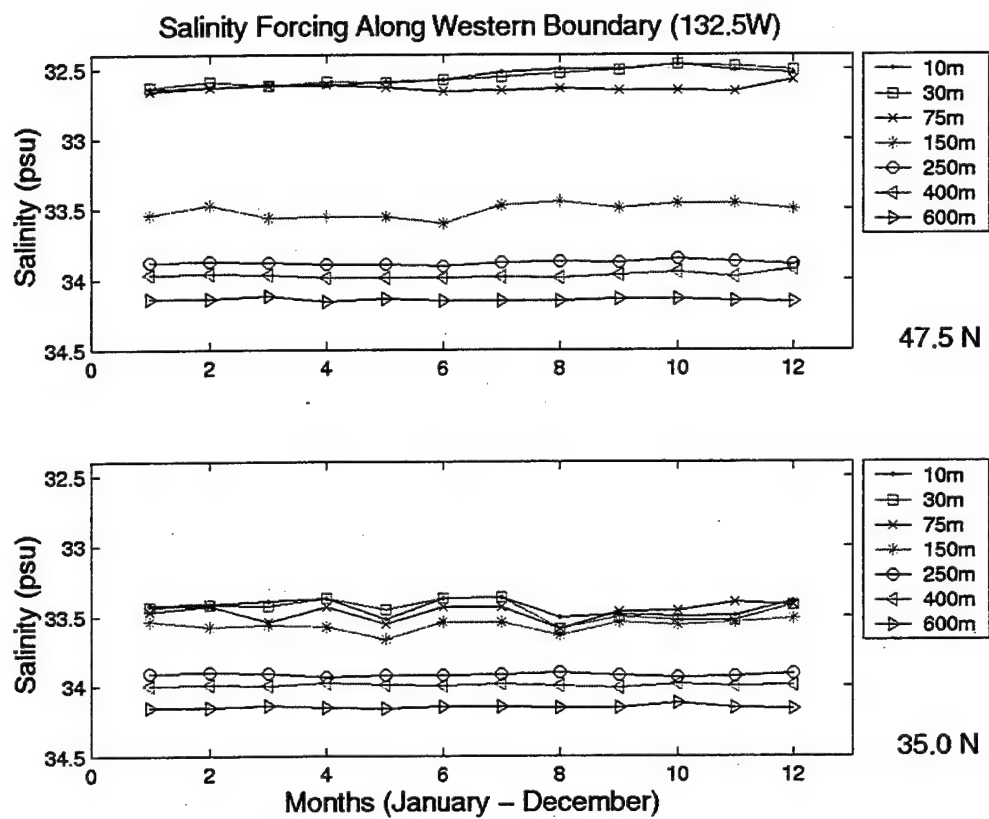
(d)

Figure 2 continued.



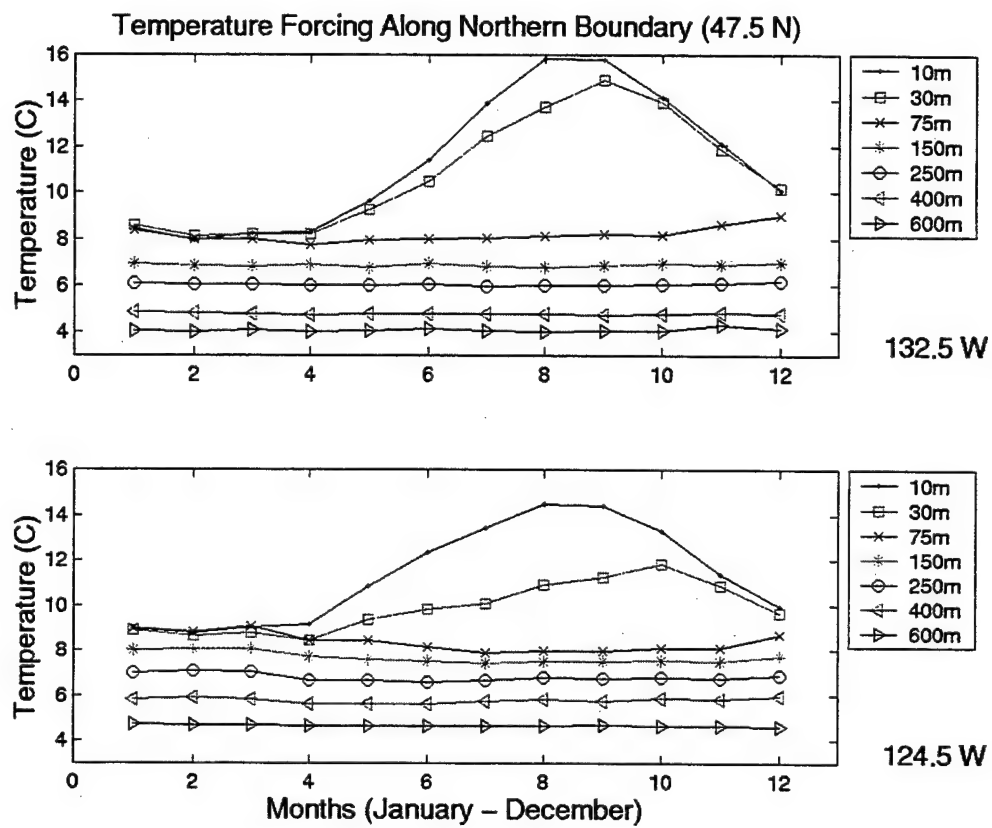
(a)

Figure 3. Plots of Levitus climatological fields used as seasonal forcing along the western boundary (132.5 W) for: (a) temperature and (b) salinity.



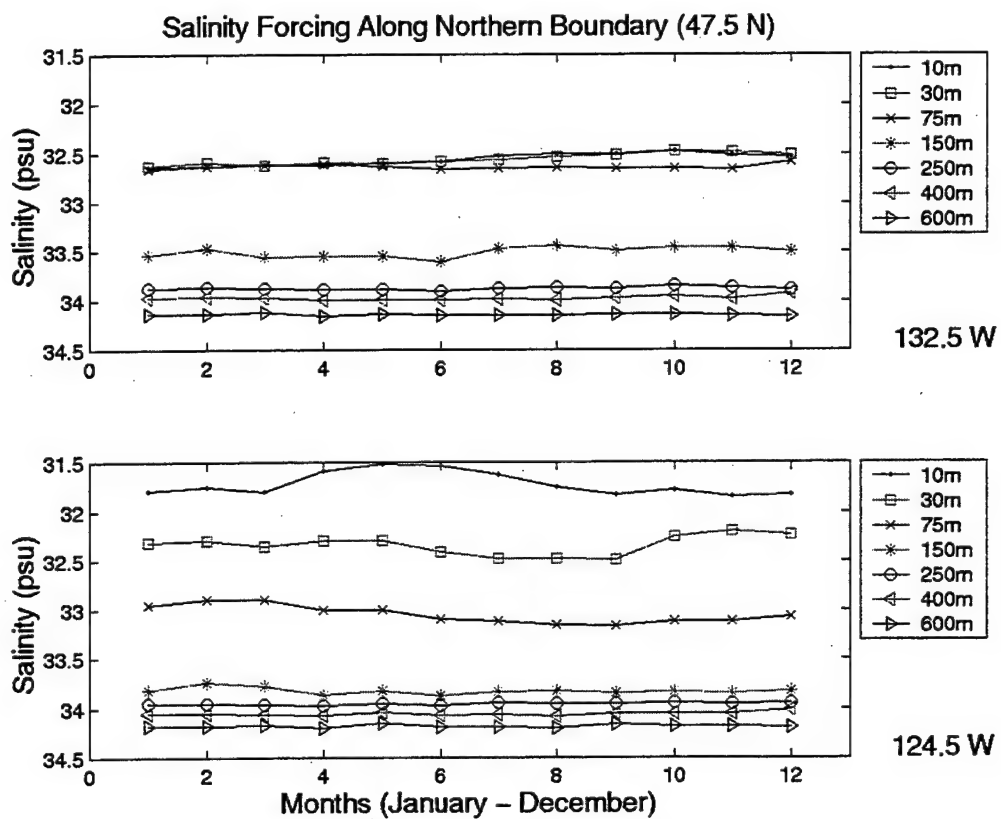
(b)

Figure 3 continued.



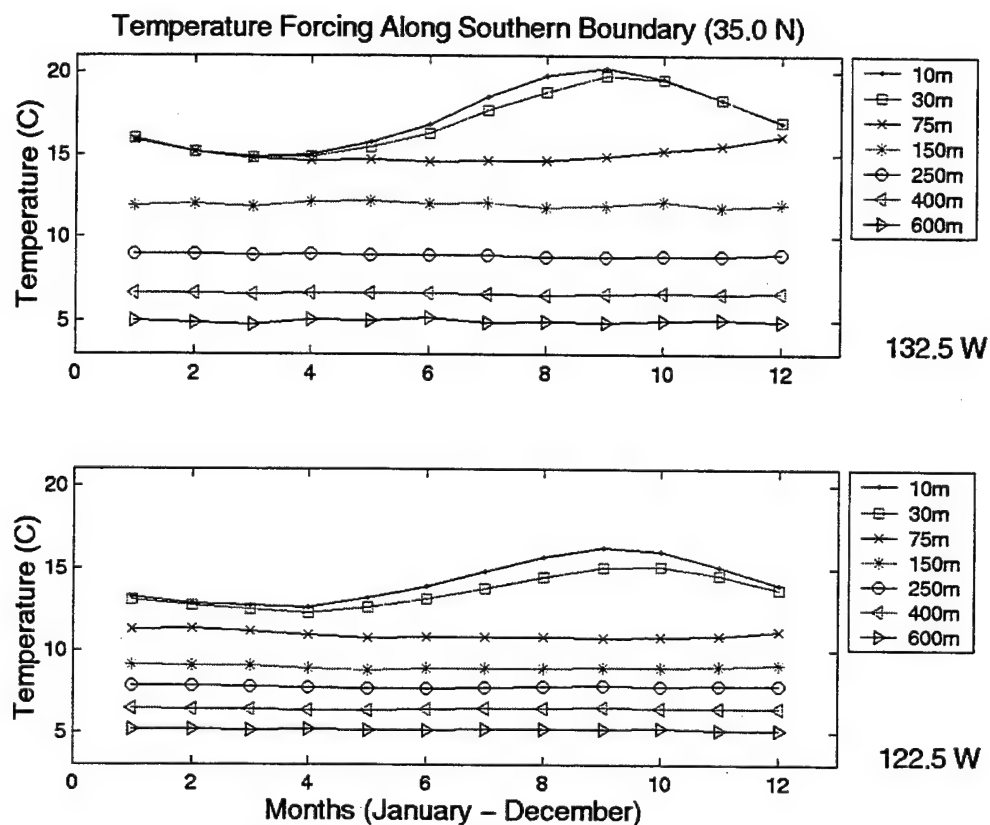
(a)

Figure 4. Plots of Levitus climatological fields used as seasonal forcing along the northern boundary (47.5 N) for: (a) temperature and (b) salinity.



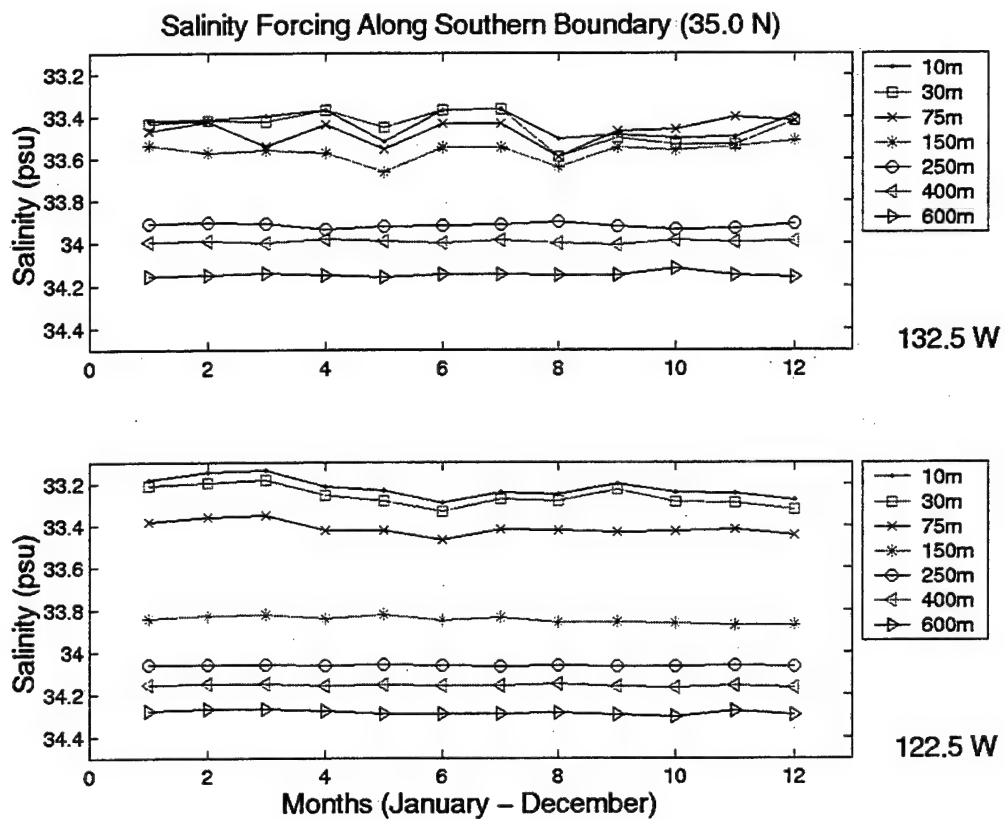
(b)

Figure 4 continued.



(a)

Figure 5. Plots of Levitus climatological fields used as seasonal forcing along the southern boundary (35.0 N) for: (a) temperature and (b) salinity.



(b)

Figure 5 continued.

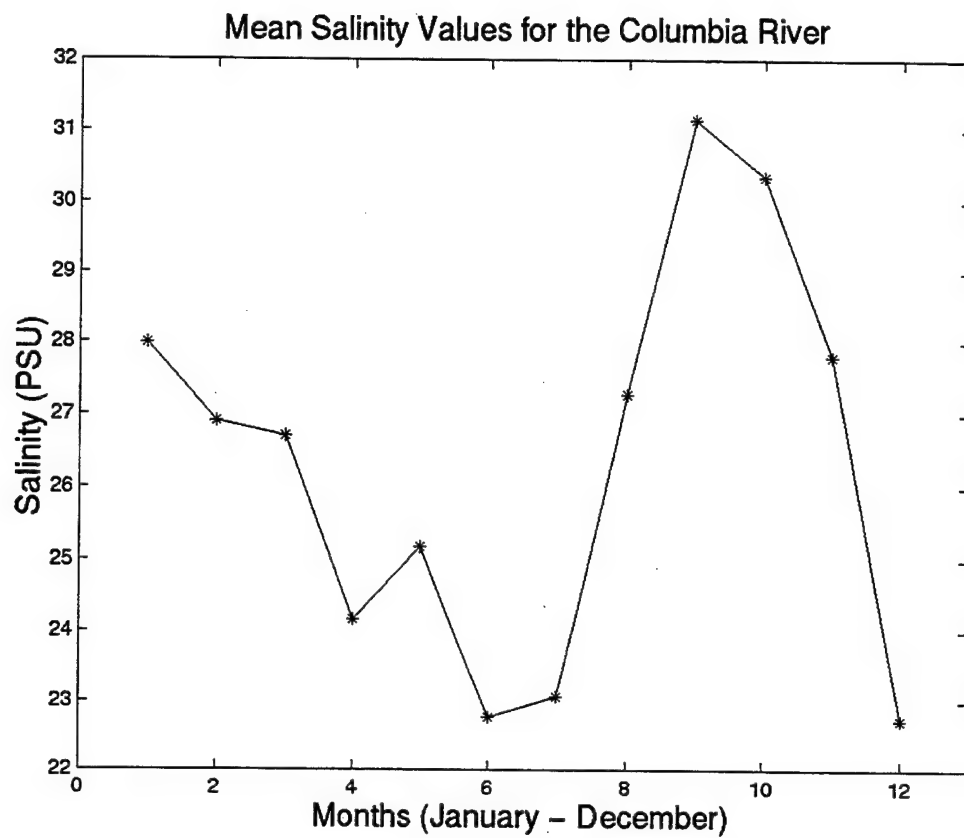
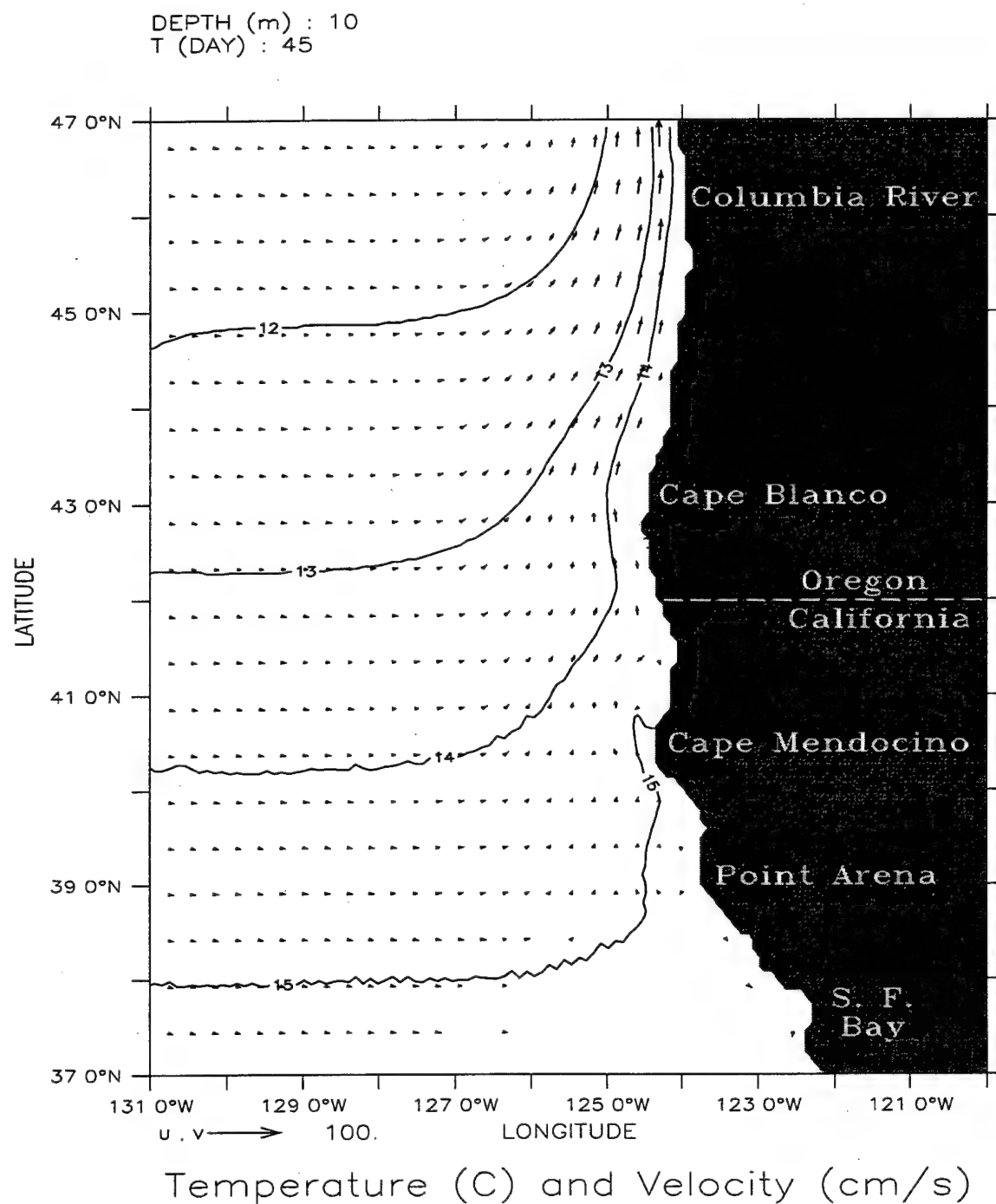


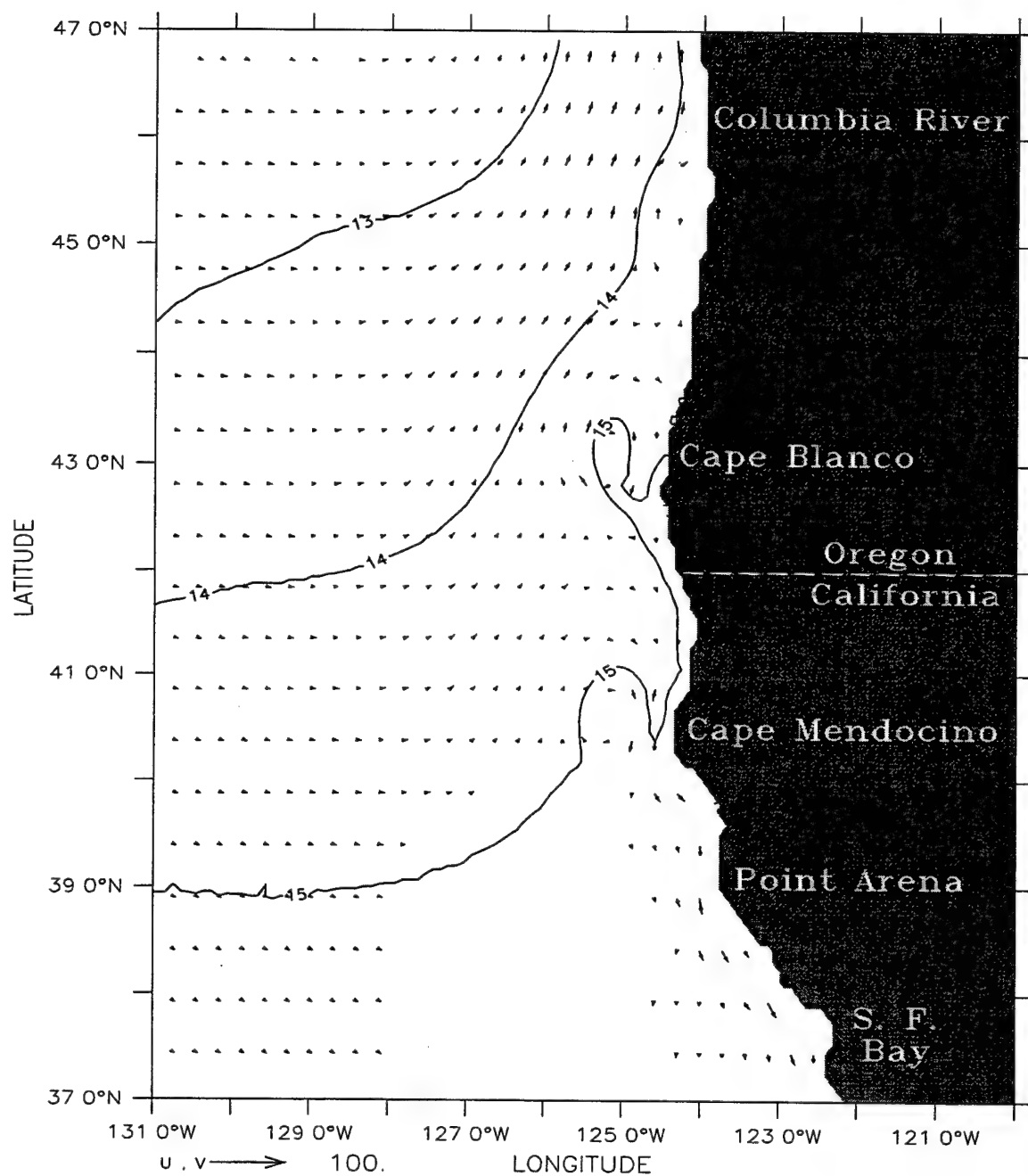
Figure 6. Monthly mean surface salinity conditions recorded at the Columbia River Lightship (46.2 N, 124.2 W), located at the mouth of the Columbia River (Bourke and Glenne, 1971).



(a)

Figure 7. Temperature contours and velocity vectors at 10 m depth for Experiment 1 at days (a) 45, (b) 84, (c) 123, (d) 237, and (e) 270. In all velocity fields presented, to avoid clutter, velocity vectors are plotted every third (fifth) grid point in the cross-shore (alongshore) direction. Contour interval is 1° C; maximum velocity vector is 100 cm/s.

DEPTH (m) : 10
T (DAY) : 84

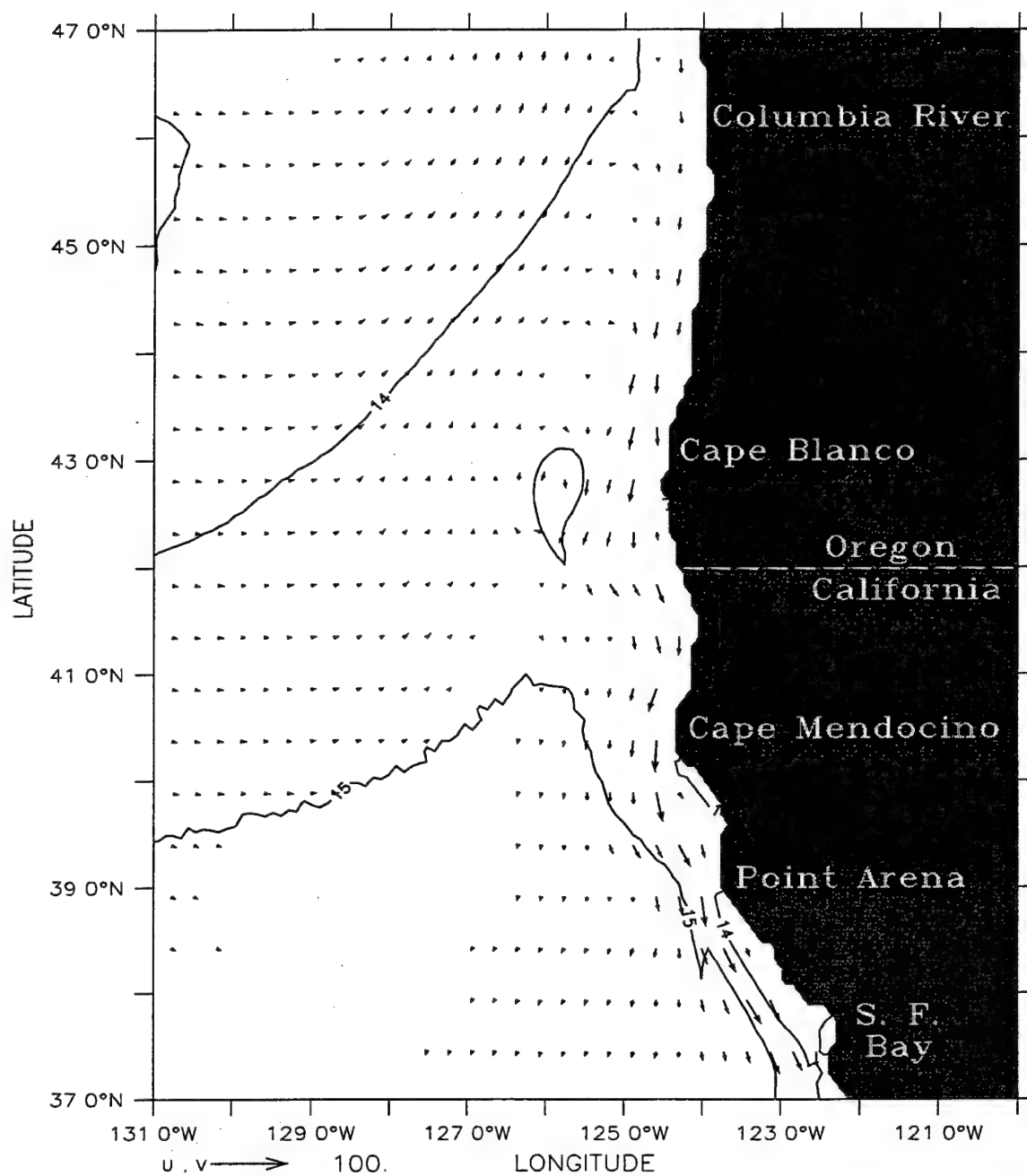


Temperature (C) and Velocity (cm/s)

(b)

Figure 7 continued.

DEPTH (m) : 10
T (DAY) : 123

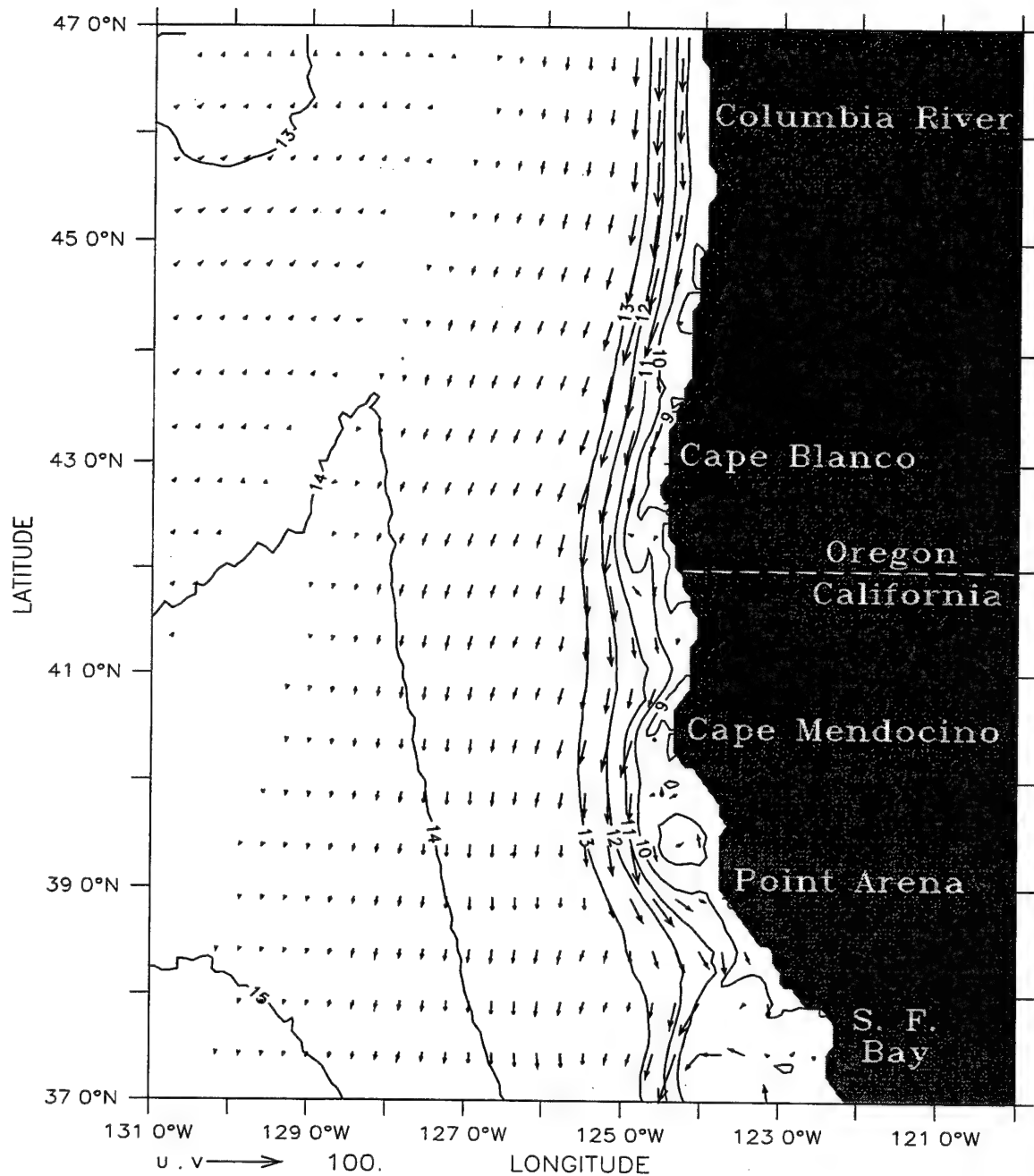


Temperature (C) and Velocity (cm/s)

(c)

Figure 7 continued.

DEPTH (m) : 10
T (DAY) : 237

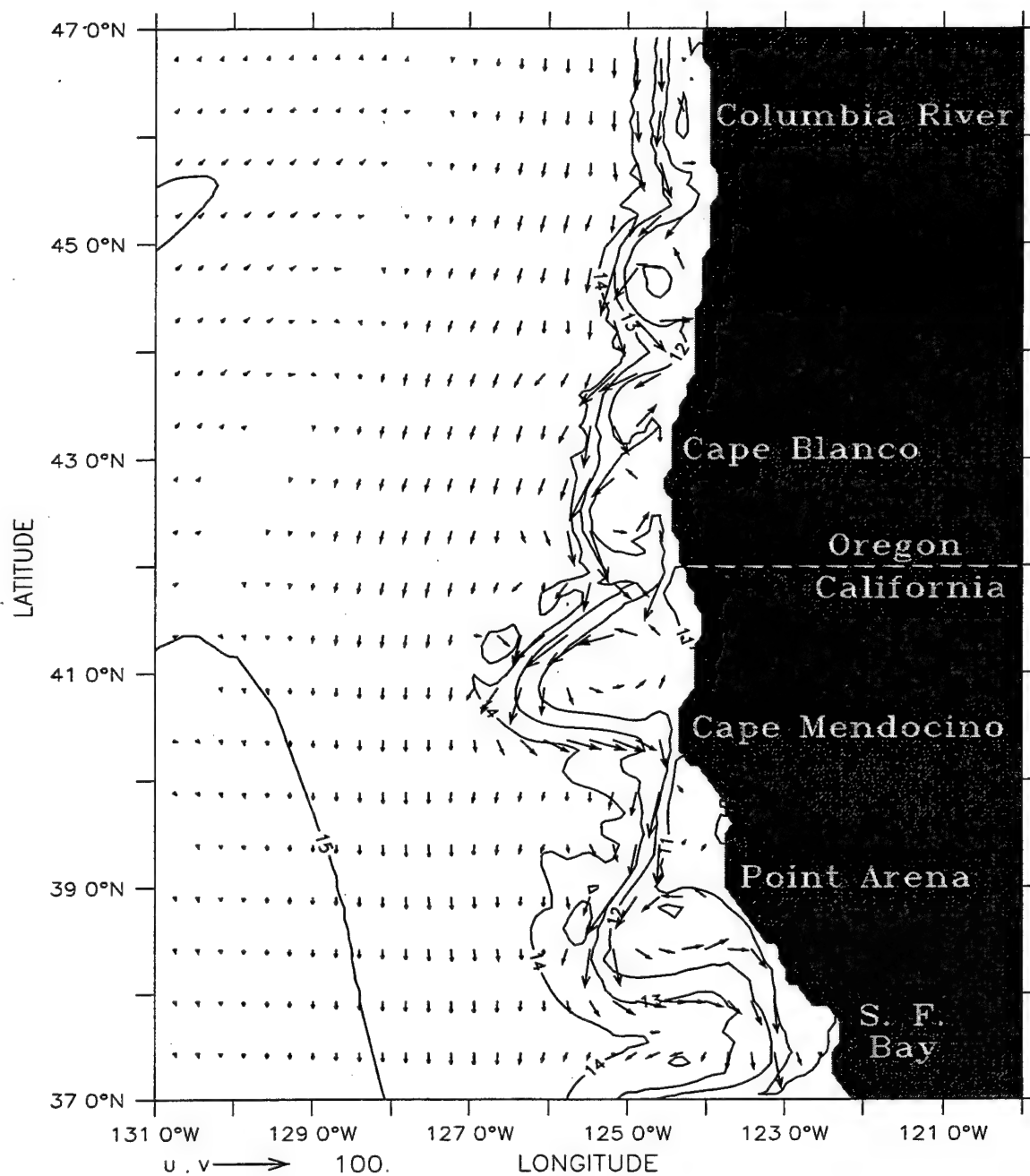


Temperature (C) and Velocity (cm/s)

(d)

Figure 7 continued.

DEPTH (m) : 10
T (DAY) : 270

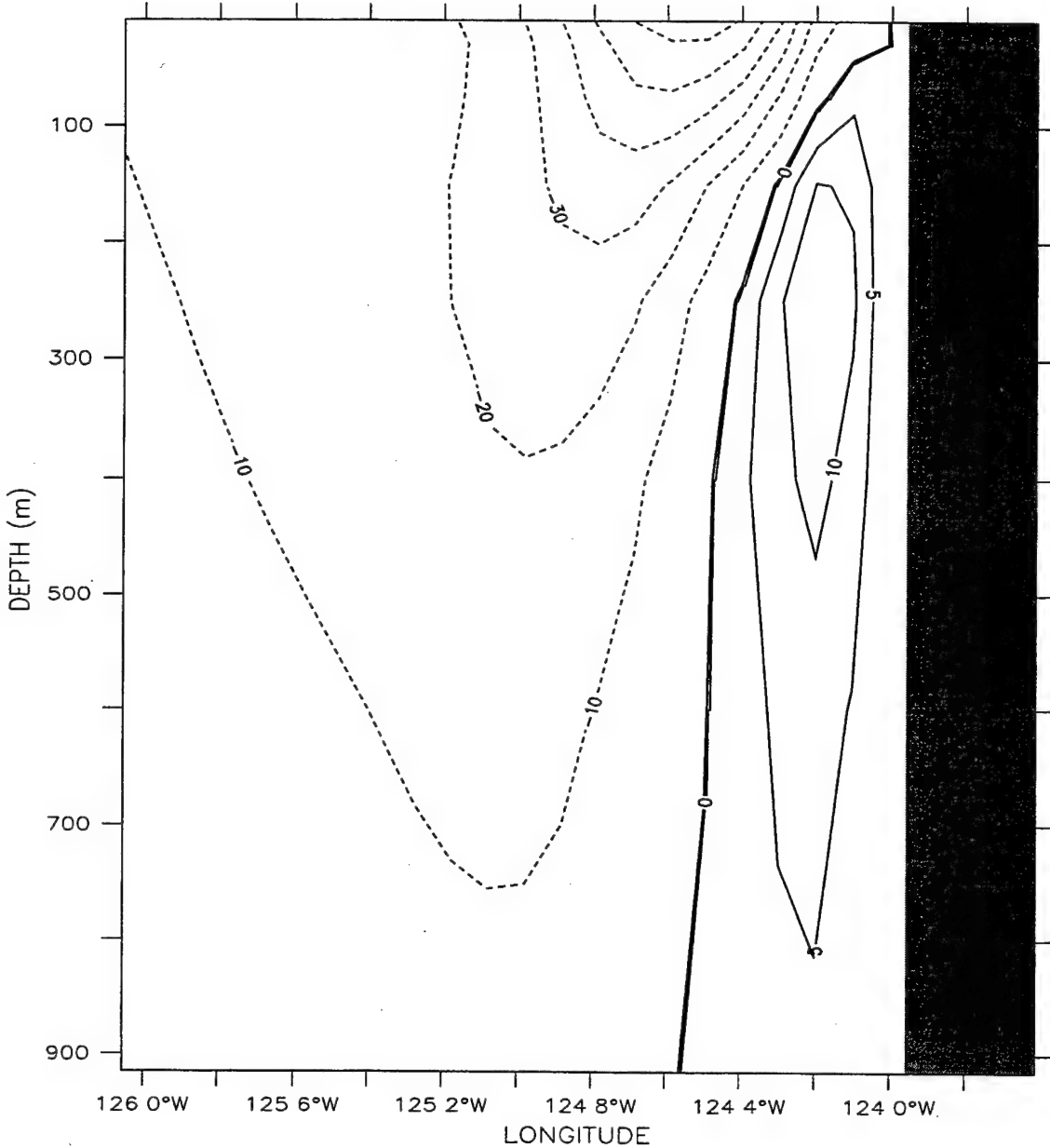


Temperature (C) and Velocity (cm/s)

(e)

Figure 7 continued.

T (DAY) : 237

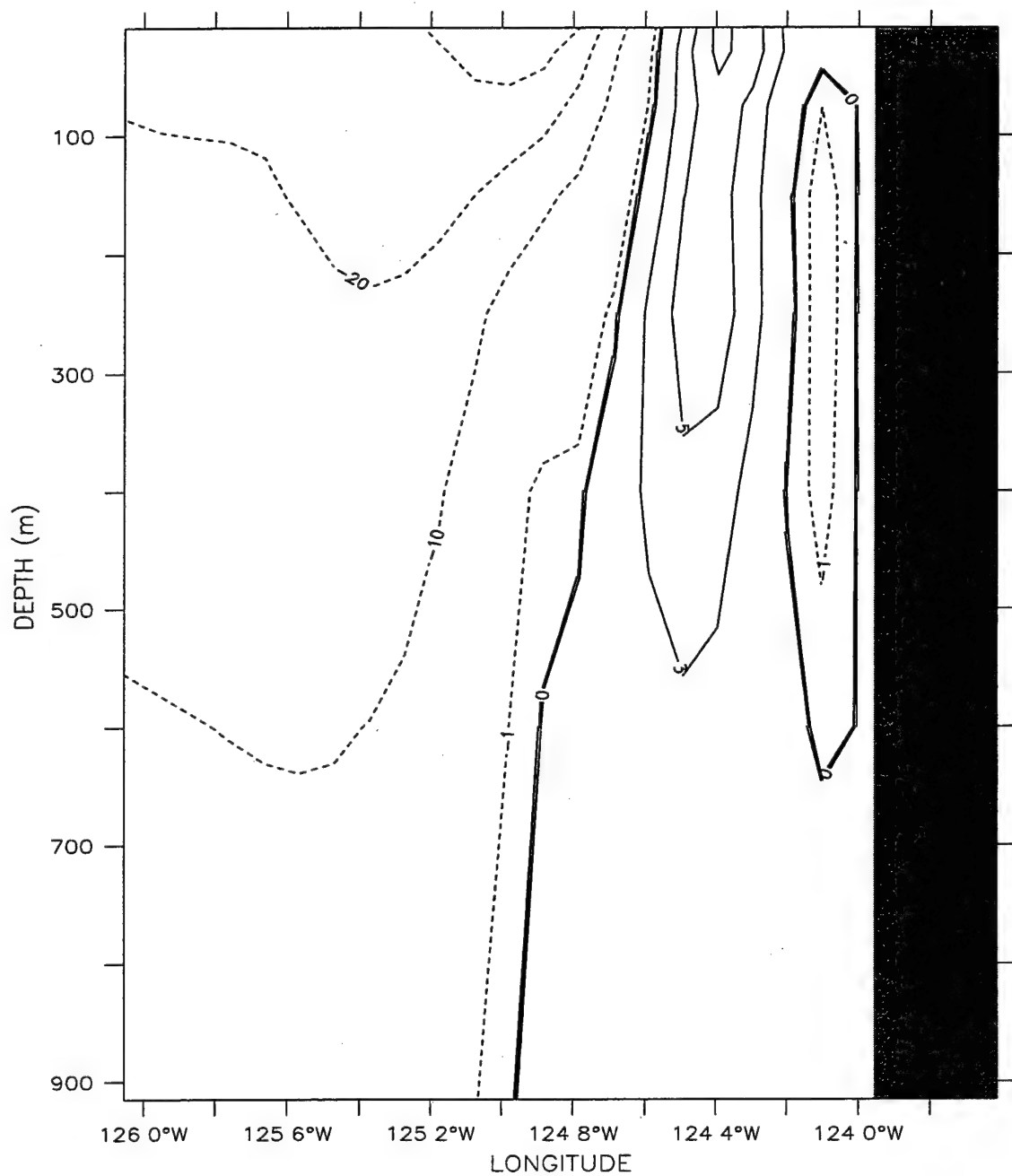


Meridional Velocity (cm/s)

(a)

Figure 8. Cross-shore section of meridional velocity (v) at 46° N for Experiment 1 at days (a) 237 and (b) 321. In (a), contour interval is 5 cm/s (10 cm/s) for poleward (equatorward) flow. In (b), contour interval for velocities greater than (less than) 5 cm/s is 10 cm/s (2 cm/s).

LATITUDE : 46N
T (DAY) : 321

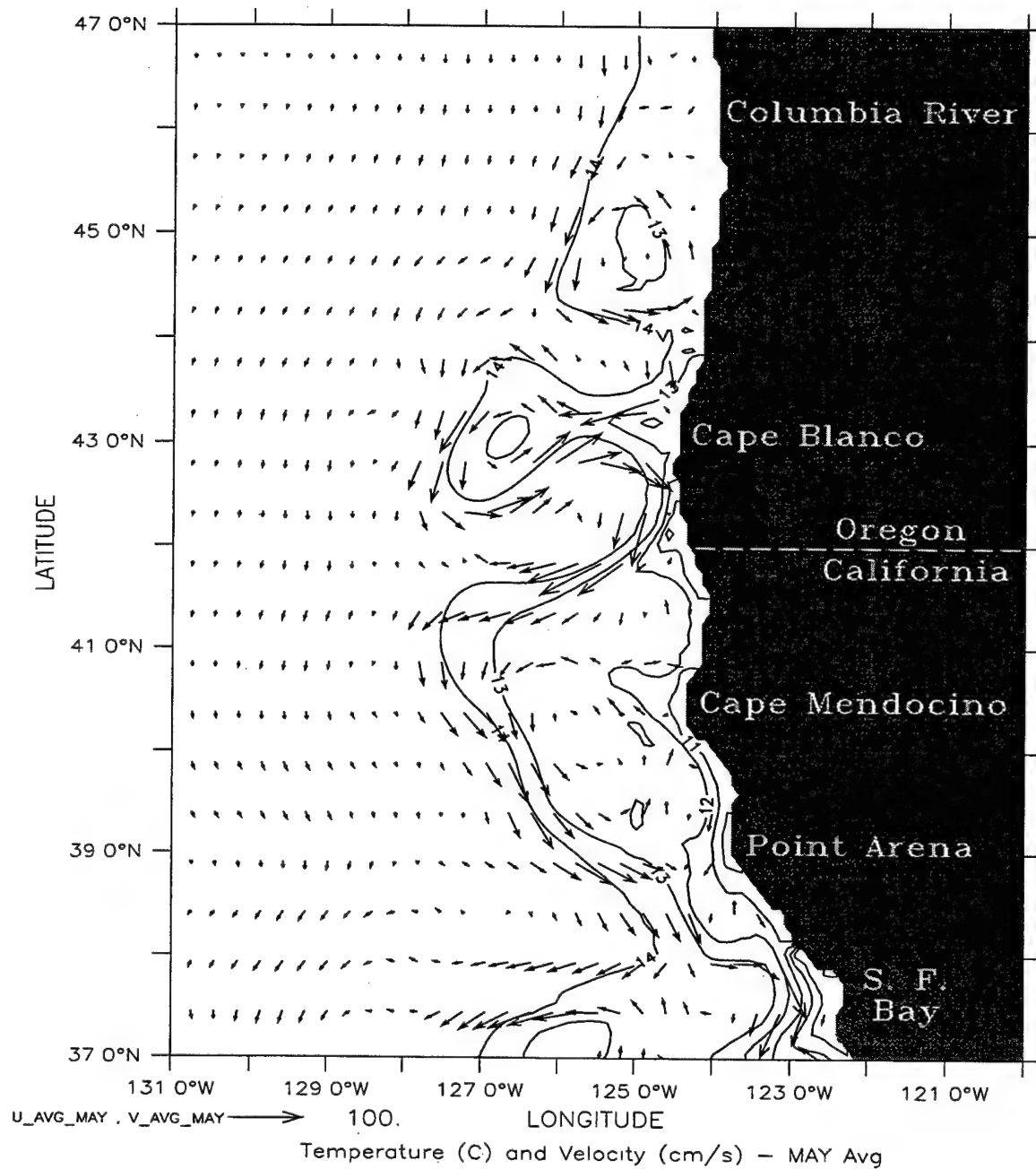


Meridional Velocity (cm/s)

(b)

Figure 8 continued.

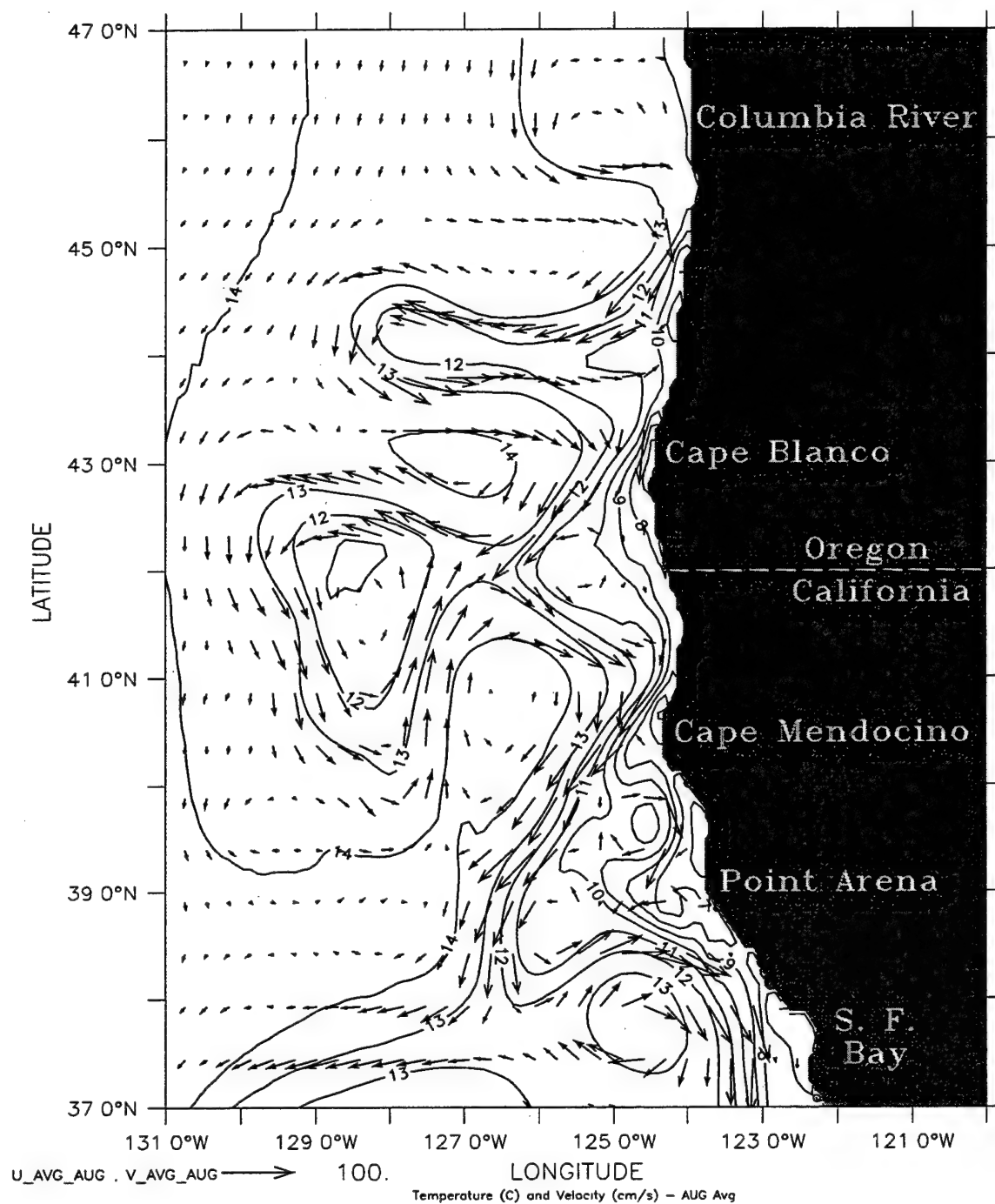
DEPTH (m) : 10
T (DAY) : 850.5 to 880.5



(a)

Figure 9. Temperature contours and velocity vectors at 10 m depth for Experiment 1 in the third year of model simulation, time-averaged over the months of (a) May, (b) August, and (c) December. Contour interval is 1° C; maximum velocity vector is 100 cm/s.

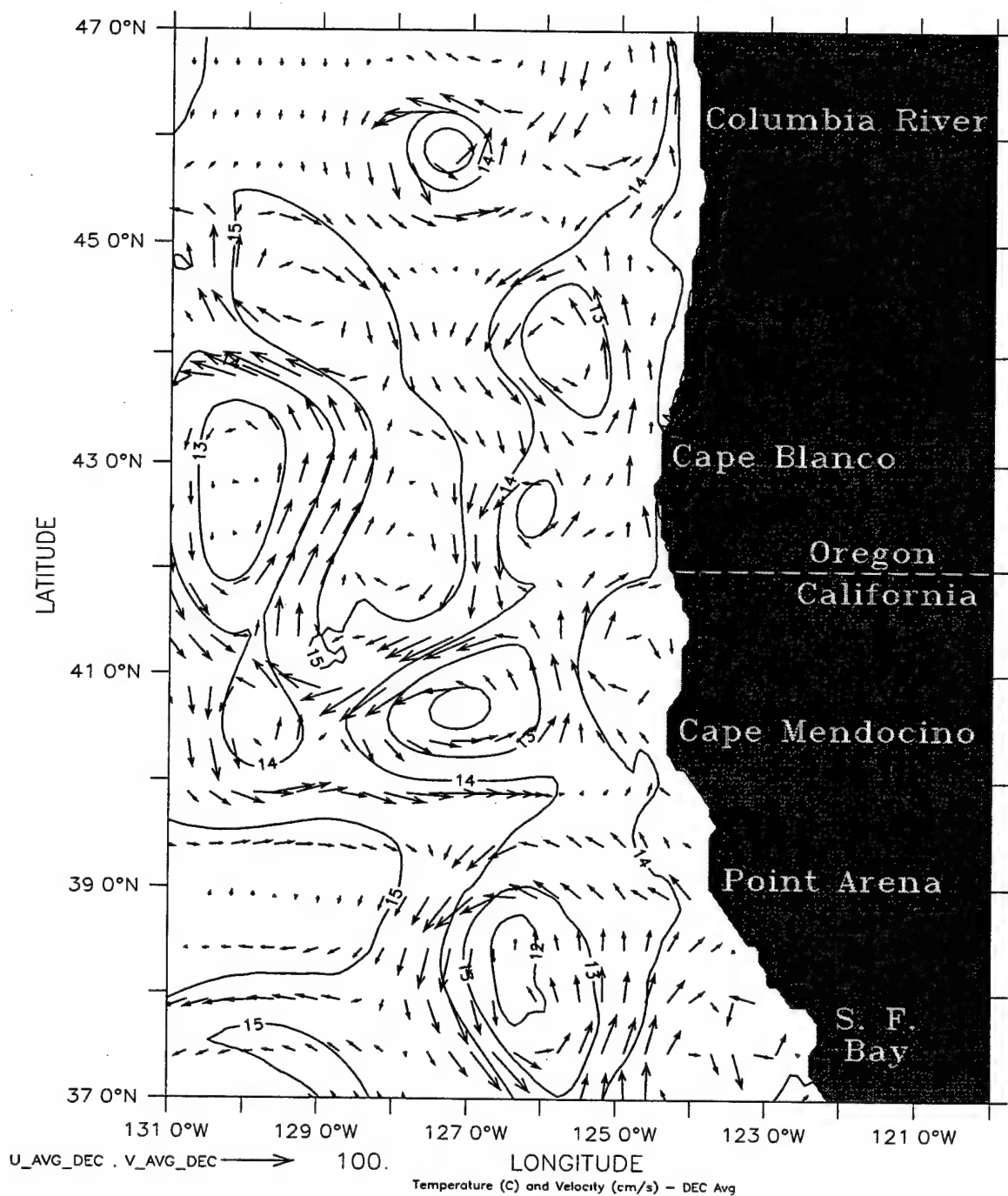
DEPTH (m) : 10
T (DAY) : 940.5 to 970.5



(b)

Figure 9 continued.

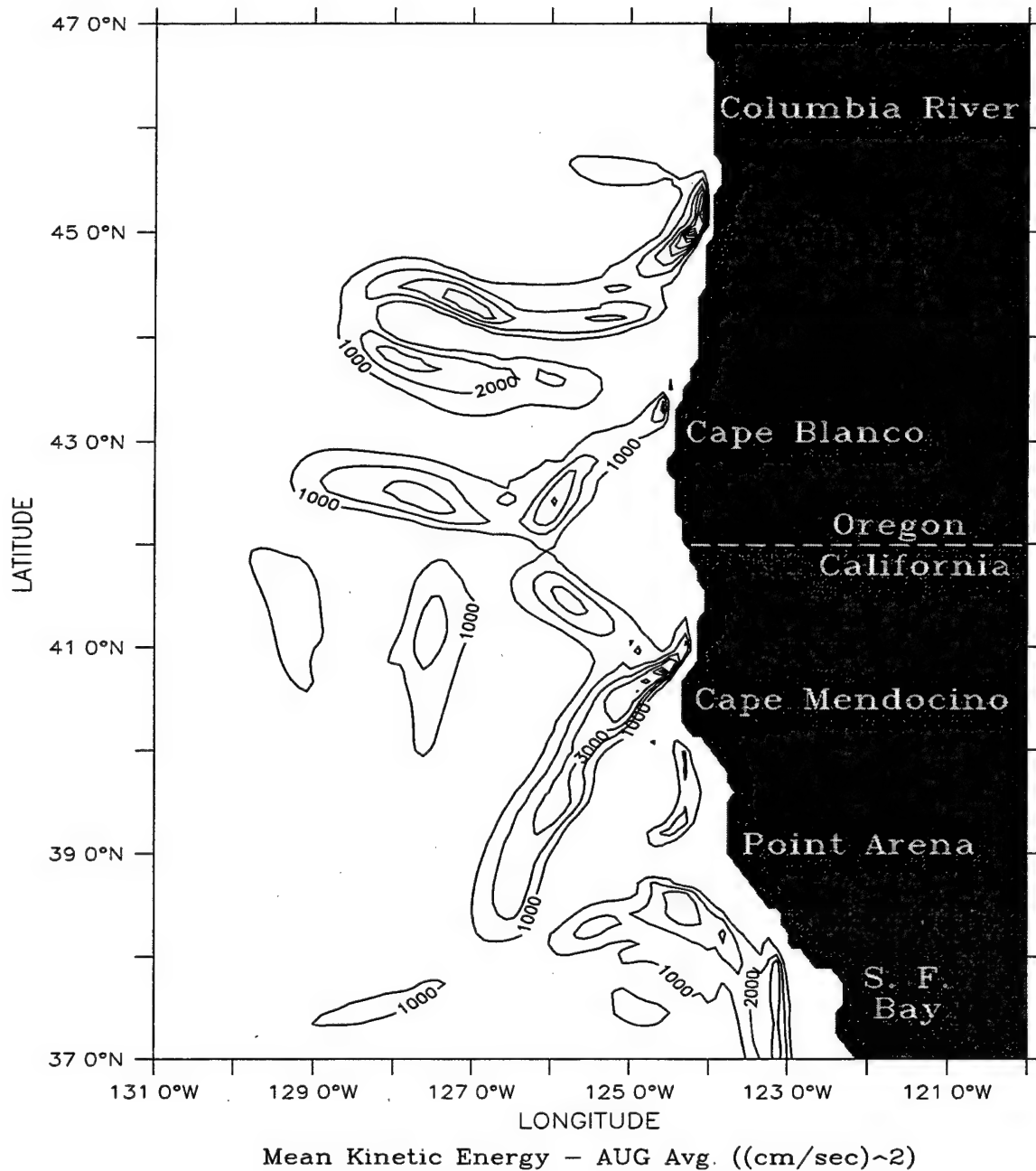
DEPTH (m) : 10
T (DAY) : 1060.5 to 1090.5



(c)

Figure 9 continued.

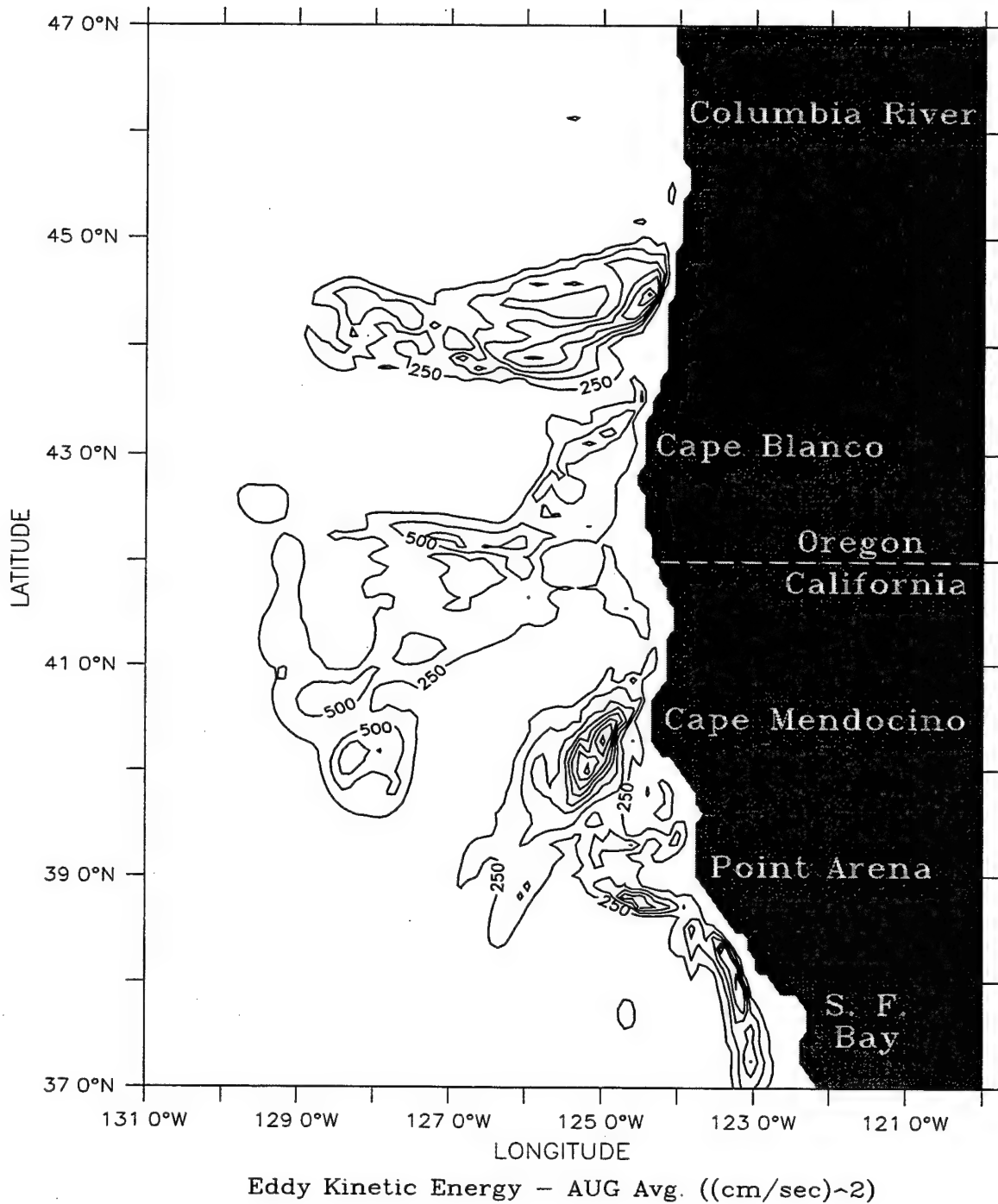
DEPTH (m) : 10
T (DAY) : 940.5 to 970.5



(a)

Figure 10. Horizontal maps at 10 m depth of (a) mean kinetic energy (MKE), and (b) eddy kinetic energy (EKE) for Experiment 1 in the third year of model simulation, time-averaged for the month of August. Contour interval is 1000 (cm/s)² for (a), and 250 (cm/s)² for (b).

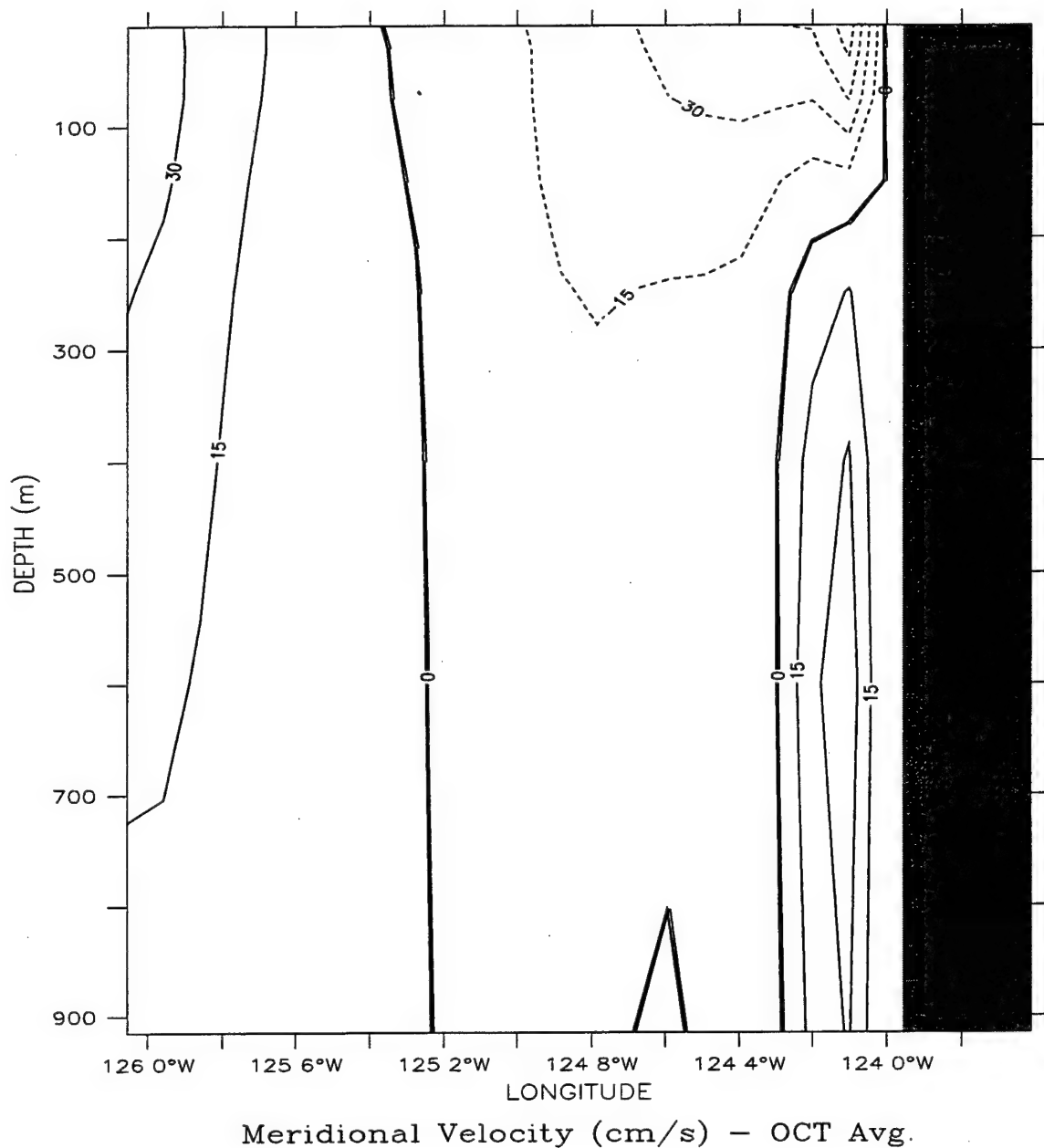
DEPTH (m) : 10
T (DAY) : 940.5 to 970.5



(b)

Figure 10 continued.

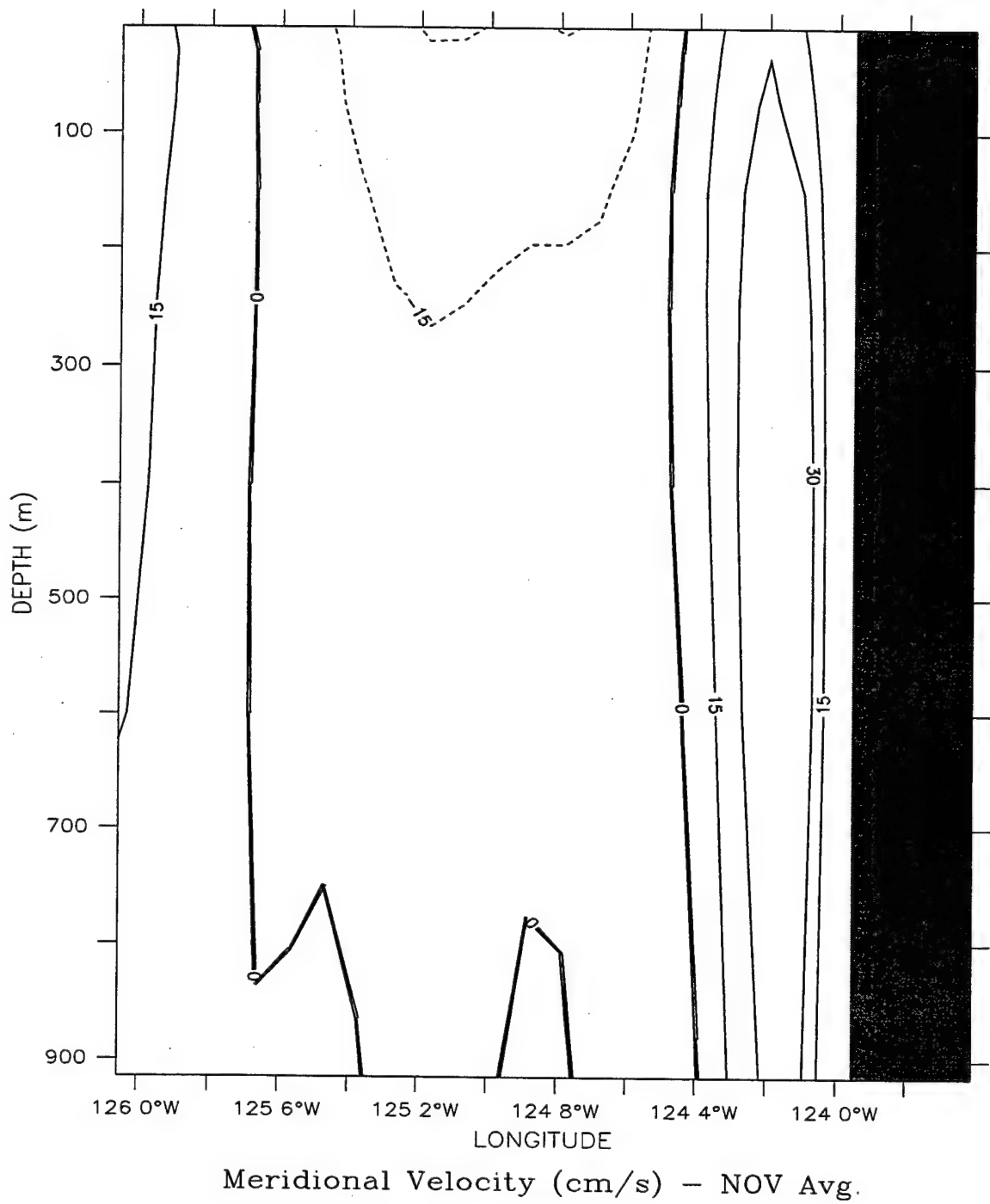
LATITUDE : 46N
T (DAY) : 1000.5 to 1030.5



(a)

Figure 11. Cross-shore section of meridional velocity (v) at 46° N for Experiment 1 in the third year of model simulation time-averaged for the months of (a) October, (b) November, and (c) December. Contour interval is 15 cm/s. The 30 cm/s contour for the coastal, poleward flow shows shoaling of the CUC from October (a) – December (c).

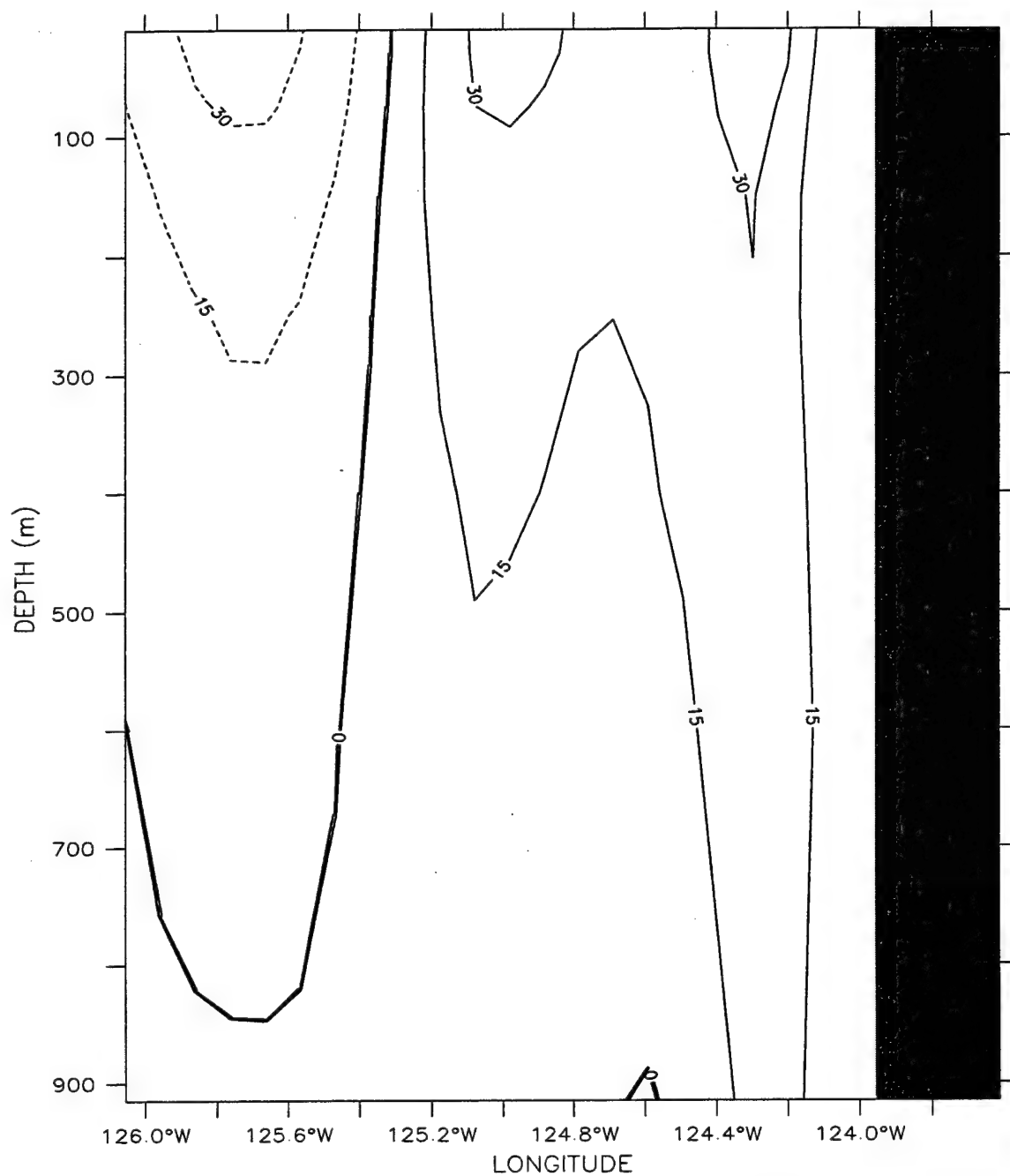
LATITUDE : 46N
T (DAY) : 1030.5 to 1060.5



(b)

Figure 11 continued.

LATITUDE : 46N
T (DAY) : 1060.5 to 1090.5



Meridional Velocity (cm/s) - DEC Avg.

(c)

Figure 11 continued.

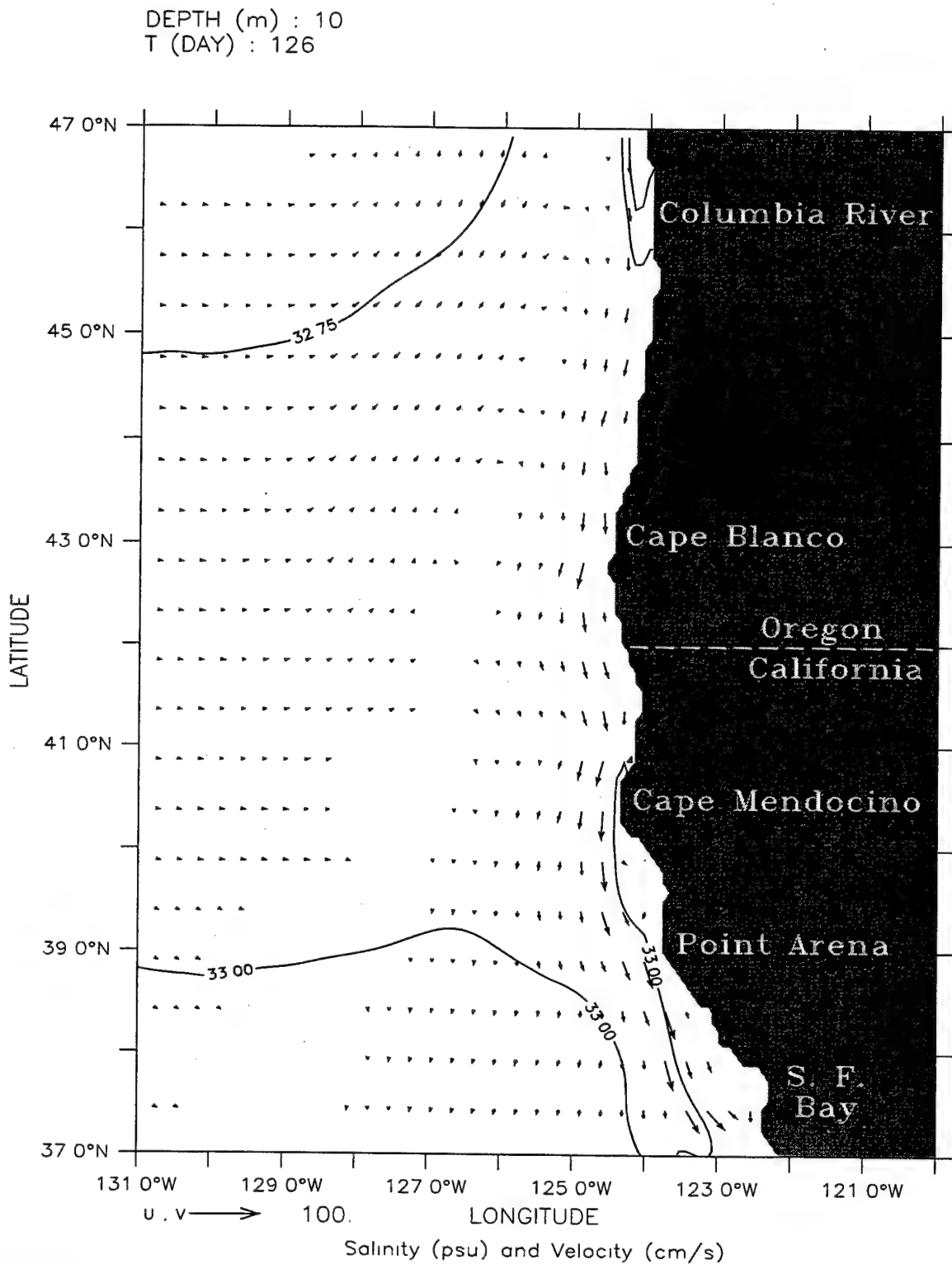
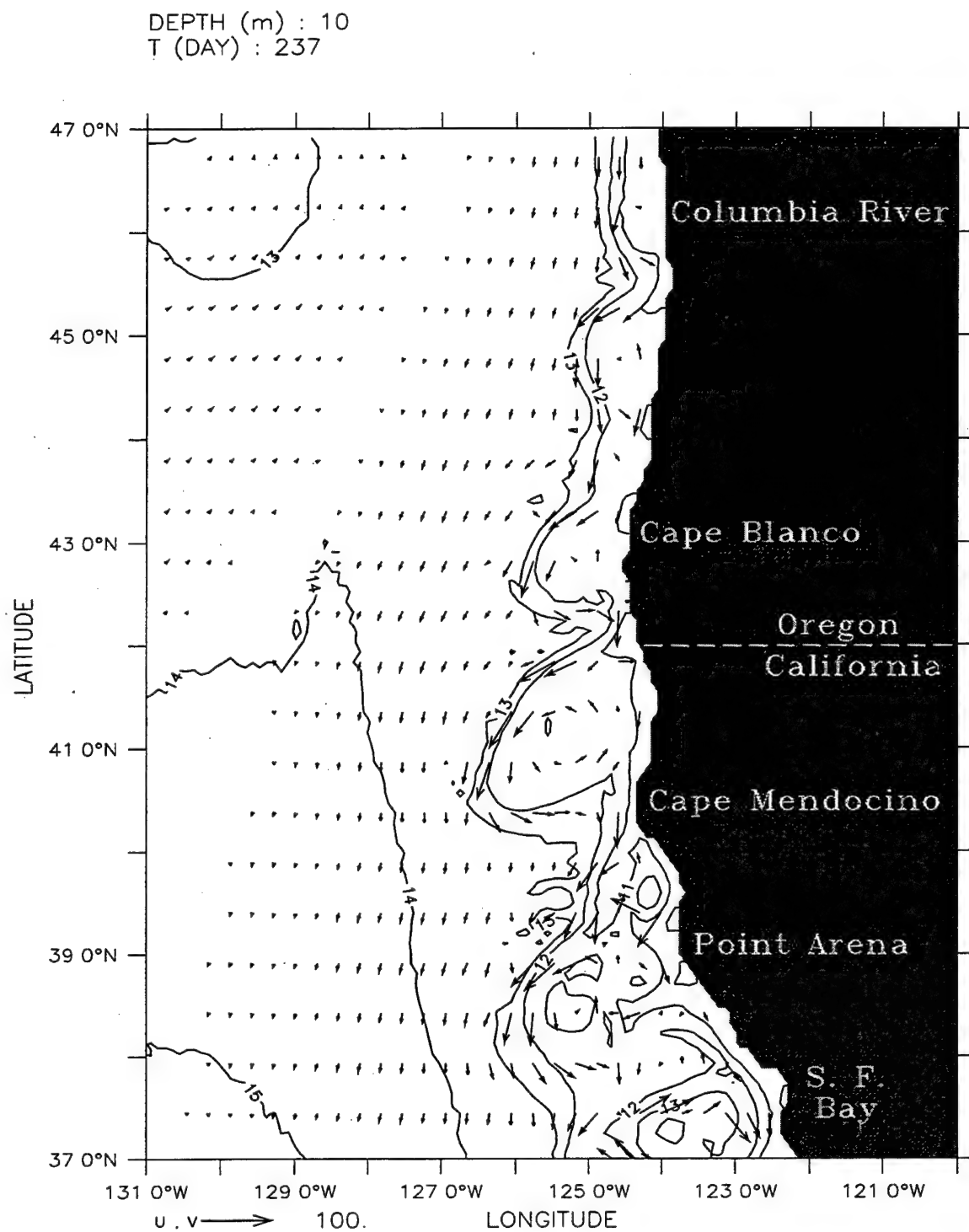


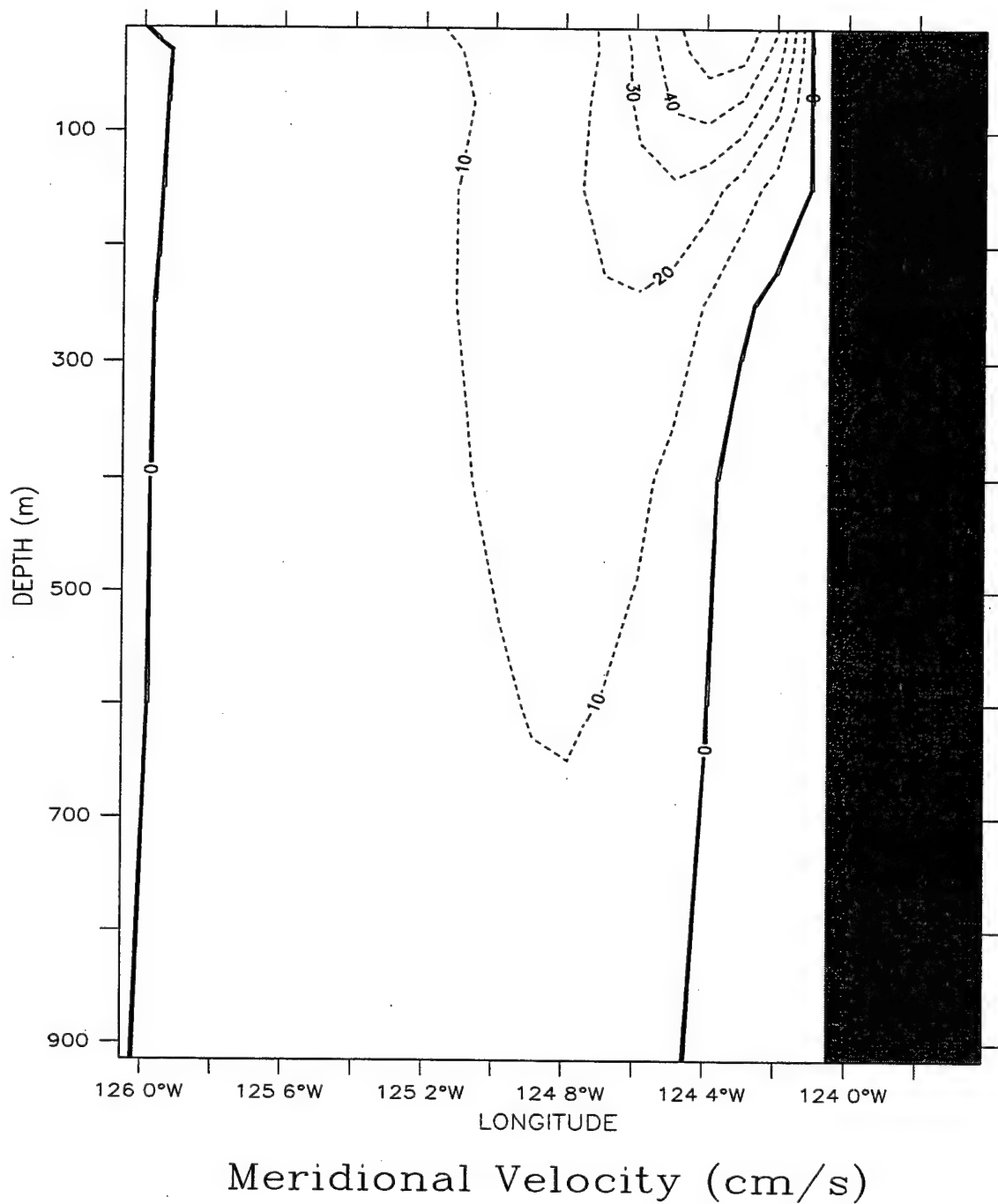
Figure 12. Salinity contours and velocity vectors at 10 m depth for Experiment 2 on day 126. Contour interval is 0.25 psu; maximum velocity vector is 100 cm/s. The 32.5 and 32.75 isohalines are present off the coast of Washington and Oregon.



Temperature (C) and Velocity (cm/s)

Figure 13. Temperature contours and velocity vectors at 10 m depth for Experiment 2 on day 237. Contour interval is 1° C; maximum velocity vector is 100 cm/s.

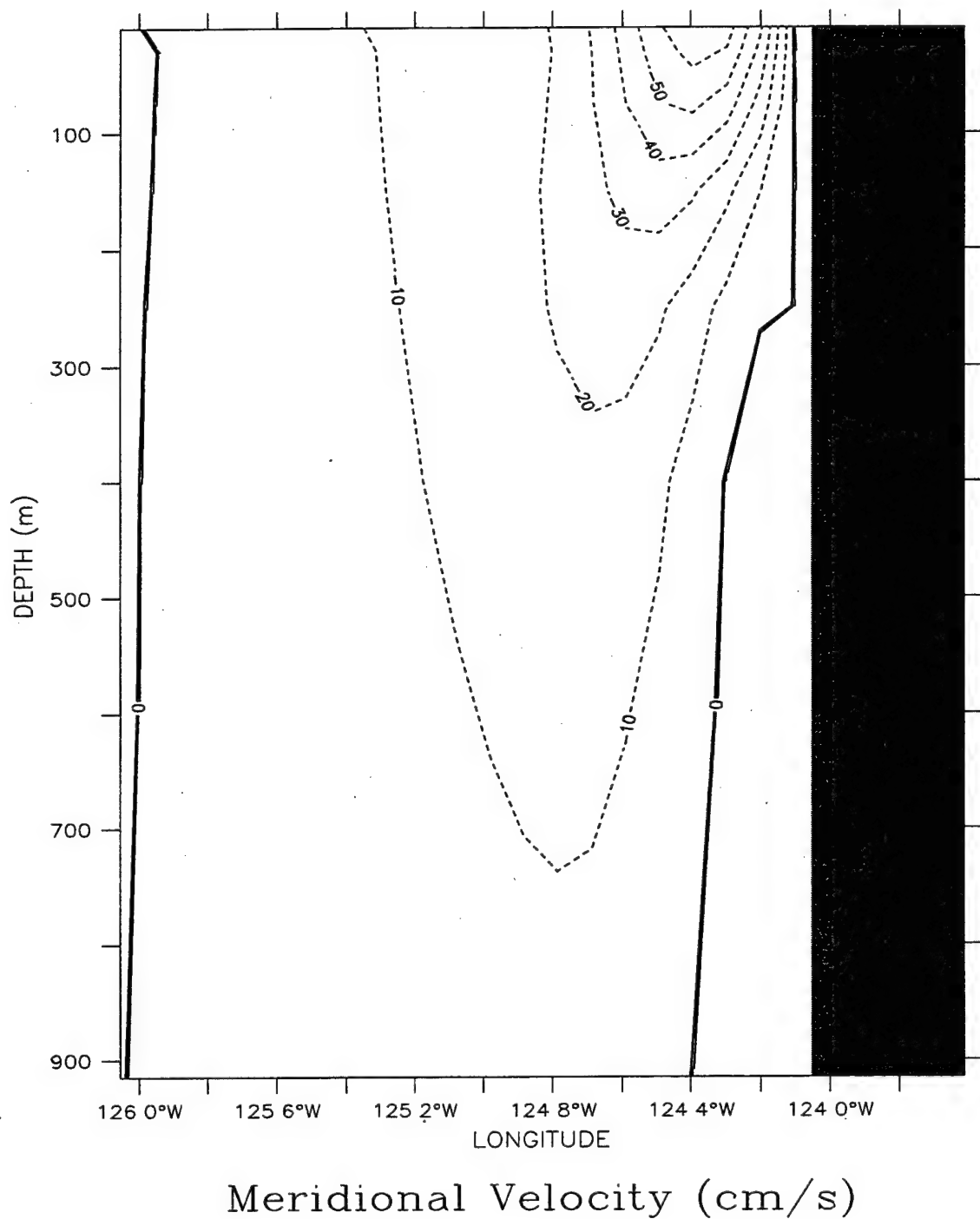
LATITUDE : 47N
T (DAY) : 183



(a)

Figure 14. Cross-shore section of meridional velocity (v) at 47° N on day 183 for (a) Experiment 2 and (b) Experiment 1. Contour interval is 10 cm/s for (a) and (b).

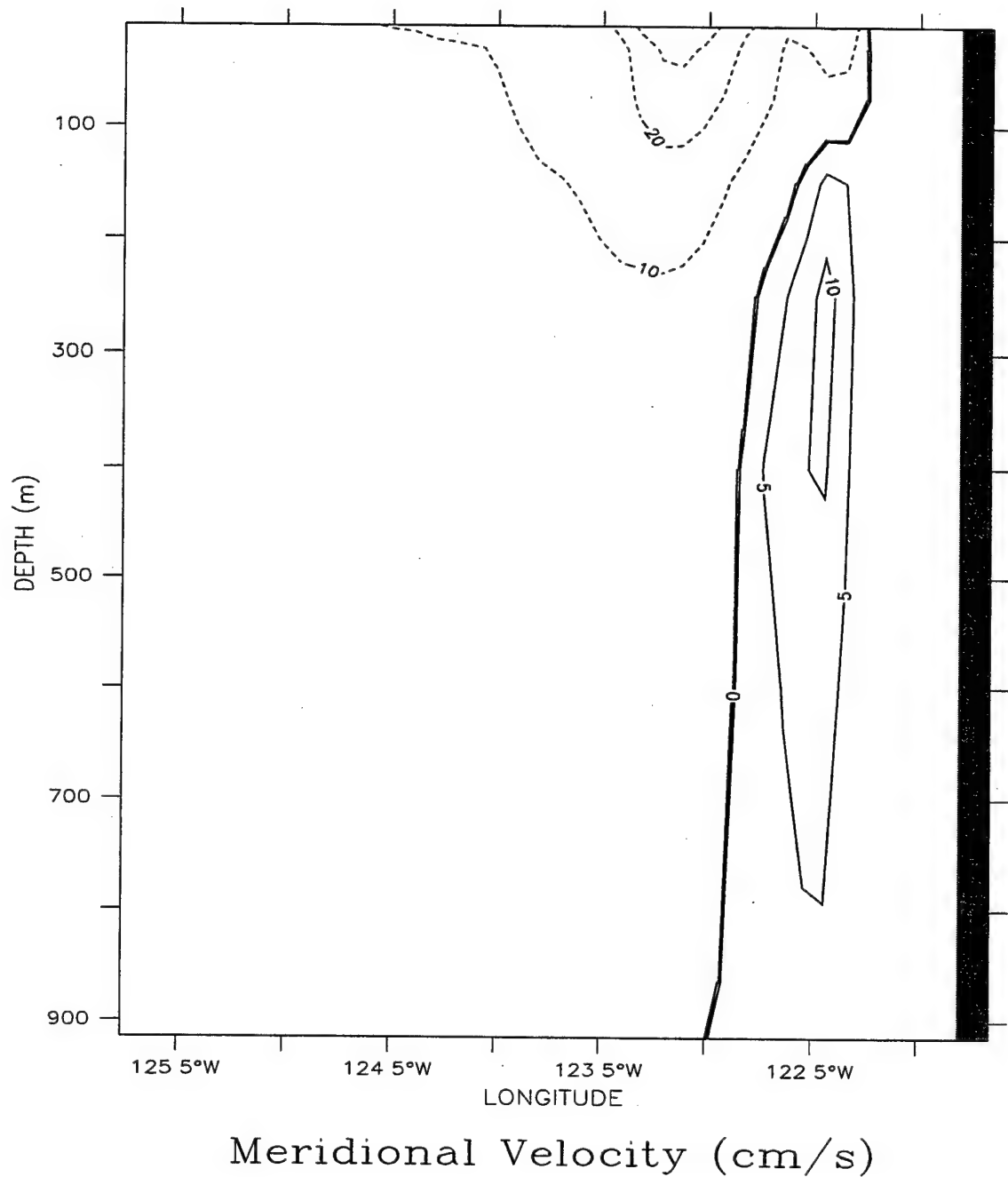
LATITUDE : 47N
T (DAY) : 183



(b)

Figure 14 continued.

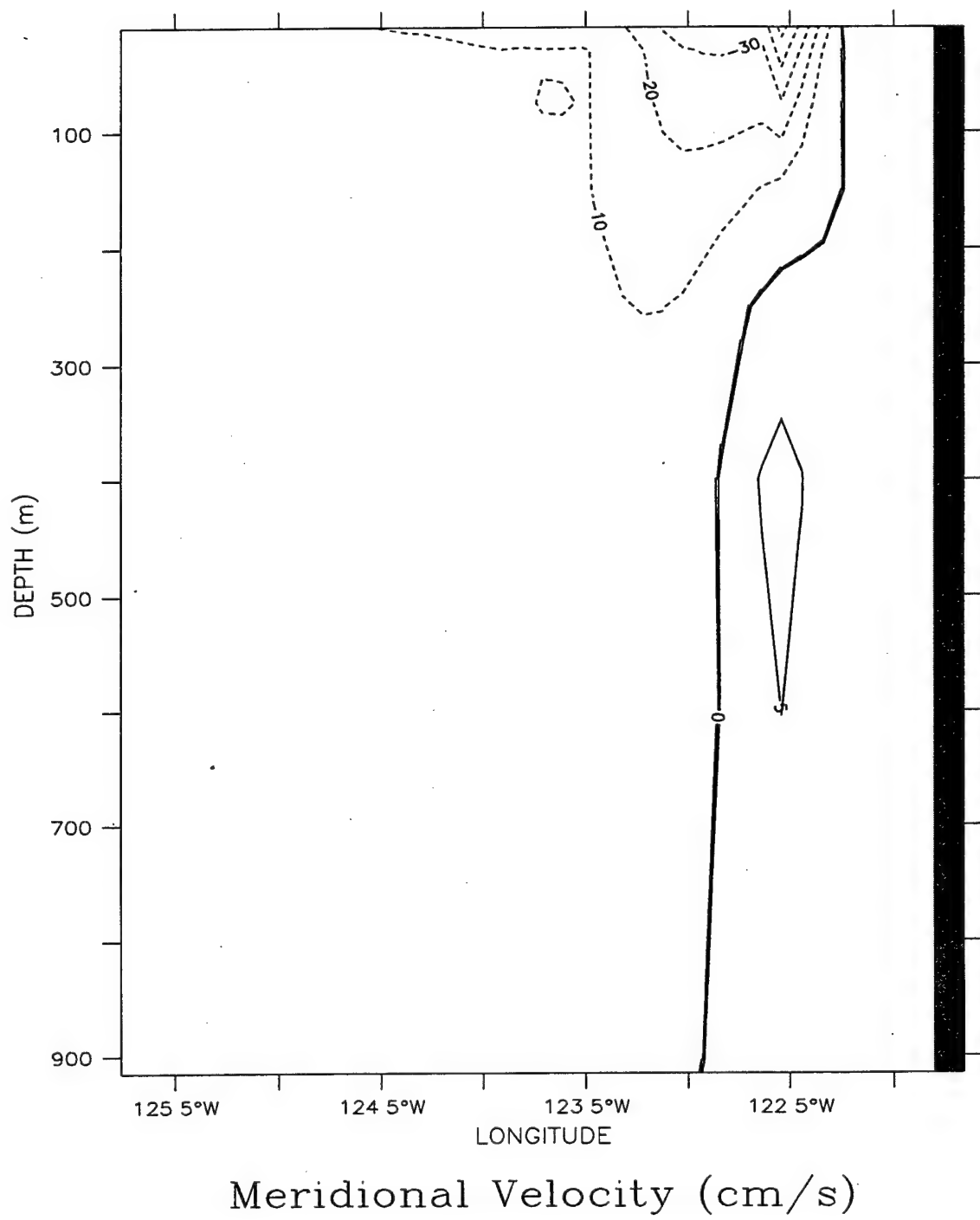
LATITUDE : 37N
T (DAY) : 141



(a)

Figure 15. Cross-shore section of meridional velocity (v) at 37° N on day 141 for (a) Experiment 2 and (b) Experiment 1. Contour interval is 10 cm/s for equatorward flow and 5 cm/s for poleward flow.

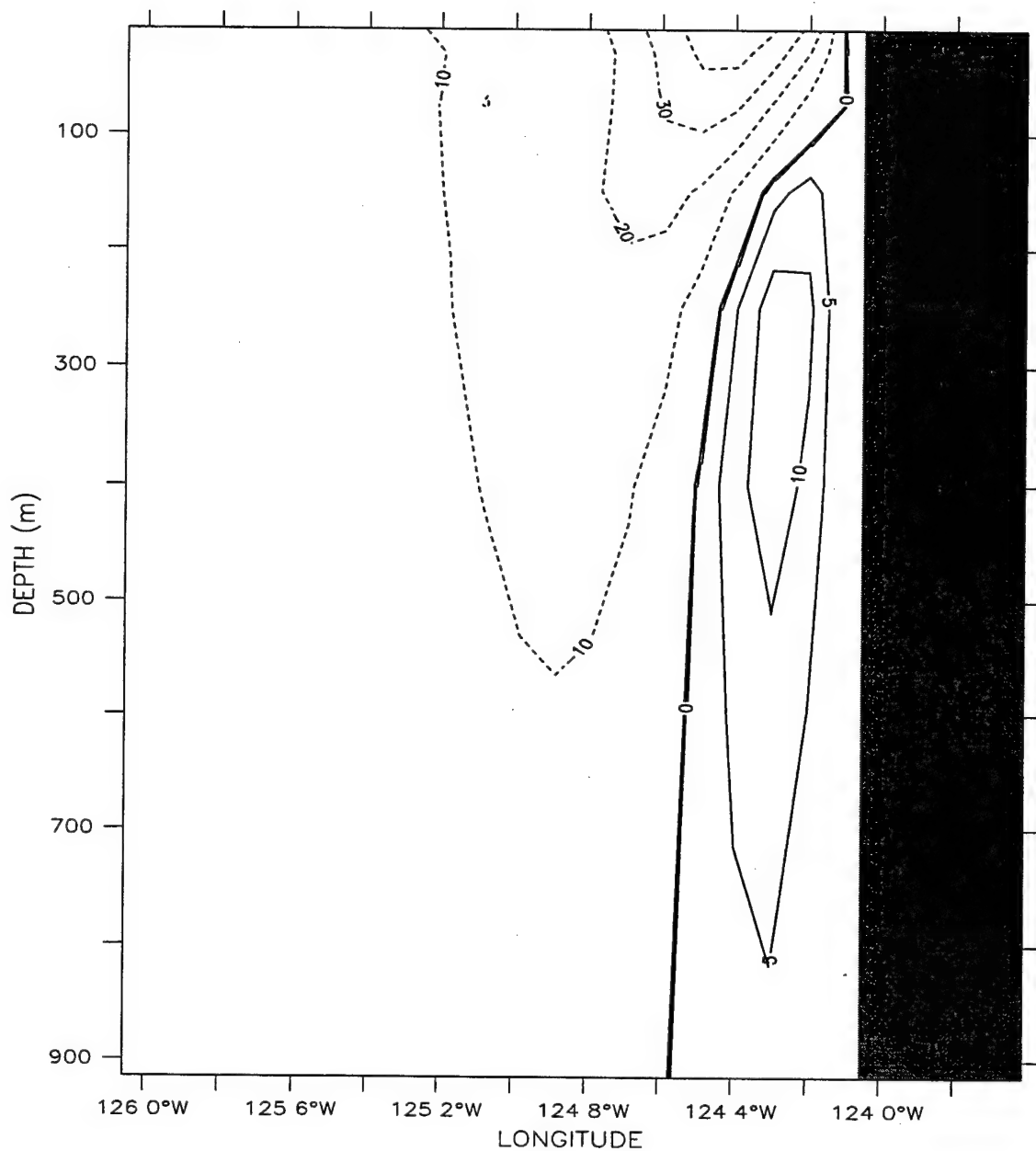
LATITUDE : 37N
T (DAY) : 141



(b)

Figure 15 continued.

LATITUDE : 47N
T (DAY) : 201

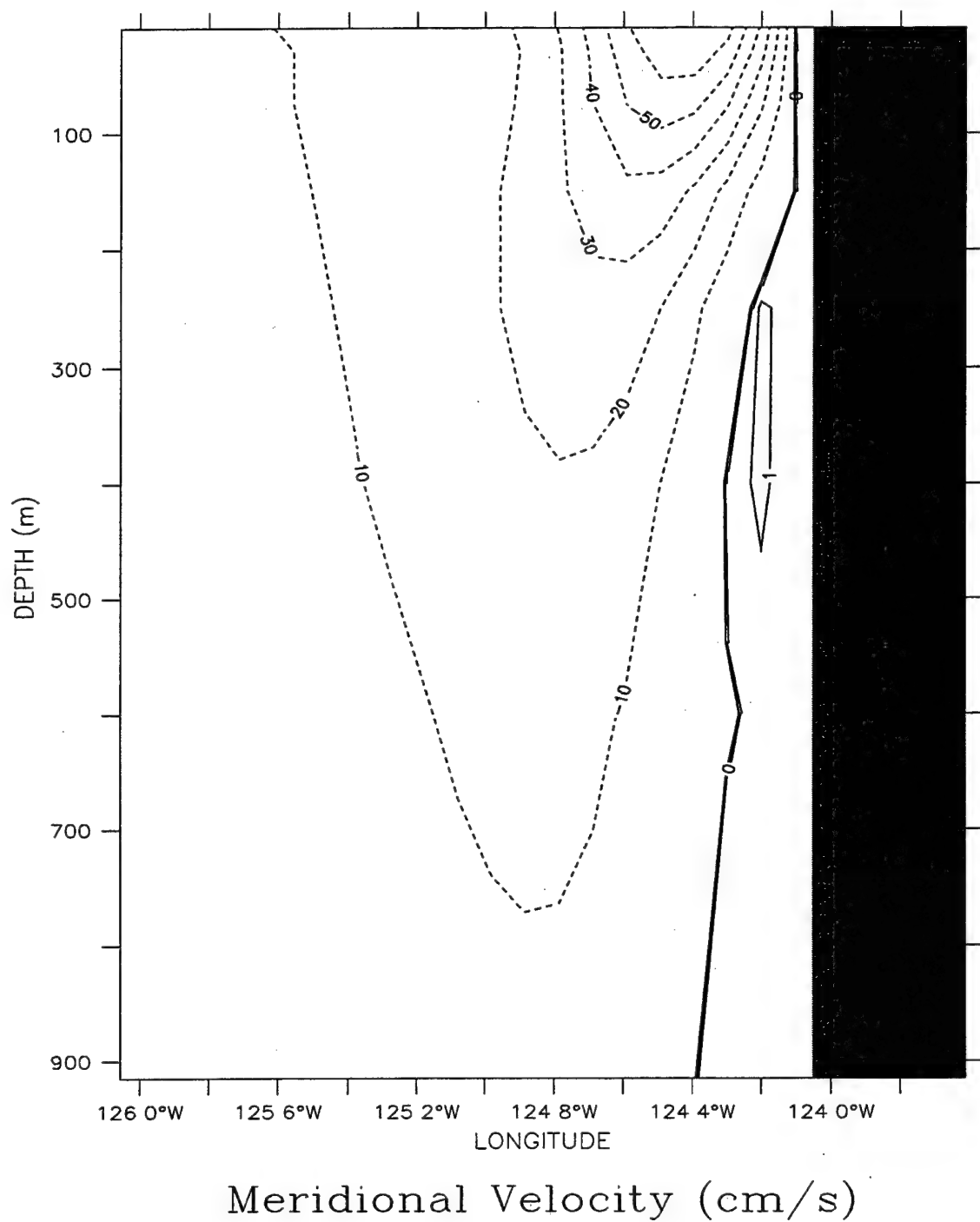


Meridional Velocity (cm/s)

(a)

Figure 16. Cross-shore section of meridional velocity (v) at 47° N on day 201 for (a) Experiment 2 and (b) Experiment 1. Contour interval is 10 cm/s for equatorward flow in (a) and (b). For poleward flow, the contour interval is 5 cm/s in (a) and 1 cm/s in (b).

LATITUDE : 47N
T (DAY) : 201



(b)

Figure 16 continued.

DEPTH (m) : 10
T (DAY) : 940.5 to 970.5

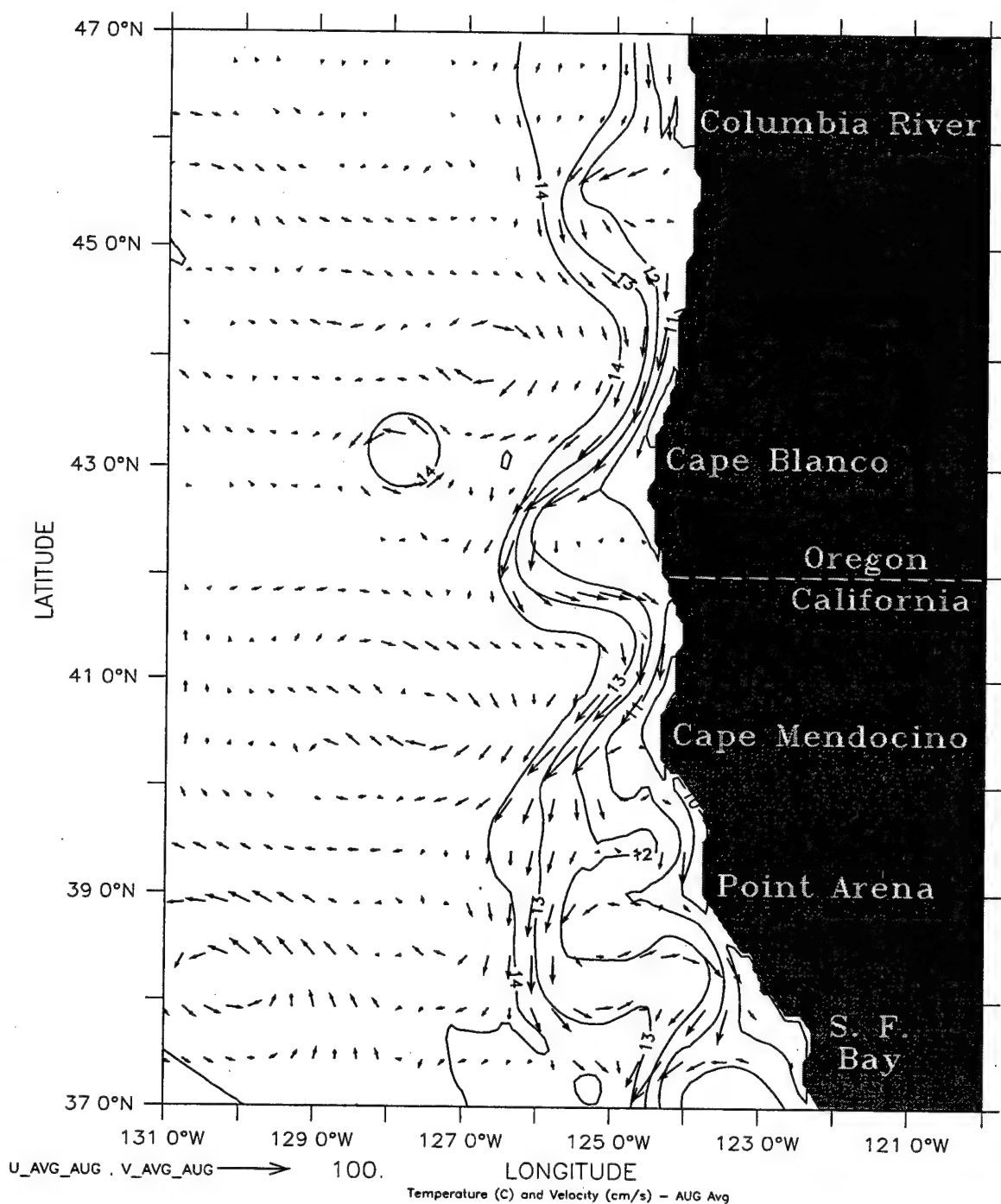
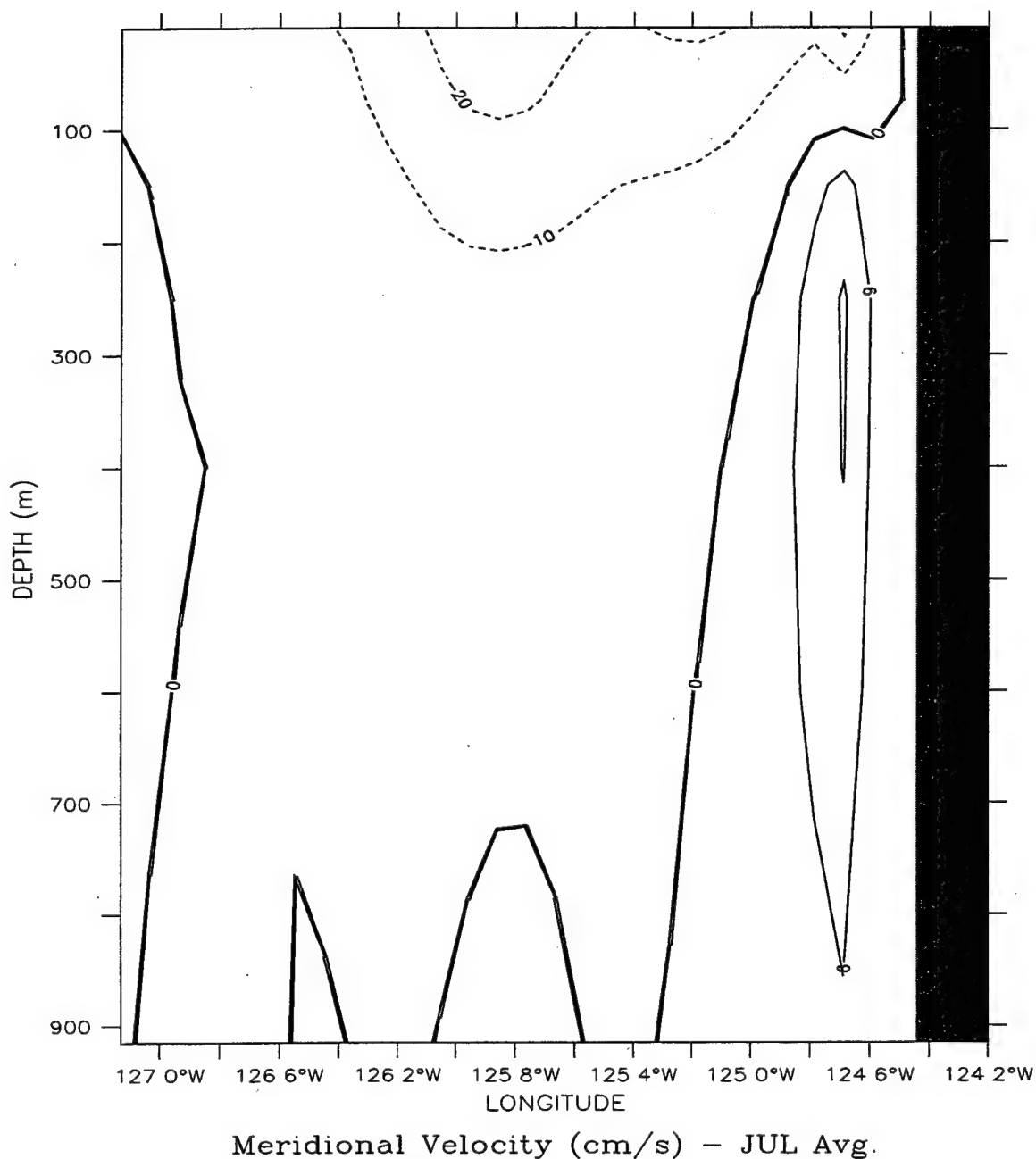


Figure 17. Temperature contours and velocity vectors at 10 m depth for Experiment 2 in the third year of model simulation, time-averaged over the month of August. Contour interval is 1° C; maximum velocity vector is 100 cm/s.

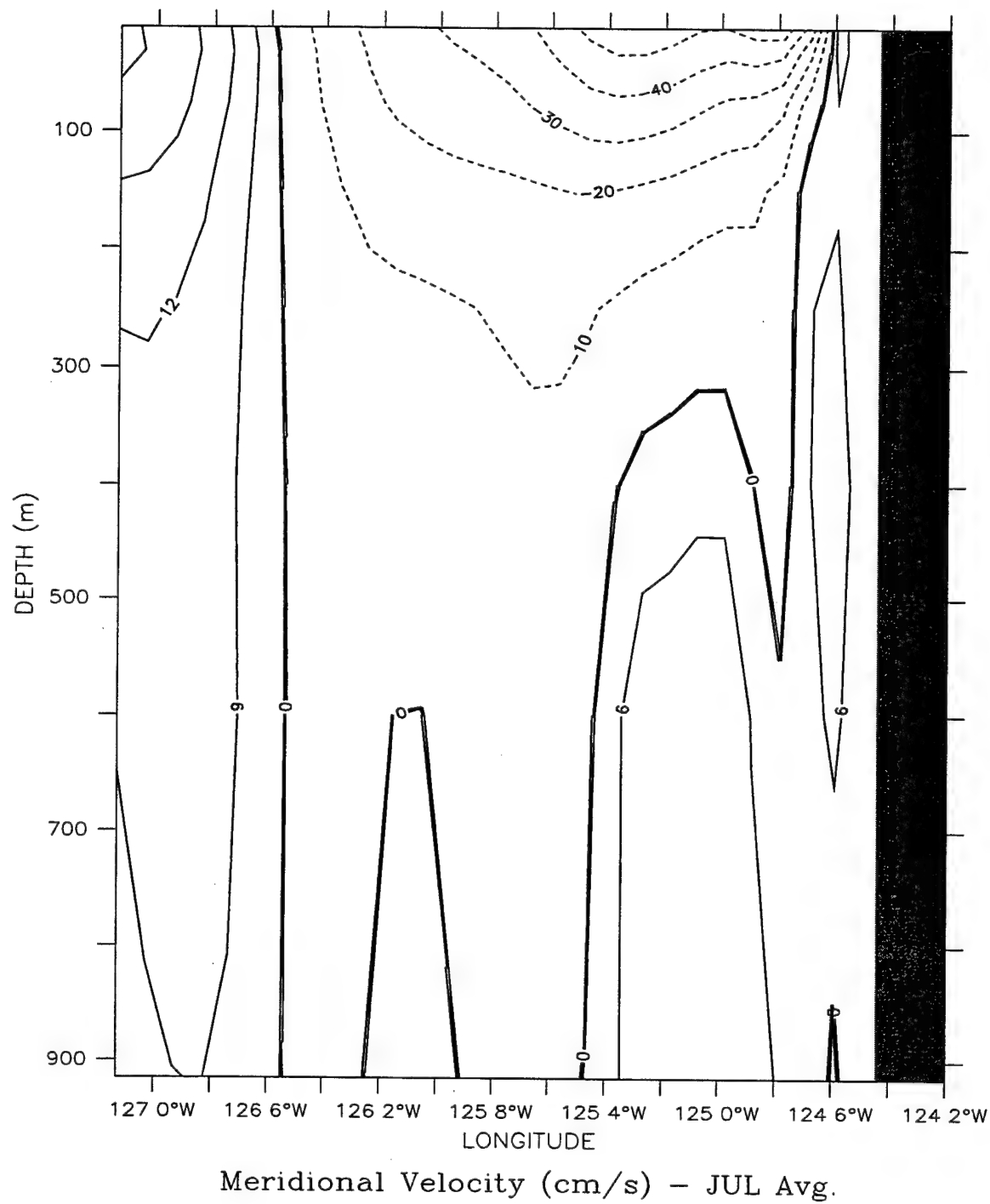
LATITUDE : 42.5N
T (DAY) : 910.5 to 940.5



(a)

Figure 18. Cross-shore section of meridional velocity (v) at 42.5° N in the third year of model simulation time-averaged over the month of July for (a) Experiment 2 and (b) Experiment 1. Contour interval is 10 cm/s for equatorward flow and 6 cm/s for poleward flow.

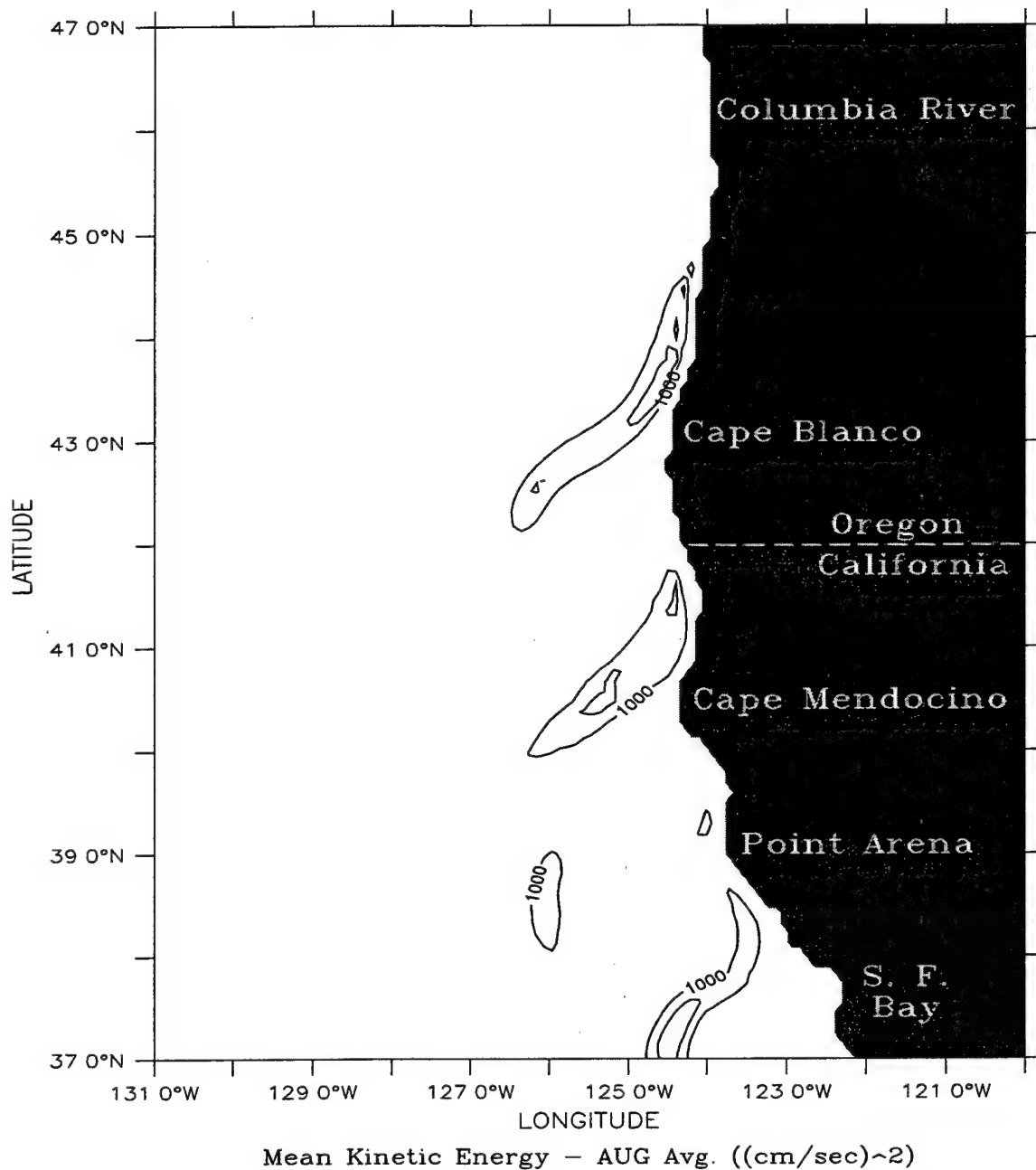
LATITUDE : 42.5N
T (DAY) : 910.5 to 940.5



(b)

Figure 18 continued.

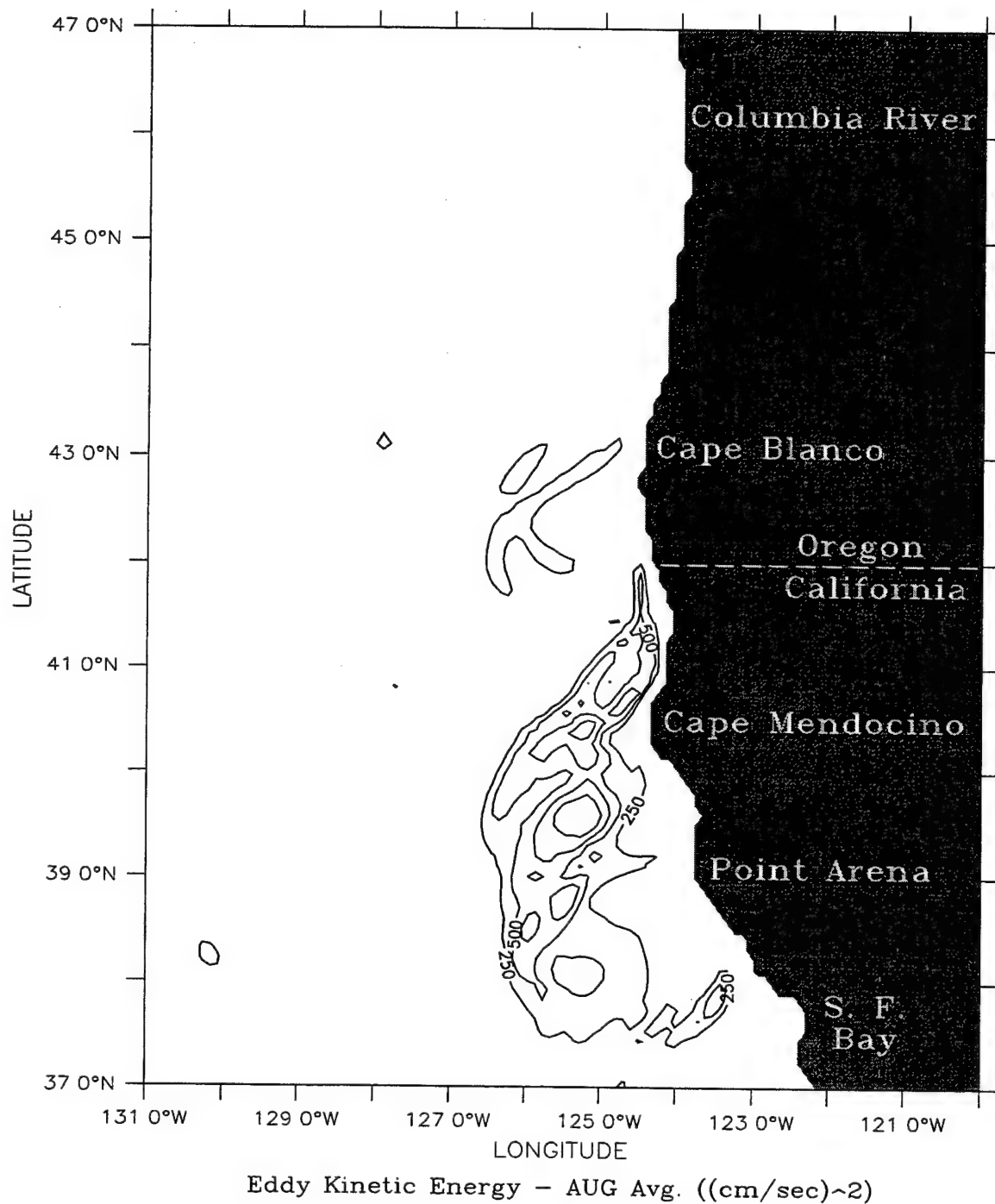
DEPTH (m) : 10
T (DAY) : 940.5 to 970.5



(a)

Figure 19. Horizontal maps at 10 m depth of (a) mean kinetic energy (MKE), and (b) eddy kinetic energy (EKE) for Experiment 2 in the third year of model simulation, time-averaged for the month of August. Contour interval is 1000 (cm/s)² for (a), and 250 (cm/s)² for (b).

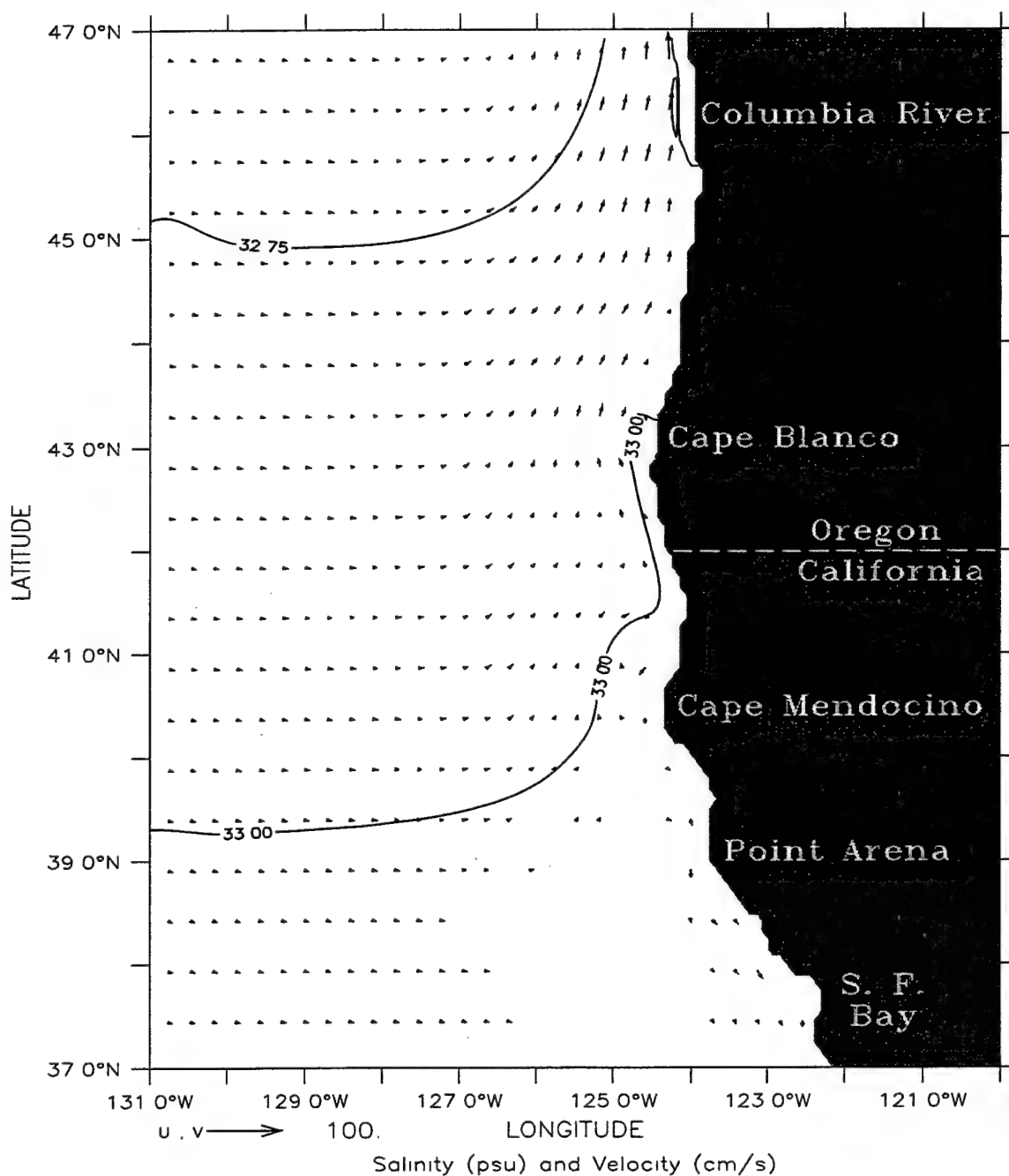
DEPTH (m) : 10
T (DAY) : 940.5 to 970.5



(b)

Figure 19 continued.

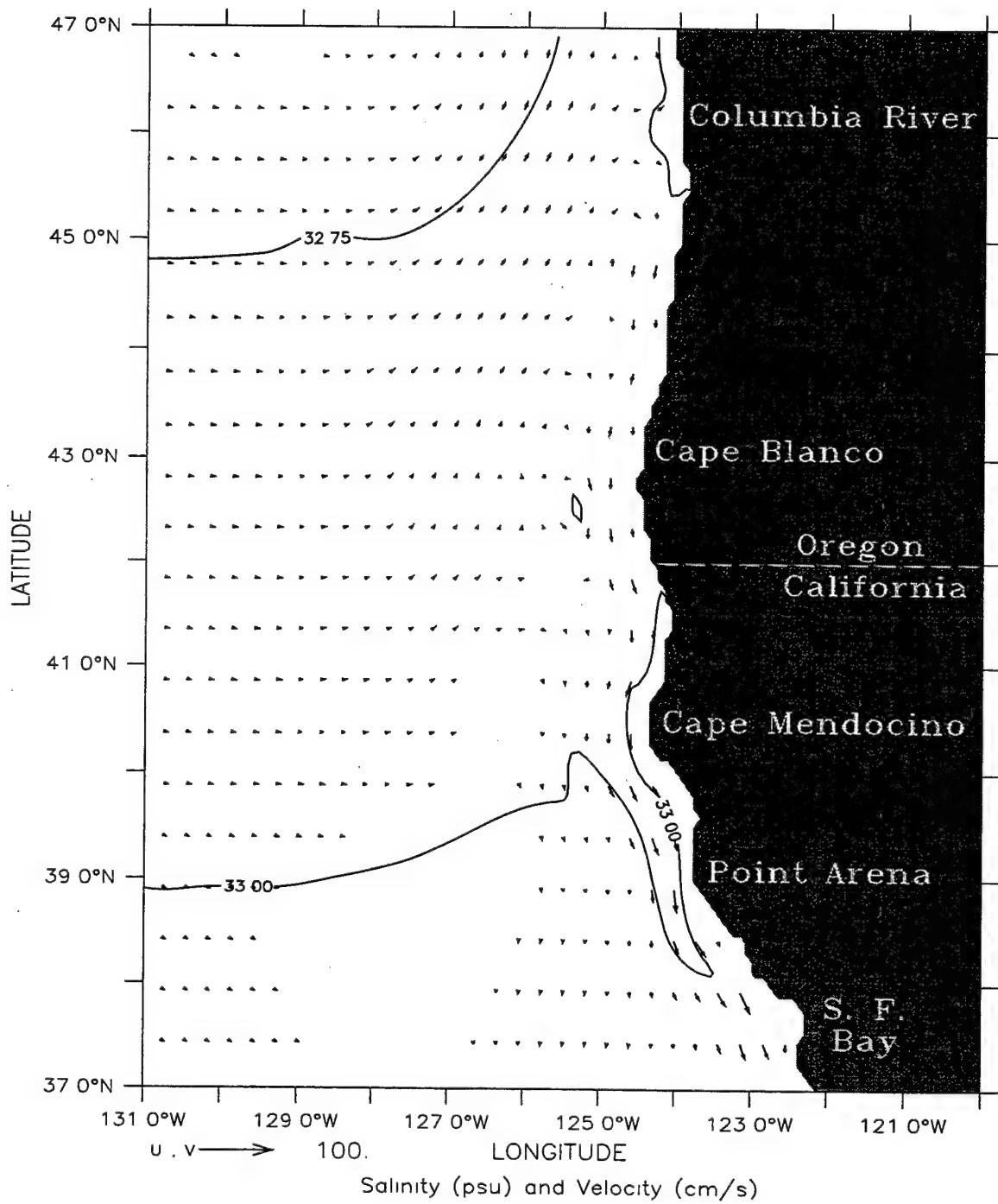
DEPTH (m) : 10
T (DAY) : 54



(a)

Figure 20. Salinity contours and velocity vectors at 10 m depth for Experiment 3 on day (a) 54, (b) 99, (c) 126, and (d) 201. Contour interval is 0.25 psu; maximum velocity vector is 100 cm/s. Salinity at the mouth of the Columbia River is ~31.72 psu for (a)–(d).

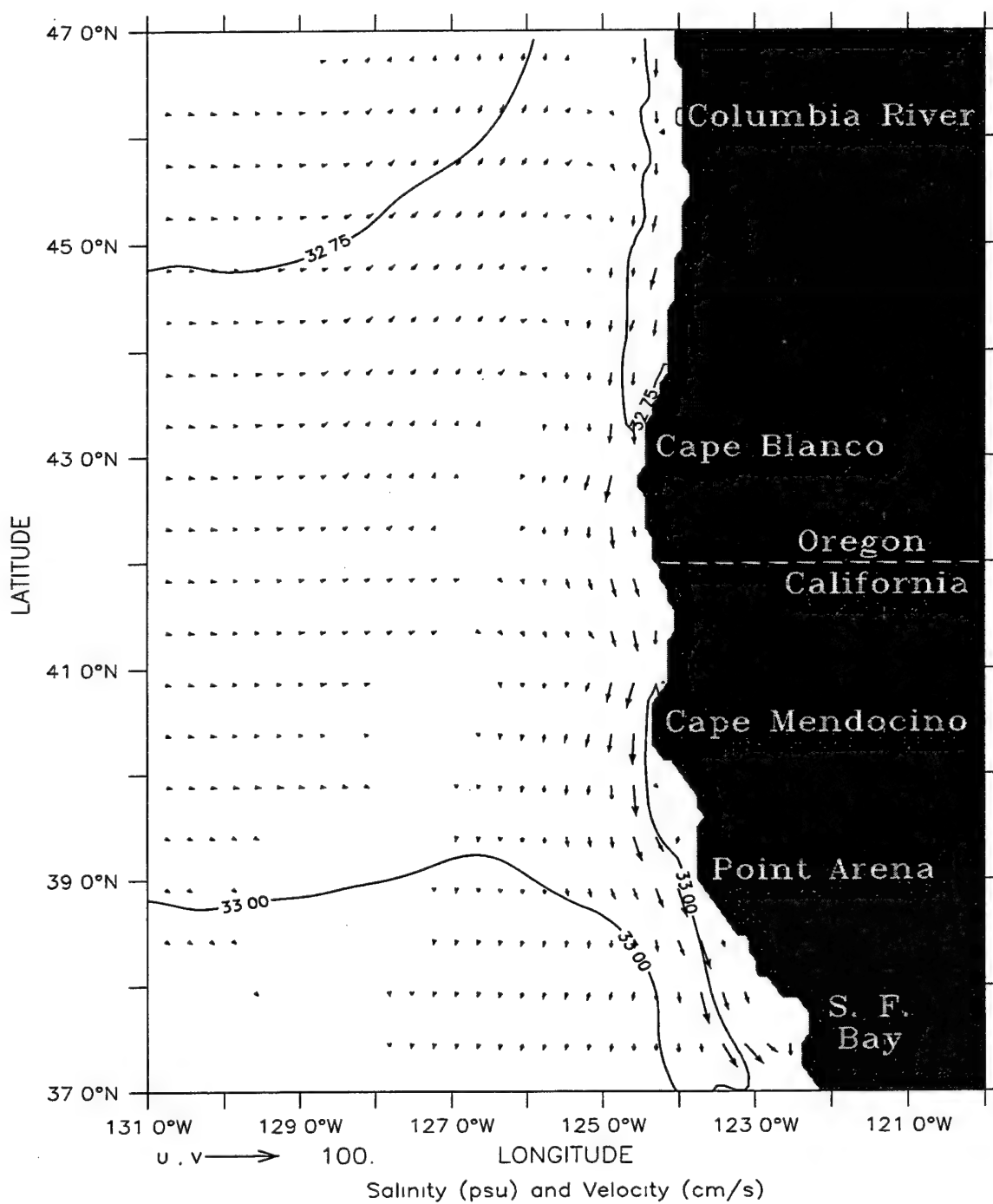
DEPTH (m) : 10
T (DAY) : 99



(b)

Figure 20 continued.

DEPTH (m) : 10
T (DAY) : 126



(c)

Figure 20 continued.

DEPTH (m) : 10
T (DAY) : 201

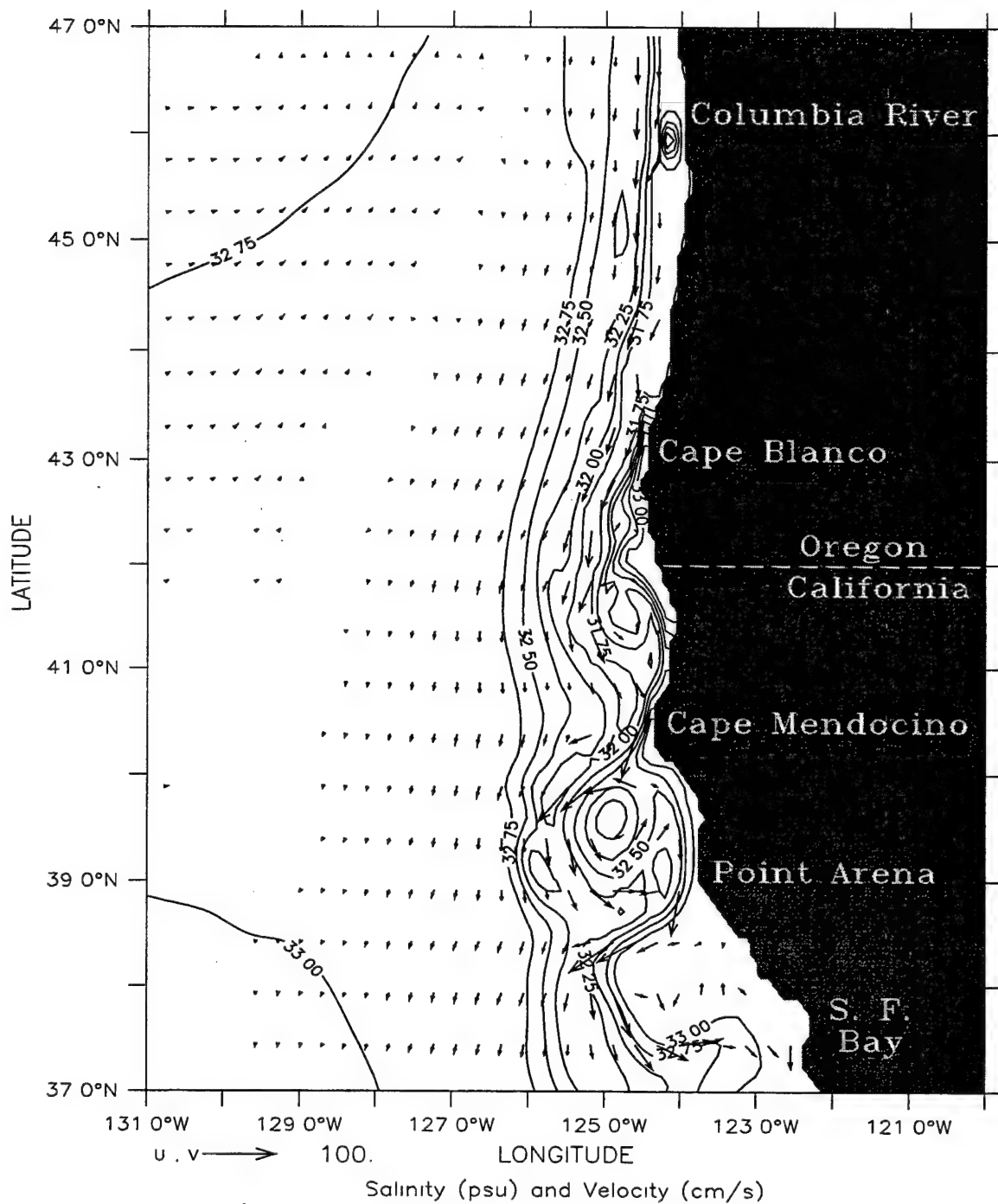
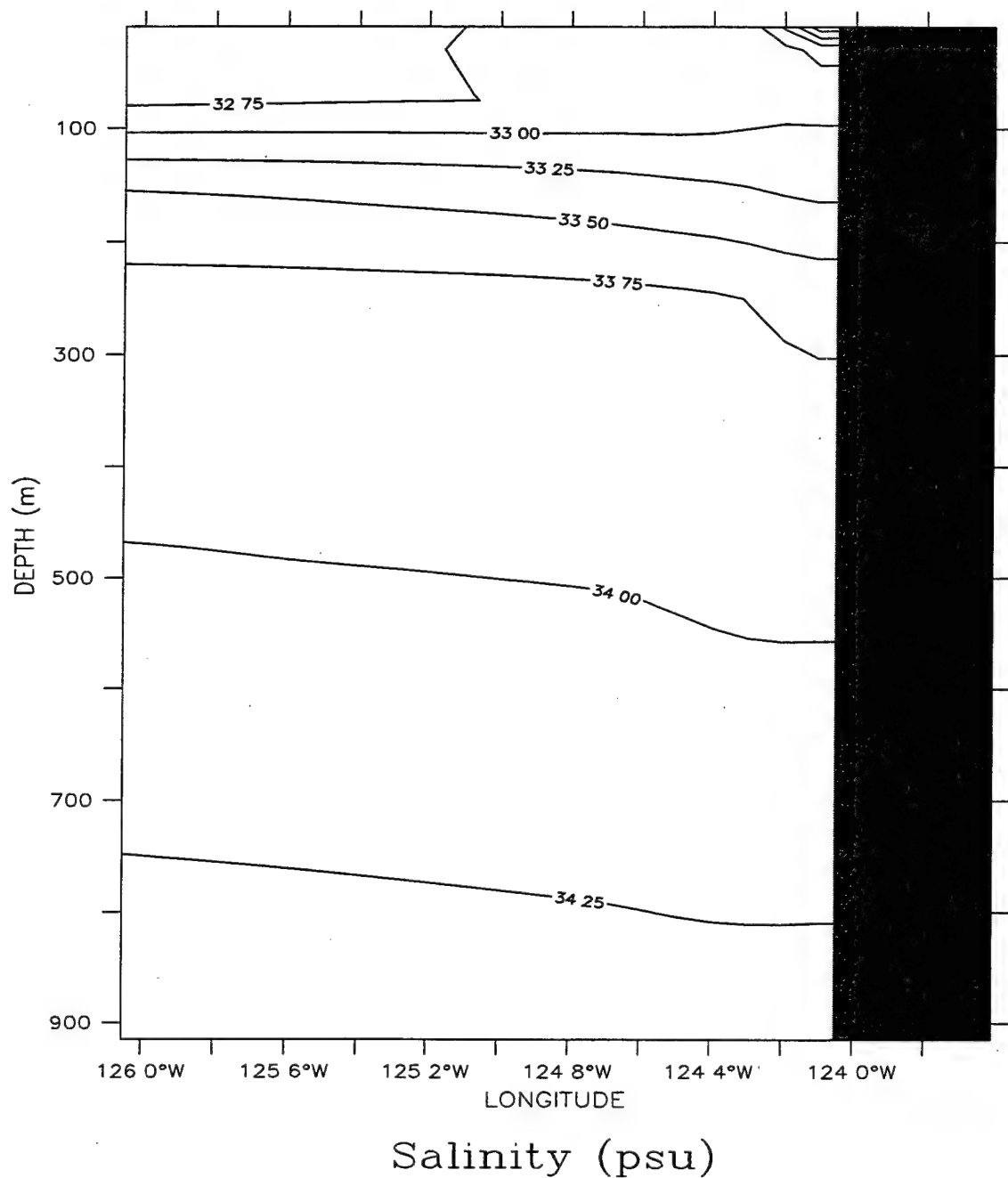


Figure 20 continued.

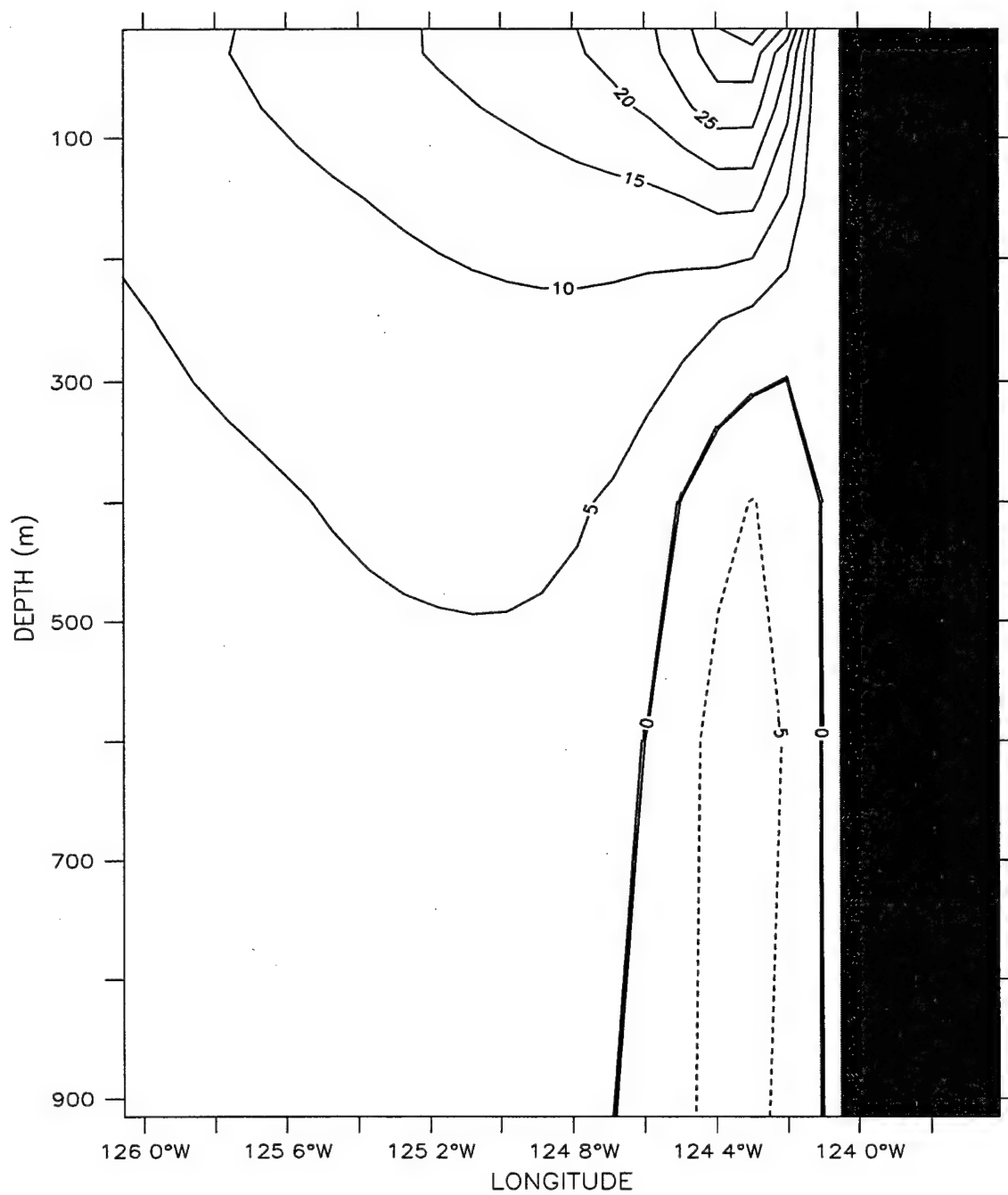
LATITUDE : 47N
T (DAY) : 54



(a)

Figure 21. Cross-shore section for Experiment 3 on day 54 at 47° N for (a) and (c) salinity to 900 m and 150m depth, respectively; (b) and (d) meridional velocity (v) to 900 m and 150m depth, respectively. Contour interval is 0.25 psu for salinity and 5 cm/s for v .

LATITUDE : 47N
T (DAY) : 54

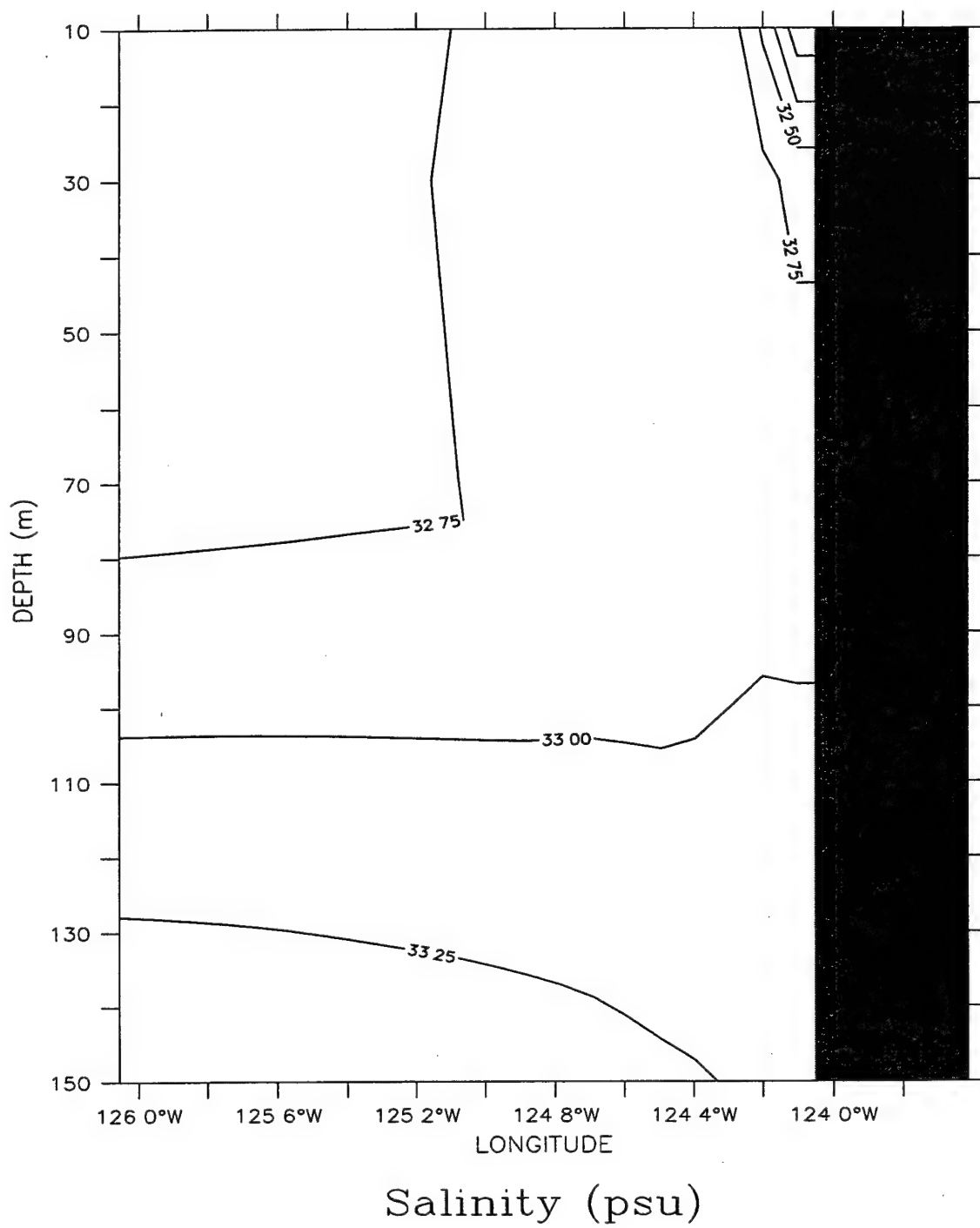


Meridional Velocity (cm/s)

(b)

Figure 21 continued.

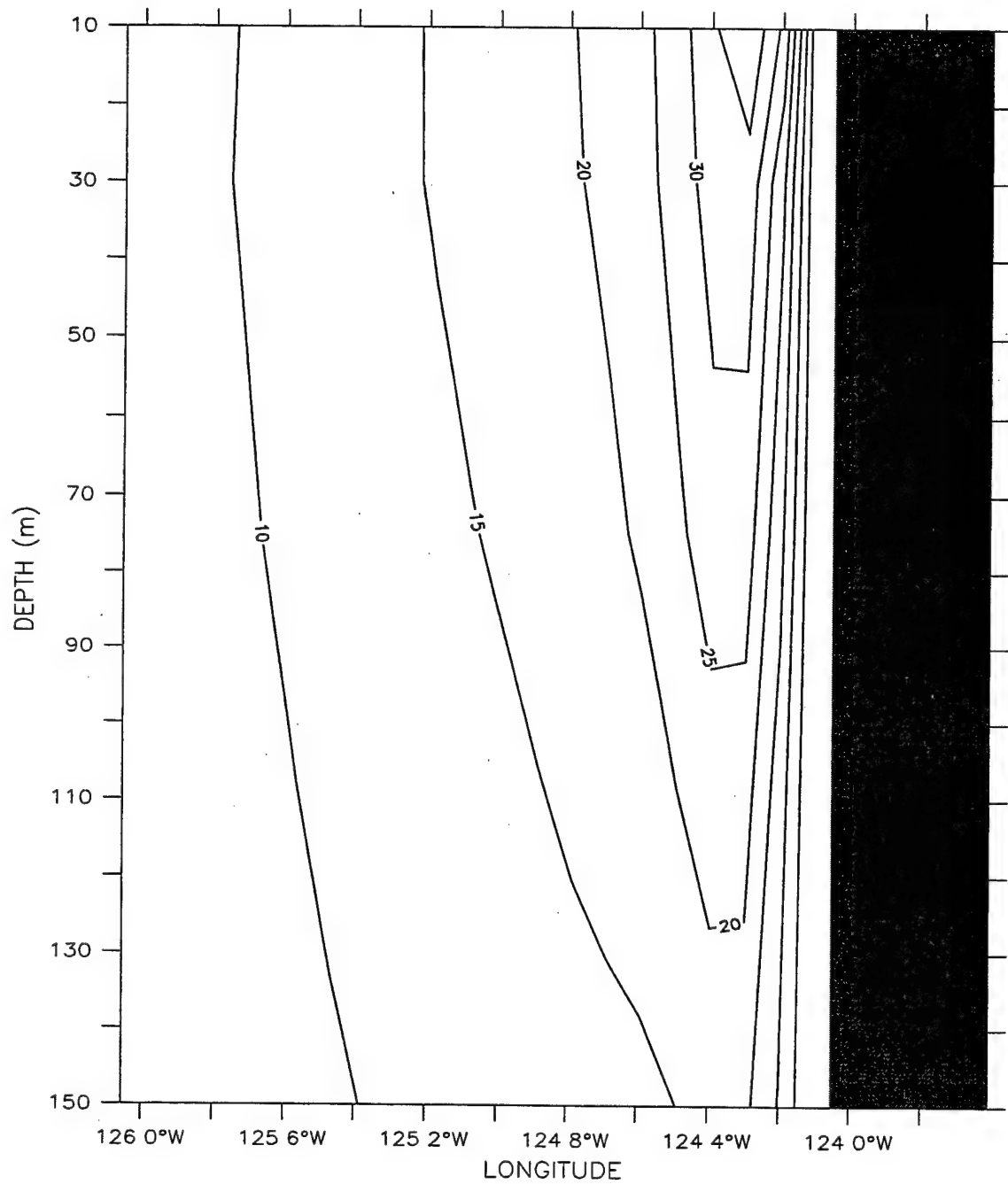
LATITUDE : 47N
T (DAY) : 54



(c)

Figure 21 continued.

LATITUDE : 47N
T (DAY) : 54



Meridional Velocity (cm/s)

(d)

Figure 21 continued.

LATITUDE : 46.2N
T (DAY) : 99

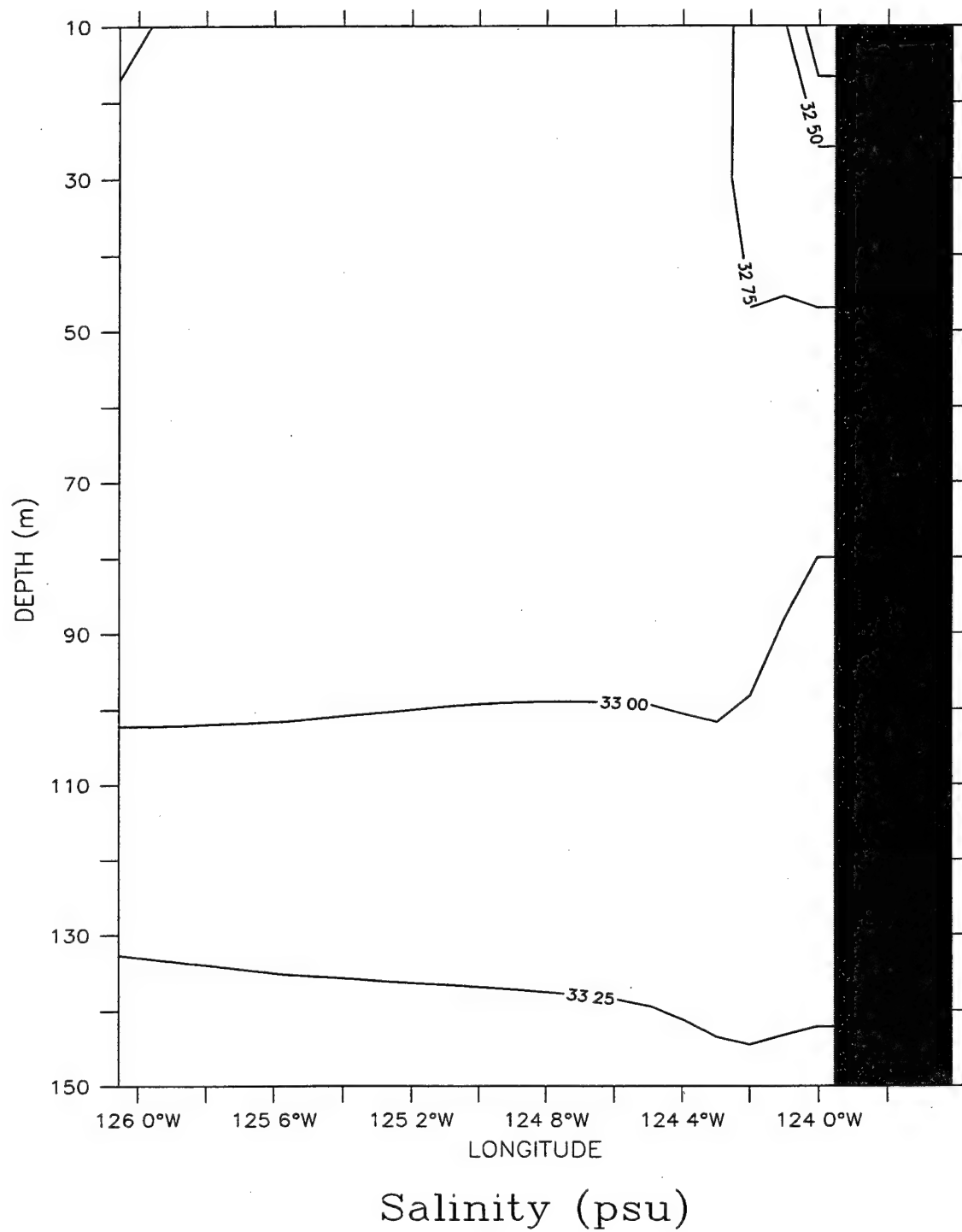
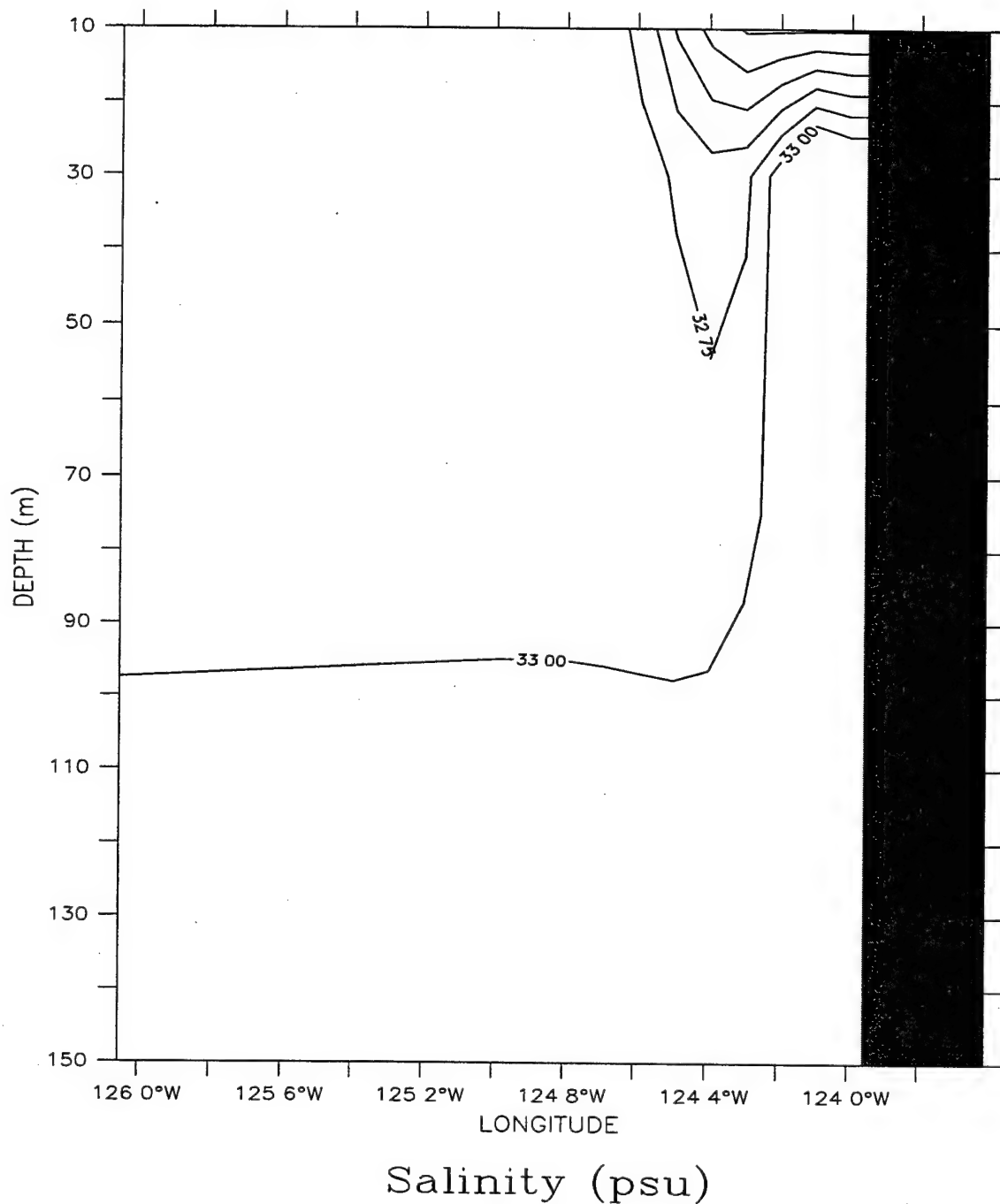


Figure 22. Cross-shore section for Experiment 3 on day 99 at 46.2° N of salinity. Contour interval is 0.25 psu.

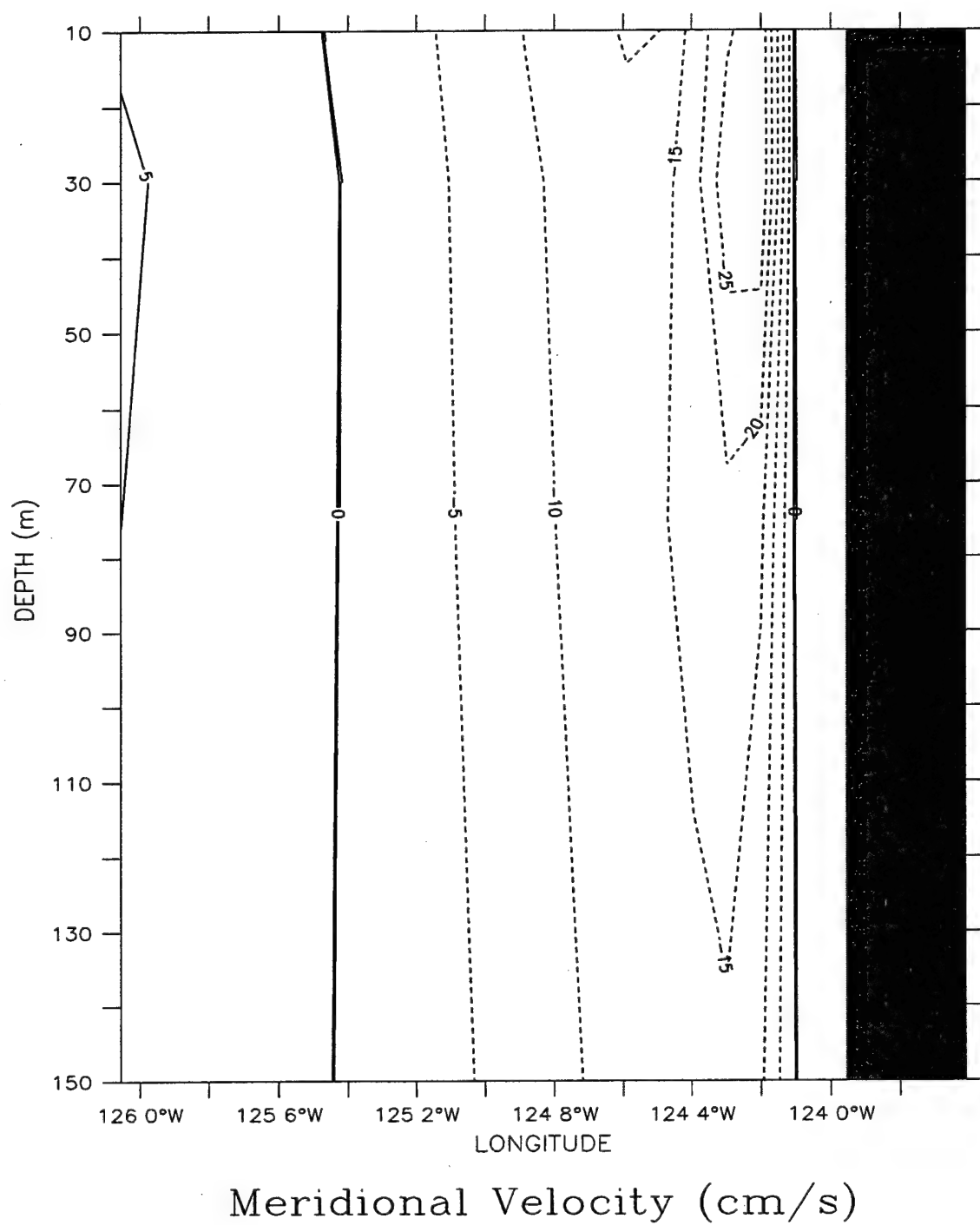
LATITUDE : 45N
T (DAY) : 126



(a)

Figure 23. Cross-shore section for Experiment 3 on day 126 at 45° N for (a) salinity and (b) meridional velocity (v). Contour interval for salinity is 0.25 psu. Contour interval for v is 5 cm/s.

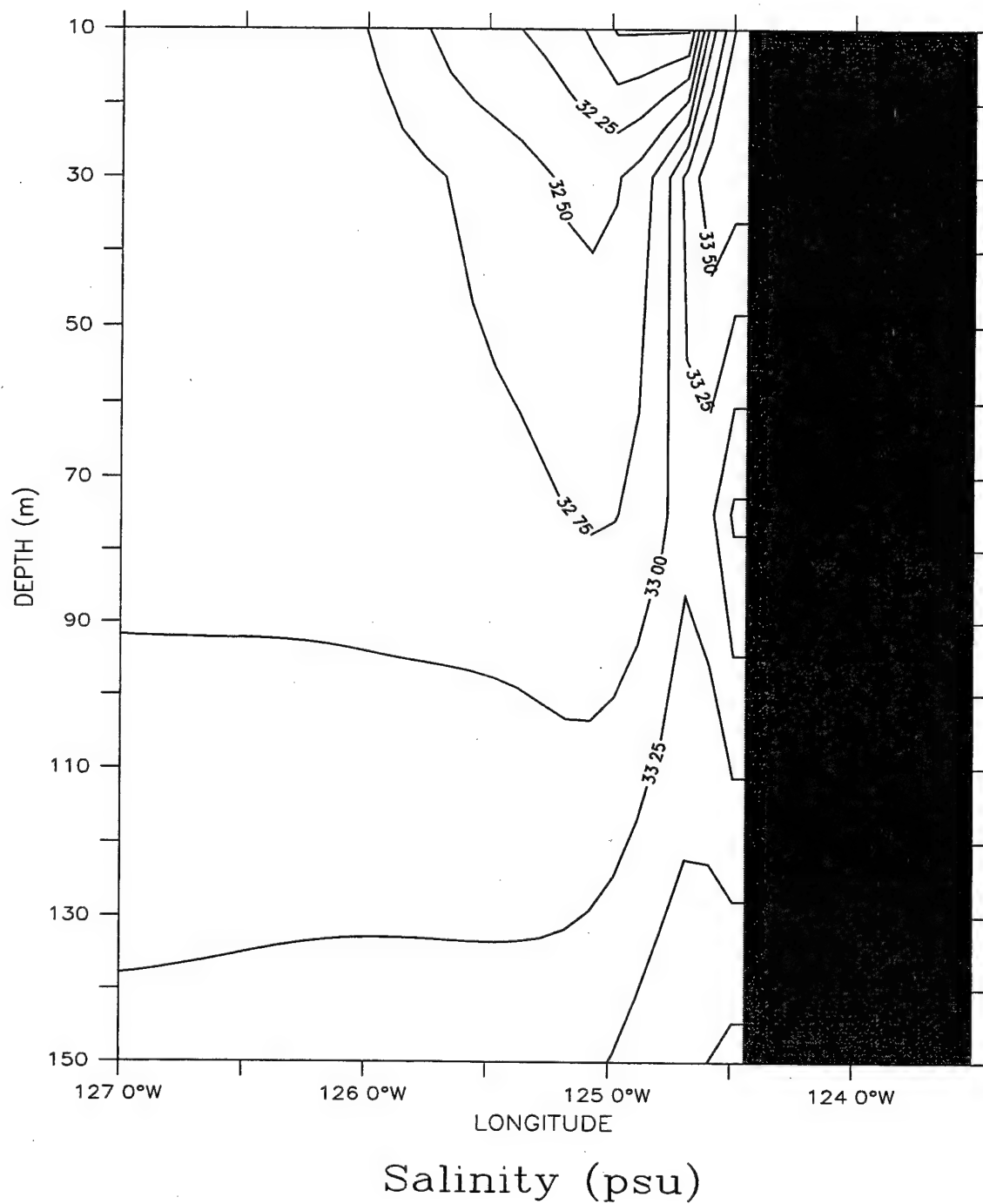
LATITUDE : 45N
T (DAY) : 126



(b)

Figure 23 continued.

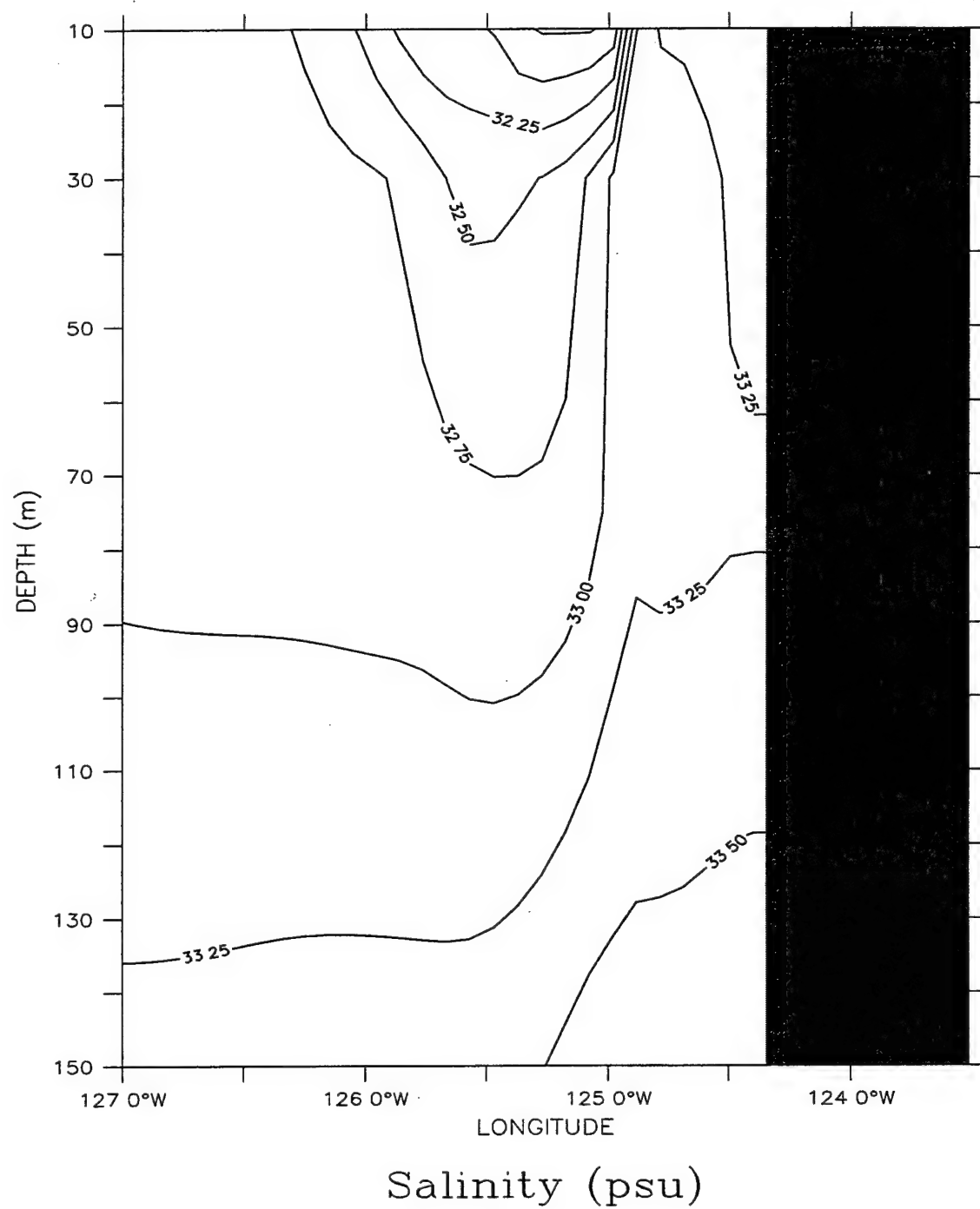
LATITUDE : 43N
T (DAY) : 201



(a)

Figure 24. Cross-shore section of salinity for Experiment 3 on day 201 at (a) 43° N and (b) 42° N. Contour interval for salinity is 0.25 psu.

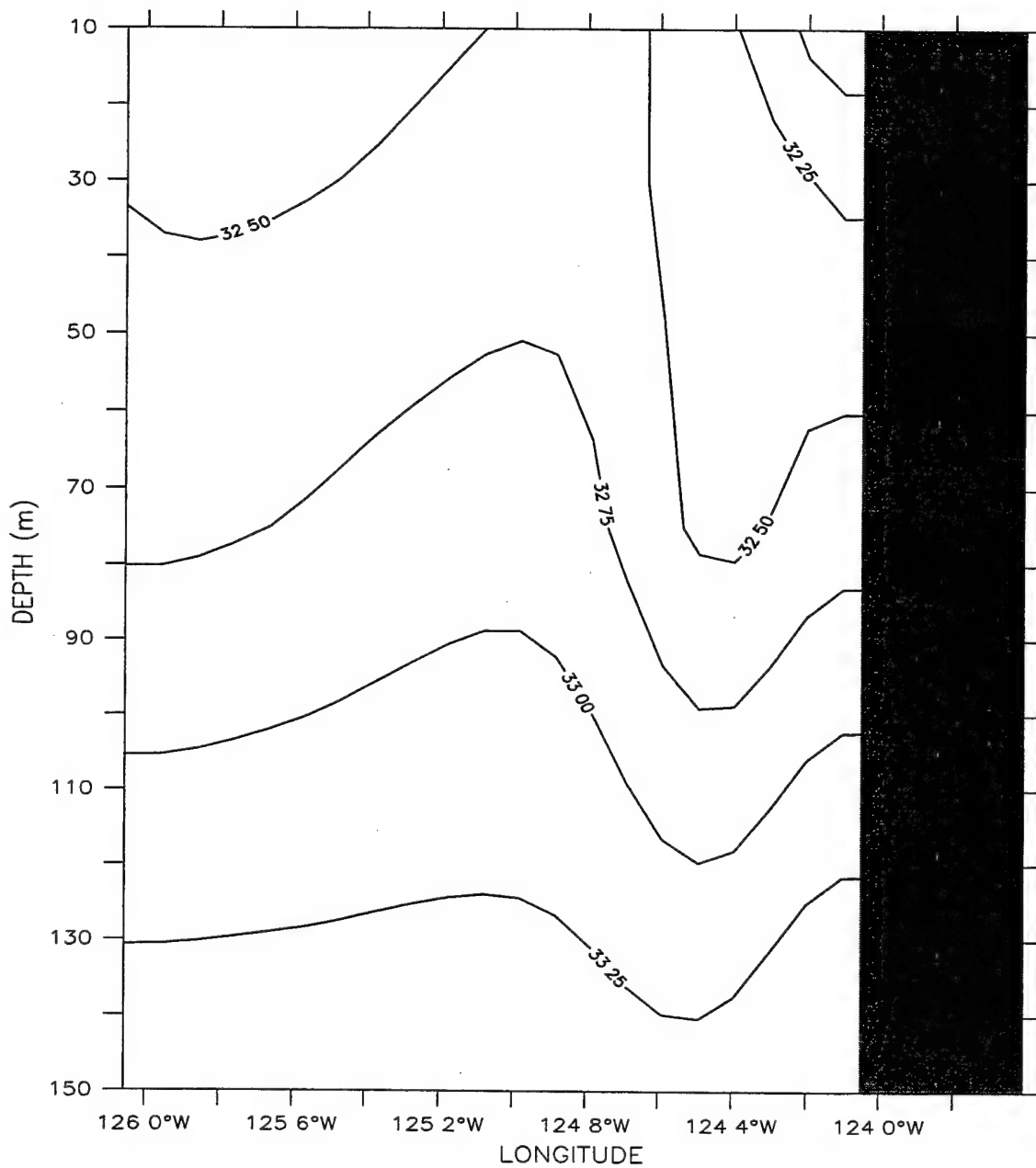
LATITUDE : 42N
T (DAY) : 201



(b)

Figure 24 continued.

LATITUDE : 47N

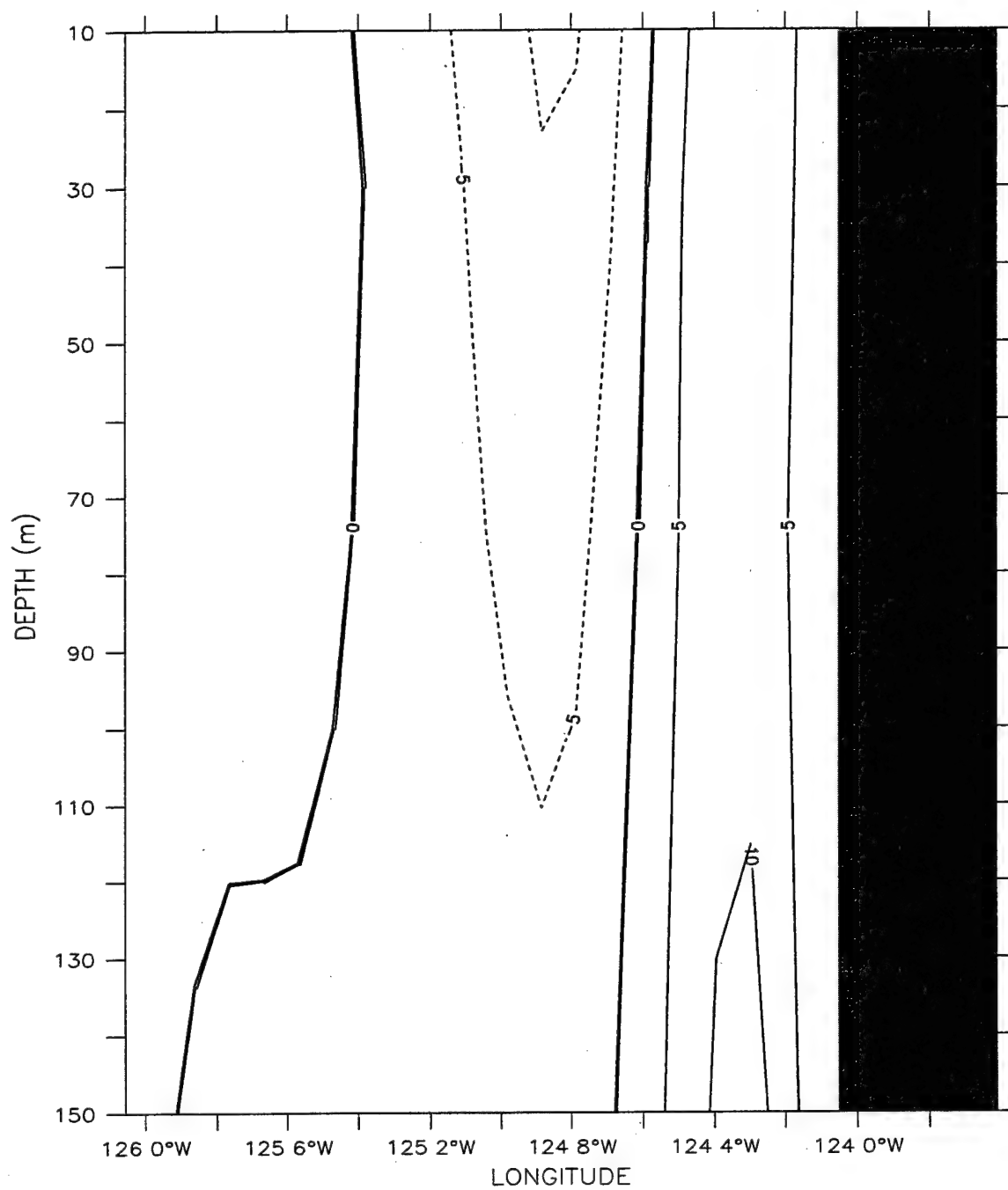


Salinity (psu) – JAN Avg.

(a)

Figure 25. Cross-shore section for Experiment 3 time-averaged over the month of January at 47° N for (a) salinity and (b) meridional velocity (v). Contour interval for salinity is 0.25 psu. Contour interval for v is 5 cm/s.

LATITUDE : 47N



Meridional Velocity (cm/s) - JAN Avg.

(b)

Figure 25 continued.

DEPTH (m) : 10
T (DAY) : 910.5 to 940.5

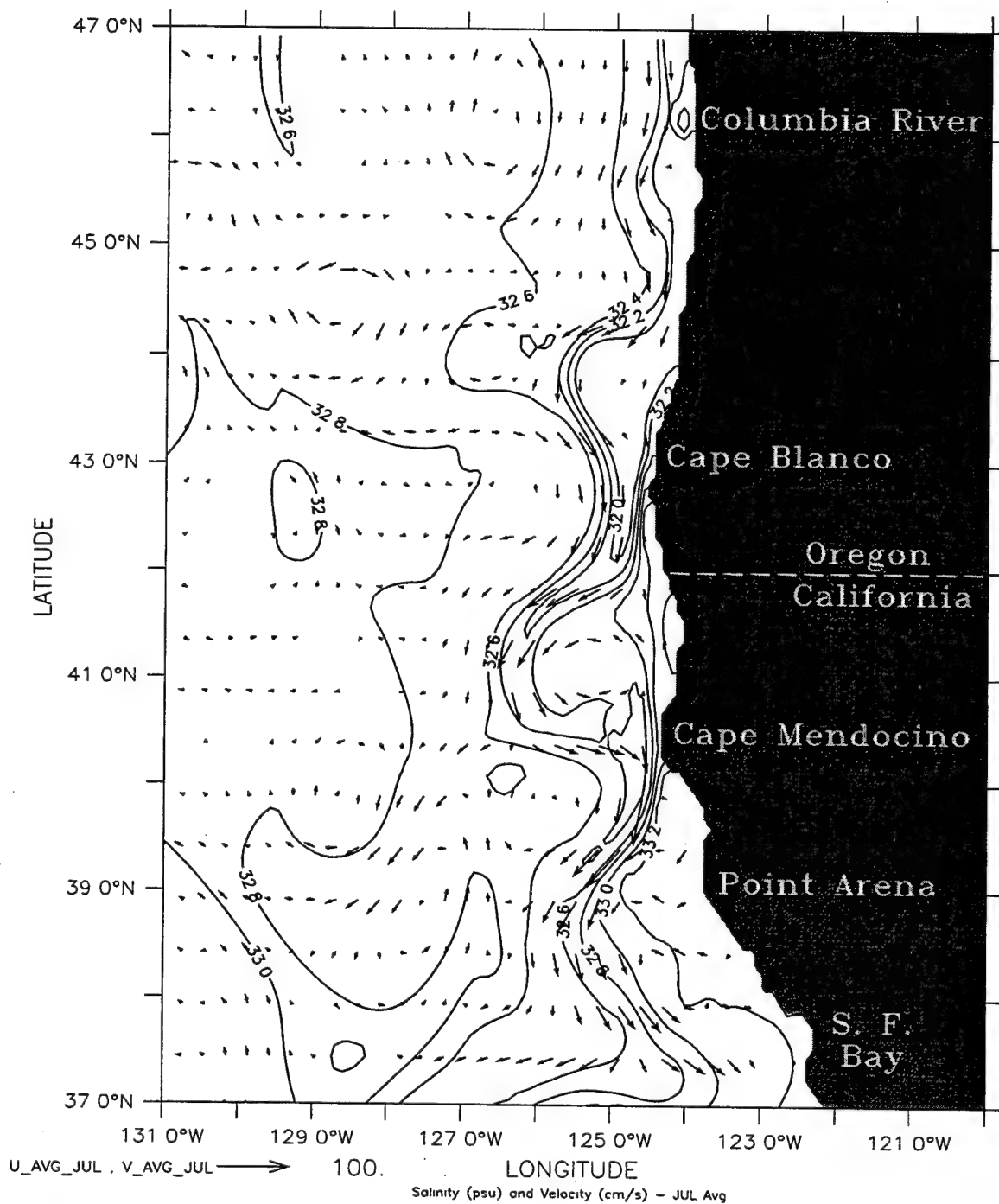
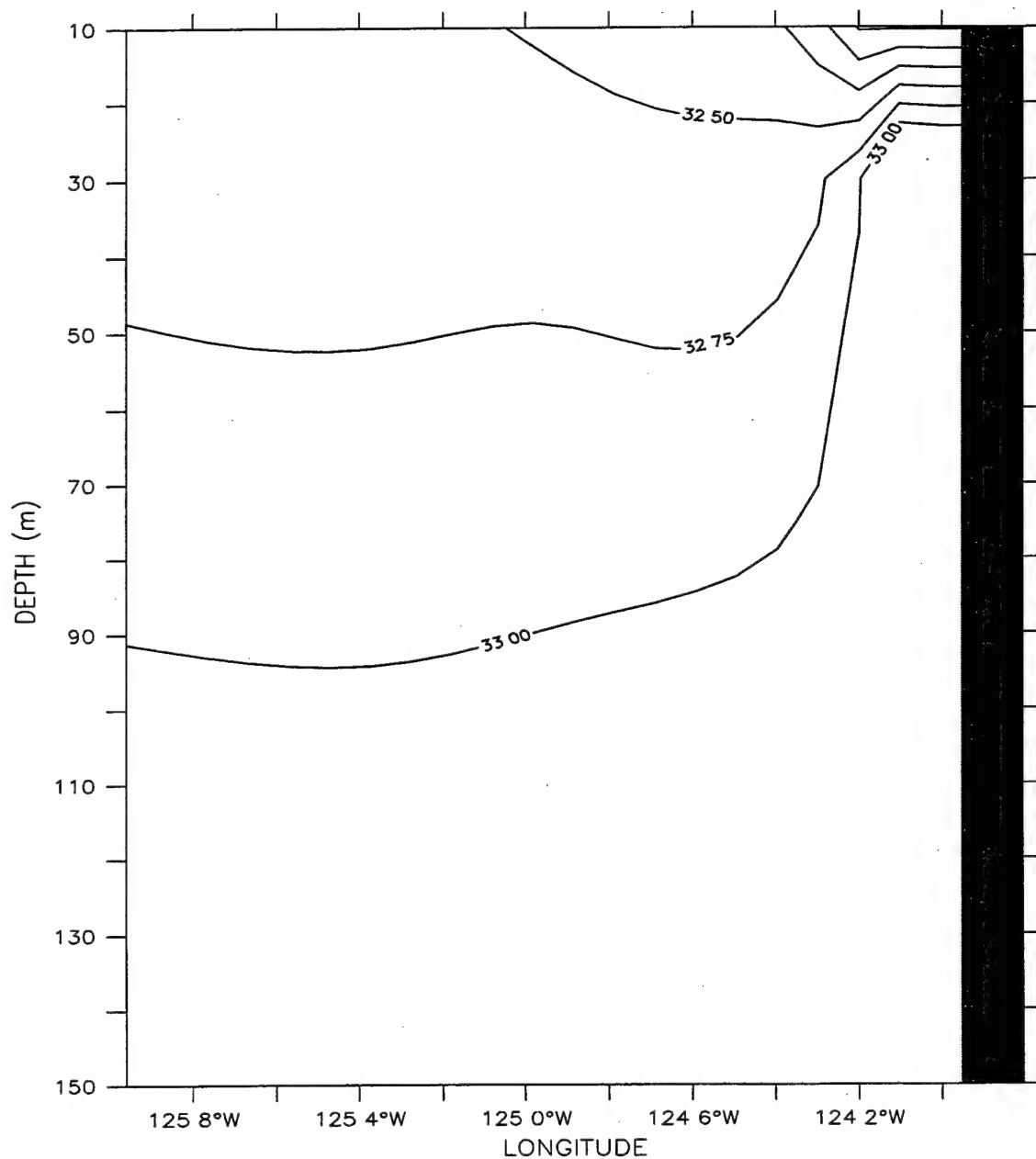


Figure 26. Salinity contours and velocity vectors at 10 m depth for Experiment 3 time-averaged for the month of July. Contour interval is 0.2 psu; maximum velocity vector is 100 cm/s. Tongue of Columbia River plume is represented by the 32.0 isohaline.

LATITUDE : 45N
T (DAY) : 910.5 to 940.5

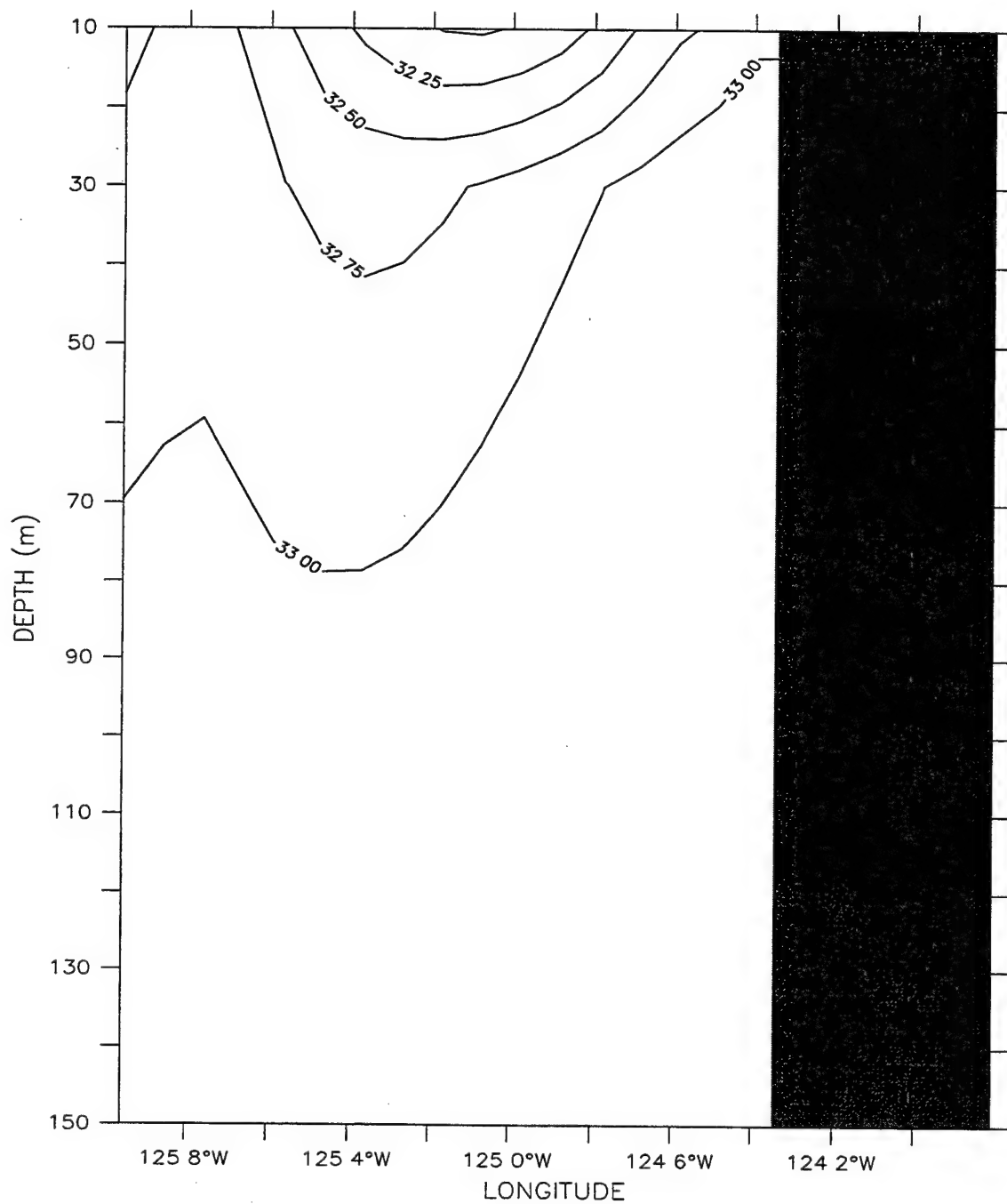


Salinity (psu) - JUL Avg.

(a)

Figure 27. Cross-shore section of salinity for Experiment 3 time-averaged for the month of July at (a) 45° N and (b) 42° N. Contour interval for salinity is 0.25 psu.

LATITUDE : 42N
T (DAY) : 910.5 to 940.5



Salinity (psu) - JUL Avg.

(b)

Figure 27 continued.

Table 1. Values of Constants Used in the Model

Constant	Value	Definition
T_0	278.2°K	Constant Reference Temperature
S_0	34.7	Constant Reference Salinity
ρ_0	1.0276 gm cm ⁻³	Density of Sea Water At T_0 and S_0
α	$2.4 \times 10^{-4} (\text{°K})^{-1}$	Thermal Expansion Coefficient
β	7.5×10^{-4}	Saline Expansion Coefficient
K	10	Number of Levels In Vertical
Δx	9.0×10^5 cm	Cross-Shore Grid Spacing
Δy	1.1×10^6 cm	Alongshore Grid Spacing
H	4.5×10^5 cm	Total Ocean Depth
Δt	800 s	Time Step
f_0	$0.84 \times 10^{-4} \text{ s}^{-1}$	Mean Coriolis Parameter
g	980 cm s^{-2}	Acceleration of Gravity
A_M	$2 \times 10^{17} \text{ cm}^4 \text{ s}^{-1}$	Bi-harmonic Momentum Diffusion Coefficient
A_H	$2 \times 10^{17} \text{ cm}^4 \text{ s}^{-1}$	Bi-harmonic Heat Diffusion Coefficient
K_M	$0.5 \text{ cm}^2 \text{ s}^{-1}$	Vertical Eddy Viscosity
K_H	$0.5 \text{ cm}^2 \text{ s}^{-1}$	Vertical Eddy Conductivity

THIS PAGE INTENTIONALLY LEFT BLANK

LIST OF REFERENCES

- Arakawa, A., and V.R. Lamb, Computational design of the basic dynamical processes of the UCLA general circulation model. In, *Methods in Computational Physics*, J. Chang, ed., Academic Press, 17, 173-265, 1977.
- Bakun, A. and C.S. Nelson, The seasonal cycle of wind stress curl in subtropical eastern boundary current regions, *J. Phys. Oceanogr.*, 21, 1815-1834, 1991.
- Batteen, M. L., Wind-forced modeling studies of currents, meanders, and eddies in the California Current System, *J. Geophys. Res.*, 102, 985-1009, 1997.
- Batteen, M. L., C. A. Collins, C. R. Gunderson, and C. S. Nelson, The effects of salinity on density in the California Current System, *J. Geophys. Res.*, 100, 8733-8749, 1995.
- Batteen, M.L., and Y.-J. Han, On the Computational noise of finite-difference schemes used in ocean models, *Tellus*, 33, 387-396, 1981.
- Batteen, M.L., R.L. Haney, T.A. Tielking, and P.G. Renaud, A numerical study of wind forcing of eddies and jets in the California Current System, *J. Mar. Res.*, 47, 493-523, 1989.
- Batteen, M.L., and P.W. Vance, Modeling studies of the effects of wind forcing and thermohaline gradients in the California Current System, *Deep-Sea Research II*, 1507-1556, 1998.
- Berdeal, I.G., B.M. Hickey, and M. Kawase, Factors Controlling the Orientation of the Columbia River Plume: A Numerical Model Study, Abstracts of the Ocean Sciences Meeting, San Antonio, TX, pp. OS168-OS169, January 2000.
- Bernstein, R.L., L.C. Breaker, and R. Whitner, California Current eddy formation: Ship, air, and satellite results, *Science*, 195, 353-359, 1977.
- Bourke, R.H. and B. Glenne, The Nearshore Physical Oceanographic Environment of the Pacific Northwest Coast, *Dept. of Oceanogr. Ref. 71-45*, 127 pp., Oreg. State Univ., Corvallis, 1971.
- Breaker, L.C., and C.N.K. Mooers, Oceanic variability off the central California coast, *Prog. Oceanogr.*, 17, 61-135, 1986.
- Camerlengo, A.L. and J.J. O'Brien, Open boundary conditions in rotating fluids, *J. Comput. Physics*, 35, 12-35, 1980.

- Chelton, D.B., Seasonal Variability of Alongshore Geostrophic Velocity off Central California, *J. Geophys. Res.*, 89, 3473-3486, 1984.
- Haney, R.L., A numerical study of the response of an idealized ocean to large-scale surface heat and momentum flux, *J. Phys. Oceanogr.*, 4, 145-167, 1974.
- Hickey, B.M., The California Current System-Hypotheses and facts, *Prog. Oceanogr.*, 8, 191-279, 1979.
- Hickey, B.M., Western North America, Tip of Baja California to Vancouver Island, In, *The Sea*, John Wiley, New York, 345-393, 1998.
- Hickey, B.M., L.J. Pietrafesa, D.A. Jay, and W.C. Boicourt, The Columbia River Plume Study: Subtidal variability in the velocity and salinity fields, *J. Geophys. Res.*, 103, 10,339-10,368, 1998.
- Holland, W.R., The role of mesoscale eddies in the general circulation of the ocean - numerical experiments using a wind-driven quasigeostrophic model, *J. Phys. Oceanogr.*, 8, 363-392, 1978.
- Holland, W.R., and M.L. Batteen, The parameterization of subgrid scale heat diffusion in eddy-resolved ocean circulation models, *J. Phys. Oceanogr.*, 16, 200-206, 1986.
- Huyer, A., Coastal upwelling in the California Current System, *Prog. Oceanogr.*, 12, 259-284, 1983.
- Ikeda, M. and W.J. Emery, Satellite observations and modeling of meanders in the California Current System off Oregon and northern California, *J. Phys. Oceanogr.*, 14, 1434-1450, 1984.
- Landry, M.R., and Hickey, B.M., *Coastal Oceanography of Washington and Oregon*, Elsevier Oceanography Series 47, Elsevier, Amsterdam, 607 pp., 1989.
- Levitus, S., R. Burgett, and T. P. Boyer, World ocean atlas 1994, Vol. 3: Salinity, *NOAA Atlas NESDI 3*, 99 pp., U. S. Dept. of Commerce, Washington, D. C., 1994.
- Levitus, S., and T. P. Boyer, World ocean atlas 1994, Vol. 4: Temperature, *NOAA Atlas NESDI 4*, 117 pp., U. S. Dept. of Commerce, Washington, D. C., 1994.
- Lynn, R.S. and J.J. Simpson, The California Current system: The seasonal variability of its physical characteristics, *J. Geophys. Res.*, 92, 12,947-12,966, 1987.
- Strub, P.T., P.M. Kosro, A. Huyer, and CTZ Collaborators, The nature of the cold filaments in the California Current system, *J. Geophys. Res.*, 96, 14,743-14,768, 1991.

Trenberth, K.E., W.G. Large, and J.G. Olson, The mean annual cycle in global ocean wind stress, *J. Phys. Oceanogr.*, 20, 1742-1760, 1990.

Weatherly, G.L., A study of the bottom boundary layer of the Florida Current, *J. Phys. Oceanogr.*, 2, 54-72, 1972.

THIS PAGE INTENTIONALLY LEFT BLANK

INITIAL DISTRIBUTION LIST

	No. Copies
1. Defense Technical Information Center.....	2
8725 John J. Kingman Rd, STE 0944	
Ft. Belvoir, VA 22060-6218	
2. Dudley Knox Library.....	2
Naval Postgraduate School	
411 Dyer Rd	
Monterey, CA 93943-5101	
3. Chairman (Code OC/Bf).....	1
Department of Oceanography	
Naval Postgraduate School	
Monterey, CA 93943-5122	
4. Chairman (Code MR/Wx).....	1
Department of Meteorology	
Naval Postgraduate School	
Monterey, CA 93943-5114	
5. Dr. Mary L. Batteen, (Code OC/Bv).....	4
Department of Oceanography	
Naval Postgraduate School	
Monterey, CA 93943-5122	
6. Dr. Curtis A. Collins, (Code OC/Co)	1
Department of Oceanography	
Naval Postgraduate School	
Monterey, CA 93943-5122	
7. LT Frank M. Schenk	4
1603 Powder Ridge Dr.	
Valrico, FL 33594	